Inertial Response from Wind Turbines

A thesis submitted to

Cardiff University

For the degree of

Doctor of Philosophy

2012

Candidate

Ian F Moore

School of Engineering

Contents

Summary of Thesis

Wind power is an essential part of the strategy to address challenges facing the energy sector. Operation of the electricity network in 2020 will require higher levels of response and reserve from generation. The provision of inertial response from wind turbines was investigated.

A model was developed for the simulation of frequency on the mainland UK system, including a simplified model for a synchronous generator to represent Full Power Converter turbines. Two different methods of inertia response, the step method and the inertia coupling method, were modelled and introduced into the turbine torque speed control. Simulations illustrated the effects on primary frequency control for a high penetration of wind turbines. Results are shown for different demand levels with generation losses of 1320GW and 1800GW. A comparison of the inertia functions is included and the effect of wind speed and the constant speed region of the maximum power extraction curve. For the scenarios modelled only a small change in turbine output was required for inertia response (0.02p.u). Without inertia response a large increase in synchronous plant response was needed.

A test rig was constructed consisting of a Full Power Converter bridge and a synchronous generator driven by a dc machine. Power converters were designed and constructed by the candidate. Vector control of both the generator converter and grid converter was implemented on a dedicated control platform. The inertia coupling function was implemented and a test frequency deviation injected to represent a load generation imbalance. Results compared closely to those from the model and demonstrated the capability to closely couple turbine speed to system frequency with adjustment of the response via a filter if desired.

The experimental work confirmed the adequacy of the simplified generator model and further confirmed the possibility of using inertia response. The inertia coupling function was considered suitable for use for the UK system.

Declarations and statements

This work has not previously been accepted in substance for any degree and is not concurrently submitted in canditure for any degree.

Signed ……..…….. (candidate) Date …….

This thesis is being submitted in partial fulfilment of the requirements for the degree of PhD.

Signed ……..…….. (candidate) Date …….

This thesis is the result of my own independent work/investigation, except where otherwise stated. Other sources are acknowledged by explicit references.

Signed ……..…….. (candidate) Date …….

I hereby give consent for my thesis, if accepted, to be available for photocopying and for inter-library loan, and for the title and summary to be made available to outside organisations.

Signed ……..…….. (candidate) Date …….

Acknowledgements

The following thanks are due:

My supervisors Dr Janaka Ekanayake and Professor Nicholas Jenkins for their constant encouragement, advice given and their enthusiasm for the subject of renewables and power systems.

The staff, researchers and PhD students within the Institute of Energy at Cardiff University for the opportunities I have been given to present and discuss my work and engage with others in the area of power systems.

Staff in the research office and graduate office for providing supporting activities and training.

The staff in the electronics workshop Denley, Paul, Mike, Wayne, Alan and Richard for their practical skills and help.

The SUPERGEN FLEXnet project and partners including Richard Hair at E.ON for my placement.

and of course by non means least support from my family.

Dedication

To my good friend Nicholas Ewart Wood who sadly passed away in the Autumn of 2008.

Copyright

List of tables

List of figures

List of symbols

General

C_p	Coefficient of performance
e_d	d-axis stator voltages (also V_{ds})
e_q	q-axis stator voltages (also V_{qs})
$e_{q\text{-}int}$	Control component of applied q-axis voltage
E_{int}	Internal voltage of the machine (phasor representation)
E_T	Terminal voltage (phasor representation)
f	Frequency
H	Per unit inertia constant
H_{eq}	Equivalent per unit inertia constant for synchronous system consisting of multiple rotating masses
H_i	Per unit inertia constant for an individual rotating mass
H_{WT}	Wind turbine per unit inertia constant
i_a, i_b, i_c	Stator currents in phases windings a, b, c
i_{dr}, i_{qr}	d and q-axis rotor currents
i_{dq_error}	Error inputs to PI compensators
i_{ds}, i_{qs}	d and q-axis stator currents
I_T	Current (phasor representation)
J	Moment of inertia
k_d, k_q	Scaling constants for dq transformation
k_i, k_p	Integral and proportional gains
L	Grid connection inductance
L_m, L_{rr}, L_s	Mutual inductance, Rotor self inductance, Stator inductance
p_f	Number of poles
P	Power
P_{acc}	Accelerating power
$P_{r\ gen}$	Power flowing via DFIG rotor circuit
R	Turbine rotor radius
R_e	Equivalent stator resistance
R_r	Rotor resistance
s	Slip or Laplace operator
S_i	VA base for an individual generator
S_{sys}	VA base for the power system
T_{acc}	Accelerating torque
T_{aero}	Torque developed at the rotor due to the wind
T_{base}	Rated torque of a generator
T_e	Electromagnetic air-gap torque
T_{e_ref}	Torque setpoint
T_m	Mechanical torque applied to the input shaft of a generator
T_{Pmax}	Curve of torque for maximum power extraction
T_{SI}	Torque employed to synthesise wind turbine inertia (subtracted from T_{Pmax})

$T_{SI'}$	Accelerating torque for inertia synthesis (before compensation)
T_{WT_acc}	Accelerating torque at the wind turbine rotor
U, U_{wind}	Wind speed
V_{abc}	Phase voltages
$V_{dc\text{-}link}$	dc link Voltage
$V_{dq'}$	d and q-axis voltage setpoints from PI compensators
V_{dq_speed}	Speed voltage components
V_e	Equivalent stator voltage
V_{dr}, V_{qr}	d and q-axis rotor voltages
V_{ds}	d-axis stator voltages (also e_d)
V_{qs}	q-axis stator voltages (also e_q)
VA_{base}	Rated power of a generator
X_e	Equivalent stator reactance
X_r	Rotor reactance
X_s	Stator impedance

Inertia response function

f_{trig}	Triggering frequency
K_c, K_T	Coupling gain, torque compensator gain
P_{step}	Step power increase
t_{recov}	Time after disturbance at which turbine speed recovery initiates
T_{dif}	Time constant of the first order filter applied to the differentiator
T_{step}	Step torque increase
ω_{min}	Minimum rotor speed

System modelling

D	Load sensitivity
P_0	Initial value of power
P_{gov}	Power response via synchronous plant governors
P_{load}	Power consumed by loads
P_{term}	Power output from synchronous generators
P_{WT}	Wind turbine power output
P_{WT_ss}	Steady state power output of wind turbine before a disturbance
T_0	Initial value of torque
T_{CH}, T_{RH}, T_{SM}	Steam turbine time constants – Steam chest, Re-heater, Servo motor
T_{gen}	Combined VSC and electrical machine time constant
F_{HP}	High pressure turbine fraction
ω_0	Initial value of rotor speed

Test rig

H_{eff}	Effective per unit inertia constant of the test rig
H_{rig}	Per unit inertia constant of the test rig
i_{acc}	dc machine armature current less current due to frictional losses

i_{dc_arm} dc machine armature current
$i_{dc\_arm\_ref}$ dc machine armature current reference
T_{ON_arm} dc machine armature duty cycle on-time
$T_{ON\_U1, U2, U3, L1, L2, L3}$ Duty cycle on-time for upper (U) and lower (L) converter switches
T_{aero_ref} Aerodynamic torque provided via dc machine
T_{dc_ref} Setpoint torque for dc machine
T_{scale} Additional shaft torque to increase effective inertia of test rig
ω_{ref_man} Speed setpoint for manual control of the test rig

Machine Modelling

L_{ad} d-axis mutual inductance
L_{aq} q-axis mutual inductance
L_d Inductance associated with total d-axis flux linkage due to i_d
L_{ffd} d-axis field self inductance
L_{fkd} Field to d-axis damper winding mutual inductance
L_{kkd} d-axis damper winding self inductance
L_q Inductance associated with total d-axis flux linkage due to i_q
L_l Leakage inductance
$P_{air\text{-}gap}$ Power transferred across the air-gap
P_t Terminal power
R_a Per phase armature resistance

ω_{mech} Mechanical speed of rotor rotation

Subscripts:

$_{ad}$	d-axis armature
$_{aq}$	q-axis armature
$_{fd}$	Field winding
$_{kd}$	d-axis damper winding
$_{kq}$	q-axis damper winding

Common subscripts

$_{acc}$ Accelerating
$_{dc}$ Direct current
$_{d, q}$ d-axis, q-axis
$_{ref}$ Reference
$_{s}$ Stator

Operators

Δ Change in value
p Rate of change

Greek Symbols

δ_T	Torque angle
Ψ, λ	Magnetising flux / flux linkage
ω_e	Rotational speed of reference frame (i.e. frequency of a.c)
ω_r	Speed of turbine rotor or generator shaft
ω_{0r}	Rated speed of a generator
ω_s	Slip speed
θ	Position of the d-axis ahead of the stationary magnetic axis
θ_r	Rotor position

List of abbreviations

ADC	Analogue to Digital Converter
CCGT	Combined Cycle Gas Turbine
C.V	Control Valve
DAC	Digital to Analogue Converter
DFIG	Doubly-fed Induction Generator
DMOL	Designed Minimum Operating Limit
DSP	Digital Signal Processor
FPC	Full Power Converter
FSIG	Fixed Speed Induction Generator
FSM	Frequency Sensitive Mode
IC	Integrated Circuit
IG	Induction Generator
IM	Induction Machine
K.E	Kinetic Energy
LFSM	Limited Frequency Sensitive Mode
MOSFET	Metal Oxide Semiconductor Field Effect Transistor
PC	Personal Computer
PCB	Printed Circuit Board
PLL	Phase Locked Loop
PI	Proportional Integral
PM	Permanent Magnet
PPM	Power Park Modules
PWM	Pulse Width Modulation
SM	Synchronous Machine
VSC	Voltage Source Converter
WT	Wind Turbine

1 Introduction

An outline is given of the challenges facing the electrical power industry and the role of large scale wind energy in making the transition to a de-carbonised electricity sector. The research objectives of the thesis are listed along with publications by the candidate. Lastly, torque speed control of a variable speed turbine is introduced, this being a key feature of the variable speed wind turbine which is the subject of this work.

1.1 Future UK electrical supply system and large scale wind

1.1.1 The energy challenge

The UK in common with many other countries is facing a number of challenges regarding the provision of adequate supplies of energy in the near term and long term future. For the UK three main issues are identified relating directly to the power generation sector (Department of Trade and Industry 2007):

- Ageing plant and infrastructure; an estimated 25% of existing capacity is due to close by 2020. These closures will consist of mainly coal fired and nuclear power stations.
- Security of supply concerns for fossil fuel based generation; a declining output from the UK Continental Shelf oil and gas fields and an increased reliance on imports from unstable regions. This is set against a general backdrop of increasing energy consumption worldwide.
- Constraints on green house gas emissions; National and international legally binding targets seek to reduce current green house gas emissions and make a substantial reduction (down 80% on 1990 levels) by 2050. A substantial part (37%) of existing emissions directly occurs from within the power generation sector.

A further challenge for the power generation sector is the planned large increase in use of electricity based technologies for heat and transport. This is because

electricity is considered easier to de-carbonise[1] and will mean that overall demand for electricity is set to increase regardless of further energy efficiency measures. In all an estimated £110billion of investment will be needed in electricity generation and transmission by 2020, a more than doubling of the current rate of investment.

Government strategy to address these challenges include energy efficiency, advanced metering, demand side management, and by no means least building of a diverse spread of low carbon generation via market based investment. Encouragement and enforcement of the necessary changes needed in the operation of markets is seen in the 'Electricity Market Reform' bill (Department of Energy and Climate Change 2011a) now being passed through parliament. This details changes which include a new Feed in Tariff to replace the existing Renewables Obligation (main mechanism which incentivises building of low carbon generation), a Carbon Price Floor (to strengthen carbon trading which functions to reflect the externalised costs of emissions), and an Emissions Performance Standard (to limit annual carbon emissions for new plant). A new market based measure is also included to incentivise the provision of plant capacity.

1.1.2 Attractive characteristics of large scale wind

Large scale wind power has a number of attractive characteristics, which make it suitable to play a large part in meeting the challenges outlined. These are:

- Established technology and competitive cost (Mott MacDonald 2010) - Comparison of Levelised Generation Costs[2] for new build, large scale generation technologies, indicates the cost of onshore wind lies in-between the cheapest option, Combined Cycle Gas Turbines (CCGTs) and those of the next cheapest option, that of coal. The future prediction is that "A modest real cost reduction over the next decade means that it [onshore wind] is projected to undercut CCGT to be the least cost substantive renewable

[1] The report 'Building a Low Carbon Economy' (Committee on Climate Change 2008) sets out emissions reduction targets for the UK and puts forward decarbonisation of the power generation sector as a key part of the strategy to achieve the targets.

[2] Levelised generation cost is "the lifetime discounted cost of an asset expressed in cost per unit energy produced". It is largely composed of the upfront capital costs and the running costs (such as fuel costs for non-renewables) over the life of the plant. It is important to note that comparative cost estimates between different types of generation is heavily influenced by the projections for fuel and carbon prices adopted and discount rates used (Mott MacDonald 2010).

option." Predicted costs for the newer technology options of offshore wind (currently costing 50% more than that of onshore), next generation nuclear and coal with carbon capture and storage (including super-critical coal) are that large reductions in costs will occur as each technology matures.

- Carbon footprint an order of magnitude lower than fossil fuelled plant (The Parliamentary Office of Science and Technology 2011) – Calculation of the 'carbon footprint' of an electricity generating technology involves assessment of the total[3] emissions over the lifetime of the plant and division of this total by the electricity output. Large scale wind is among the low carbon technologies which have emissions largely due to construction as opposed to conventional fossil fuel plant where emissions are largely due to their operation. Data from a range of peer reviewed studies indicates the carbon footprint of large scale wind to be approximately 15gCO_2eq/kWh. This compares to median estimates for the carbon footprint of existing gas and coal plant of approximately 500 and 900gCO_2eq/kWh respectively. Median estimates for coal and gas generating plant equipped with Carbon Capture and Storage is approximately 200gCO_2eq/kWh.
- Resource availability – The UK has a large potential resource of wind energy especially offshore. This is reflected in the 'UK Renewable Energy Roadmap' (Department of Energy and Climate Change 2011b) which analyses trends in recent deployment of renewables with reference to 2020 targets. It reported levels of wind capacity as 4GW onshore and 1.3GW offshore with the potential to achieve 13GW onshore and 18GW offshore by 2020. The Gone Green scenario presented by National Grid (2011a) as a plausible scenario to meet climate change objectives includes planned capacities of 9GW onshore and 17GW offshore by 2020 and 10GW onshore and 37 GW offshore by 2030.

1.1.3 System operation with high proportion of wind power

National Grid is responsible in the UK for the provision of adequate and reliable network capacity and the task of balancing supply and demand. In their consultation

[3] Total emissions will for example include "construction and maintenance; the extraction, processing and transport of their fuels (if applicable); and their ultimate decommissioning and disposal" (The Parliamentary Office of Science and Technology 2011).

document National Grid (2011b) present their analysis and view on operation of the network in 2020 with a generation mix based on their 'Gone Green' scenario. A key aspect highlighted is the change in the generation mix due to the increasing proportion of renewable and other low carbon generation sources. Some of the important issues arising from this change are listed below (note reserve and response are explained in 2.1.1):

- Reserve – Higher levels needed and greater variability seen as scheduling of plant becomes more influenced by the effect of weather as installed wind capacity rises.
- Response – Increase needed due to largest in-feed loss going up from 1320 to 1800MW. This is to cater for connection of offshore wind farms and also the expected larger size generators from new build power stations.
- Operation at minimum demand – The need to curtail wind plant during minimum demand will become necessary (predicted 38 days per year) although the curtailment will rarely coincide with high output from wind generation.
- Thermal plant operating regimes – An increase in the required operational flexibility of CCGTs and a reduction in their load factor[4].
- Other issues – Increase in the size of interconnectors and increased variability of these flows. In general an increase in the number of balancing actions is predicted, this in turn creating a need for further automation in the despatch of generation and demand.

1.2 Wind turbine torque speed control

Synthesis of turbine inertia requires control of turbine speed and torque. This section introduces the power and torque characteristics of the variable speed turbine, the practical division of the torque speed control into regions and explains how turbine speed control may be implemented.

[4] Load factor is a measure of the utilisation of a plant and is calculated by dividing the actual output from the plant in a year by the maximum theoretical output in a year if it ran constantly at full output.

1.2.1 Turbine power and torque characteristics

The relationship between turbine power output and wind speed is cubic and is given by (Burton et al. 2001):

$$P = \frac{1}{2} C_p \rho U^3 \pi R^2$$

where ρ is the density of air, U is the upwind free air speed, R is turbine rotor radius and C_p (explained next section) is the coefficient of performance of the turbine.

An example of the torque T_{aero} and the power P developed for a horizontal axis wind turbine is shown in Figure 1.1 for three different wind speeds with rotor pitch held constant. Per unit scaling of power and torque is based upon rated operation at a wind speed of 13m/s. Hence at rated output, wind speed 13m/s, the maximum power and the torque corresponding to maximum power are both 1p.u. The power and corresponding torque value for maximum power operation for a wind speed of 10.2m/s is also indicated.

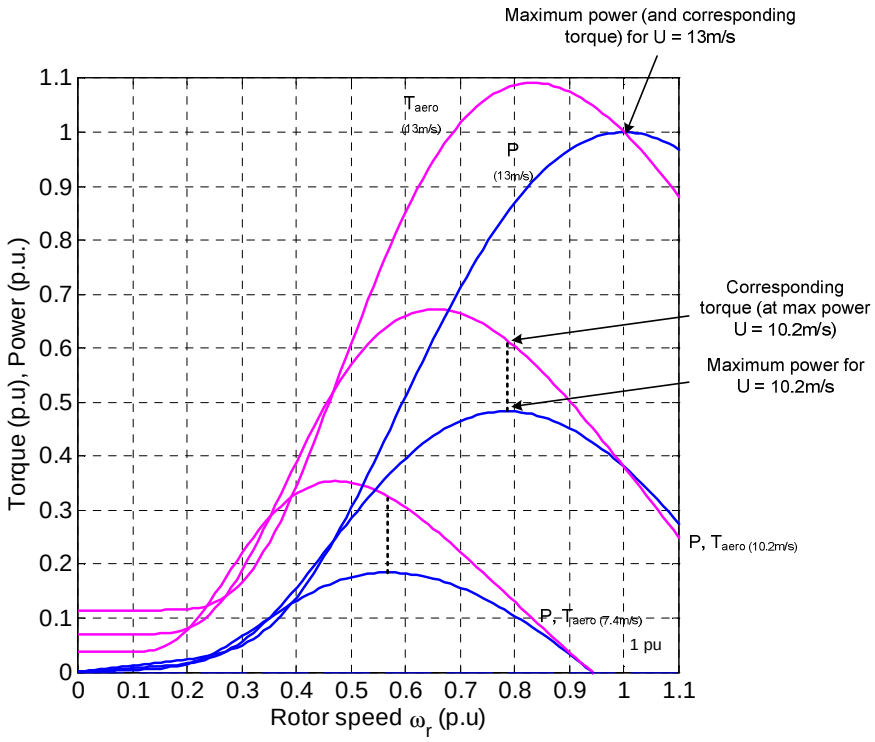

Figure 1.1 – Torque developed by the rotor, T_{aero} (magenta) and developed power P (blue) as rotor speed varies for three different wind speeds for a horizontal axis variable speed turbine.

1.2.2 Maximum power extraction curve

The efficiency of a turbine in converting the available power from the wind into power available at the turbine, the developed torque multiplied by speed, is described by the power coefficient C_p. For a particular turbine rotor design the C_p value will peak (become optimum) at a particular ratio of wind speed to rotor speed, this ratio which is non-dimensional is known as the tip speed ratio λ and is given by (Burton et al. 2001):

$$\lambda = \frac{\omega_r R}{U}$$

where ω_r is rotor speed, R is the rotor radius and U is the upwind free air speed.

If turbine speed is controlled such that the optimum tip speed ratio is maintained across a range of wind speeds then the power production of the rotor will be maximised[5]. The set of points which prescribe this operation form a maximum power extraction curve, this curve is shown in Figure 1.2. Division of the curve by rotor speed results in a curve of torque, T_{Pmax}, which corresponds to maximum power and is typically used in the turbine control as the generator torque setpoint. Note the C_p-lambda curve for the turbine featured in this thesis is included in Appendix B2.

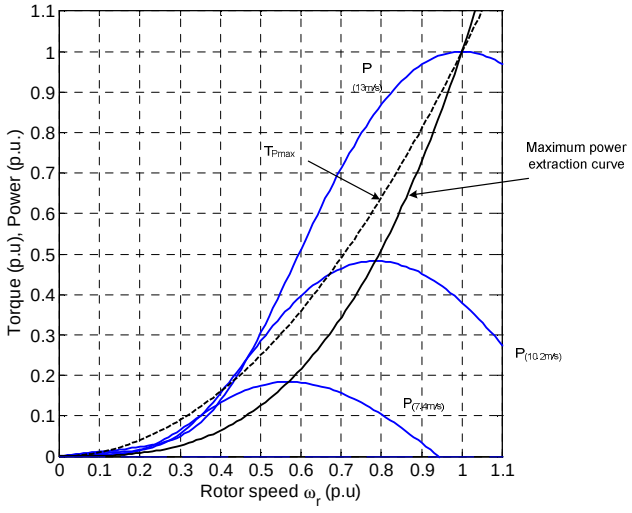

Figure 1.2 – Turbine power characteristics including maximum power extraction curve and corresponding torque curve T_{Pmax}.

[5] This assumes the aerodynamic performance of the blades does not deteriorate as apparent wind speed changes. Note that operation at a constant tip speed ratio means the apparent angle of attack of the wind to the rotor blade is also constant i.e. blade pitch is held constant.

1.2.3 Operating regions for the variable speed turbine

The primary objective for a turbine control scheme is that of maximizing energy capture whilst remaining at the same time within operational limits and designed loading limits. Economic design of a turbine means that operation on the maximum power extraction curve is not possible for all wind speeds[6]. Torque speed control of the turbine is thus typically divided into three distinct regions which are illustrated in Figure 1.3 and listed below:

- Variable speed region - follows T_{Pmax} as closely as possible in order to maximize energy capture; point **a** to **b**.
- Constant speed region - maintains rotational speed constant and adjusts torque as wind speed changes (this helps reduce acoustic noise); **b** to **c**.
- Pitch regulation region - maintains torque near constant and limits aerodynamic rotor power by blade pitching as wind speed increases; **c** to **d**.

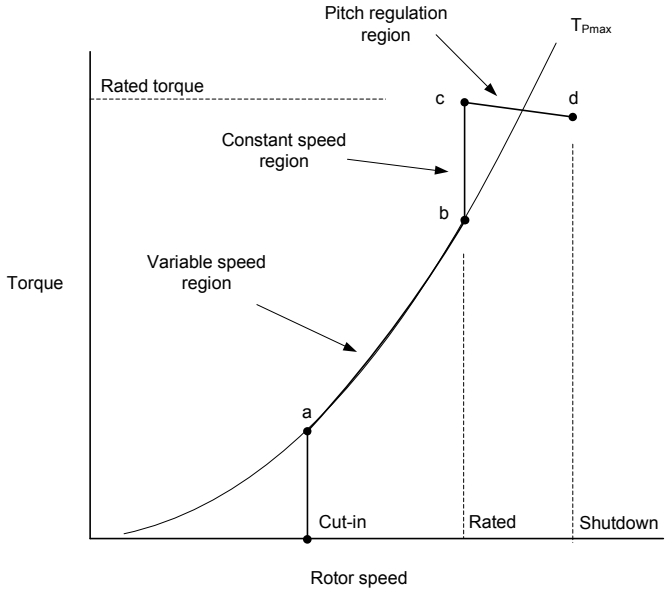

Figure 1.3 – Operating regions for a variable speed turbine.

[6]A comprehensive treatise on the design of wind turbines is given in Jamieson (2011)

1.2.4 Torque speed control in the variable speed region

Ideally speed control of the turbine in the variable speed region might be implemented by measuring wind speed and controlling generator torque to adjust rotor speed to the optimum tip-speed ratio (Manwell et al. 2002). However a more practical method that does not use wind speed measurement is to set the generator torque reference to the value of torque obtained from T_{Pmax} curve for the existing value of rotor speed. The behaviour of the turbine when using this speed control method for a step change in wind speed is illustrated in Figure 1.4 and is explained below:

i) At point **a** aerodynamic torque T_{aero} is equal to the torque setpoint for generator T_{Pmax} and speed is constant.
ii) A step increase in wind speed occurs. The generator setpoint initially remains unchanged at point **a** but T_{aero} has increased to point **b**.
iii) The turbine now undergoes acceleration, of magnitude T_{WT_acc}. As speed increases the torque setpoint, T_{Pmax}, gradually increases and T_{aero} gradually decreases. This results in a gradually reducing accelerating torque and thus a gradually reducing acceleration until the turbine reaches a new equilibrium operating speed at point **c**.

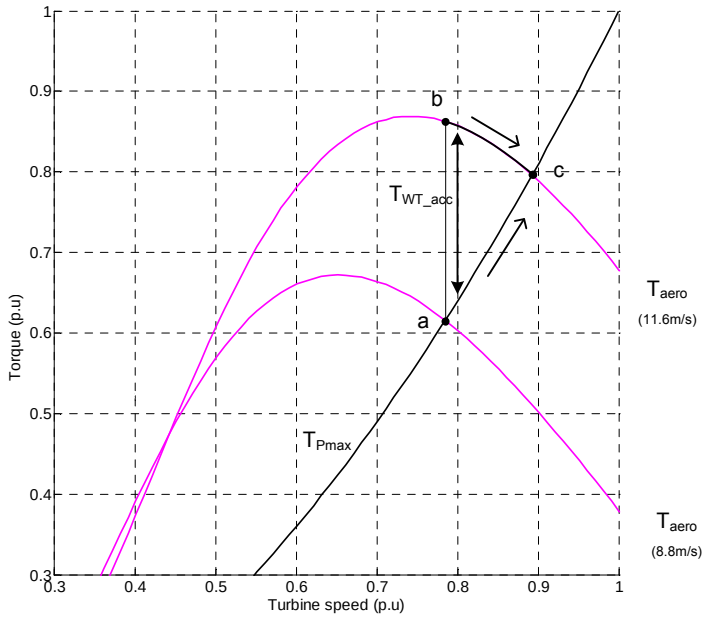

Figure 1.4 – Operation of the simple torque speed control method for a sudden increase in wind speed.

For simplicity the modelling and experimental work in this thesis uses the above method of speed control. Johnson et al. (2006) refers to the method as ‘standard control’ and states its shortcomings to include:

- Maximum power extraction curve derived during design of the turbine may be inaccurate.
- Actual wind regime is turbulent (i.e. wind speed continually changing) so the turbine will spend much of its time away from the optimum power point as described by the maximum power extraction curve.
- The maximum power extraction curve needed for optimum energy production will need to change as blade conditions change; aerodynamic performance of a blade is affected by dirt, ice and long term erosion.

A more sophisticated version of the above method is outlined by Bossanyi (2000) who presents a speed error based control, this method being more likely to be used in a real implementation. Advantages of the method are tuning of compliance via PI compensators, possibility for speed exclusion zones to avoid turbine resonance and smoother transitions between regions.

1.3 Thesis overview and research contributions

Overview

The overall research objective was to investigate the provision of inertial response from variable speed wind turbines for the mainland UK system. This is becoming important due to the expansion of wind energy and the effect a reduction in inertia will likely have on the regulation of frequency during large load generation disturbances.

Research tasks were broken into the three key activities, with thesis chapters indicated, as below:

- Review of published research/literature (Chapter 2).
  - Fundamental coupling properties of turbine generator topologies.
  - Proposed methods of inertia response.

- Simulation of the UK system in terms of frequency regulation to include wind turbines with inertia response (Chapter 5).
- Experimental testing of an inertia response function (Chapter 6).

Contributions

The contributions of the thesis are listed below:

- Review of European technical requirements for the regulation of frequency by conventional plant and large scale wind installations
- Development of a UK frequency model (Chapter 5) - Provided the platform to evaluate the potential impacts of the increasing quantity of wind power on the UK system and the possible use of inertia response to improve or remediate primary frequency control performance.
- Development of a simplified model of a Full Power Converter turbine (Chapter 3) - Enabled representation of turbine torque control for use in the UK frequency model.
- Construction of a wind turbine test rig (Chapter 4) - Allowed testing of an inertia response function, thus contributing to evaluation of the performance capability of variable speed, converter based wind turbines.

1.4 Publications

A number of papers were published describing the work, (1 to 3 below) and additionally two reports (4 & 5):

1. Moore, I., Ekanayake, J., Jenkins, N., "Control and Dynamics of Wind Turbine Generators for Existing and Future Grid Code Compliance", *Journal of Energy & Environment*, Volume1, April 2009, pp. 15-24.
2. Moore, I., Ekanayake, J., "Frequency Response from Wind Turbines", in *Universities Power Engineering Conference (UPEC), 2009 Proceedings of the 44th International*.

3. Moore, I., Ekanayake, J., “Design and Development of a Wind Turbine Simulator” in *Universities Power Engineering Conference (UPEC), 2010 Proceedings of the 45th International*.
4. Moore, I., “Review of Transmission System Connection Requirements”, report for *E.ON Technology Centre, Ratcliffe-on-Sour, Nottinghamshire*, 2011, available MooreIF@Cardiff.ac.uk
5. Ekanayake, J., Moore, I., Jenkins, N., “Control & Dynamics of Wind Turbine Generators for Existing and Future Grid Code Compliance”, report for the *Centre for Distributed Generation and Sustainable Electrical Energy*, 2009, available at http://energy.engineering.cf.ac.uk/technology-reviews

2 Literature review on inertial frequency response

2.1 Introduction

2.1.1 Frequency balancing services

Regulation of system frequency is principally managed through a combination of automatic and scheduled (non-automatic) changes in generator output. In the UK these are termed response and reserve respectively and are shown in Figure 2.1 with response further subdivided. They exist as one component of the 'balancing services' which a system operator employs for adjustment of real and reactive power to cope with a range of operational scenarios.

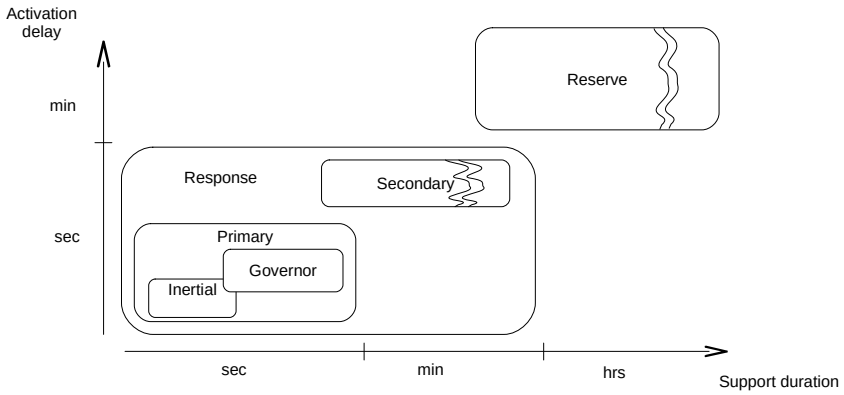

Figure 2.1 – Hierarchy of frequency balancing services for the UK grid in terms of activation delay and support duration.

In the UK, increased power output from generators responding within 10 seconds and maintaining their extra output for at least a further 20 seconds is termed primary response. Increased output from generators responding within 30 seconds and maintained for no less than 30 minutes is termed secondary response.

The function of primary response is to provide an immediate balancing action to contain the frequency deviation. Secondary response then progressively relieves the primary response and by further changes in output restores system frequency to within its normal operating range.

Reserve is the slowest acting frequency balancing type service. In addition to being used for restoration of frequency and response capability it is used to make up for demand forecasting errors and plant loss. Partitioning and functioning of reserve

services in the UK is explained in the National Grid Balancing Principles Statement (2008).

For a synchronously connected power system the instantaneous imbalance between prime mover input power and system load is met by changes in the K.E of the rotating plant, this 'response' from rotating plant inertia being entirely automatic.

2.1.2 Frequency control in the UK (Erinmez et al. 1998)

In the UK, frequency services are classified as either continuous or occasional, the latter consisting of primary and secondary response from generators and also relay initiated load response. Frequency control from generators is indicated in Figure 2.2 which shows the frequency deviation profile as might occur after a sudden large generation loss or connection of a large load.

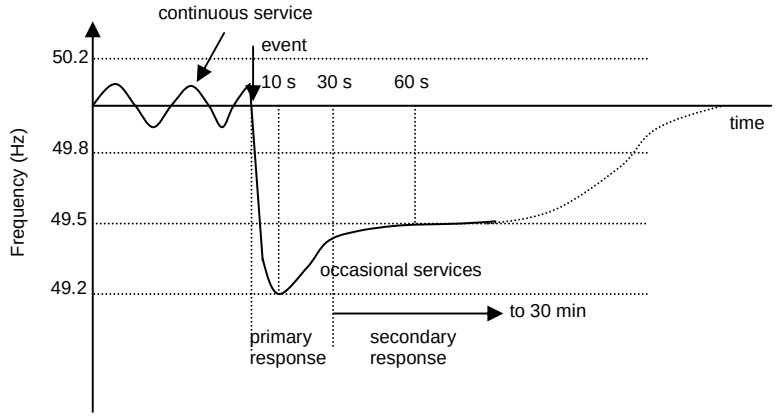

Figure 2.2 – Modes of operation of frequency control on the UK grid (Erinmez et al. 1998)

The system operator implements a policy of containment and regulation of frequency to within certain limits and procures and dispatches frequency control services in order to achieve this. The limits are specified depending on generation loss size and are summarized in Table 2.1.

Table 2.1 – Frequency containment policy for the UK electricity system

Operating Condition	Requirement
Supply Regulations	50 Hz ±1.0 except in exceptional circumstances
Normal ('continuous') control target	50 Hz ±0.2
Sudden loss < 300MW	50 Hz ±0.2
300 MW < Sudden loss < 1000MW	50 Hz ±0.5
1000 MW < Sudden loss ≤ 1320MW	50 Hz -0.8 return to 49.5Hz by 1 minute
Emergency load shedding at 48.8 Hz	

To ensure adequate plant performance minimum requirements for governors are specified in the connection 'grid codes' as well as requirements to meet target output and frequency setpoints. The main requirement for primary response from synchronous plant is that it is "released increasingly with time, through automatic governor action". Average response capability for particular types of plant, those of coal, oil and CCGT was noted to vary between 11 to 14% of registered capacity for primary, secondary and high frequency response services.

Regarding the commercial arrangements for frequency control services in the UK, payments are made to reflect costs due plant de-load efficiency, start-ups, lost opportunity, maintenance, ageing effects incurred and inclusion of a profit margin. For the year 2009/10 payments made to service providers for frequency response services which consisted of a 'Holding' payment and a 'Response Energy' payment totalled £112 million (National Grid 2010a).

2.1.3 Frequency balancing services in other countries

Differences in terminology of frequency services and performance requirements of frequency response are compared by Rebours et al (2007) across a selection of ten different countries. Classification is divided into 'primary control', 'secondary control' and 'tertiary control' these broadly being equivalent to primary response, secondary response and reserve within the UK.

In the comparison, UK primary and secondary response are classified as both being part of 'primary control', its subdivision in the UK reflecting the technical and commercial importance of primary control for a relatively small power system with

low interconnection. European countries are noted to require a relatively slow primary response capability; full deployment within 30 seconds or before deviation of 200mHz and support length of at least 15 minutes (UCTE 2004).

2.1.4 Characteristics of response for the UK grid

Although automatic and scheduled services from generators act to redress a load generation imbalance, the dynamics and magnitude of a frequency deviation is additionally influenced by frequency dependant characteristics of loads and generator plant types.

An example of loads exhibiting frequency sensitivity is pumps and fans where power consumption will typically vary as the cube of input shaft speed (IET 2009; Searle 1997). Some loads have no frequency dependency such as switch mode power supplies where power output and hence power consumed is electronically regulated. Using data from power station outputs during system disturbances Pearmine et al. (2006) calculated that the UK system load sensitivity can vary between a 1 and 7 % reduction in load per Hz depending on the time of day and season. In order to maintain desired levels of security, for scheduling purposes the load sensitivity factor is taken as a constant 2%.

Generating plant not participating in frequency control may also exhibit a frequency sensitive characteristic but one which results in declining power output capability as frequency drops, thus potentially worsening the load generation imbalance. Limiting factors for generating plant output below nominal frequency are described in ANSI/IEEE C37.106 (1993). For steam turbine plant these comprise of reductions in auxiliary plant output and prohibited and time restricted areas of turbine shaft speed operation. For combustion turbine plant a major restriction is the increase in blade temperature as shaft speed and (thus) air-flow decreases which eventually leads to over-temperature protection systems reducing fuel input.

The combined interaction of responsive and non- responsive generating plant and loads during frequency disturbances along with the size of the generation load imbalance will determine the frequency response ‘holding’ required.

2.1.5 Power system inertia

Contribution to system inertia

Utility scale electrical power systems consist of a number of large generators and a multitude of loads, the interconnection of these items is illustrated in Figure 2.3. Rotating electrical machinery such as the synchronous turbo generators illustrated and the Synchronous Machine (SM) and Induction Machine (IM) loads will all contribute to system inertia. For the synchronous machine this is due to the rotor shaft being synchronously coupled to the stator field, the angle between the fields depending on the torque. For the induction machine the rotor shaft is also coupled to the stator field but asynchronously by a slip velocity which is proportional to torque (this may typically be around 2% at rated output). The variable speed wind turbine will conversely not contribute to system inertia. This is due to the fact that the electromagnetic machine torque T_e for the wind turbine is controlled via a power electronic converter. For explanation of this decoupling see 2.2.

Total contribution to system inertia will also depend on the relative size of the electrical machine and any connected rotating masses such as turbine assemblies. The relationship between rotor dimensions, weight and the output of an electrical machine means that system inertia is principally held in the rotating mass of large synchronous generators and their turbines. Inertia for a range of rotating machine sizes is given in Appendix B1.

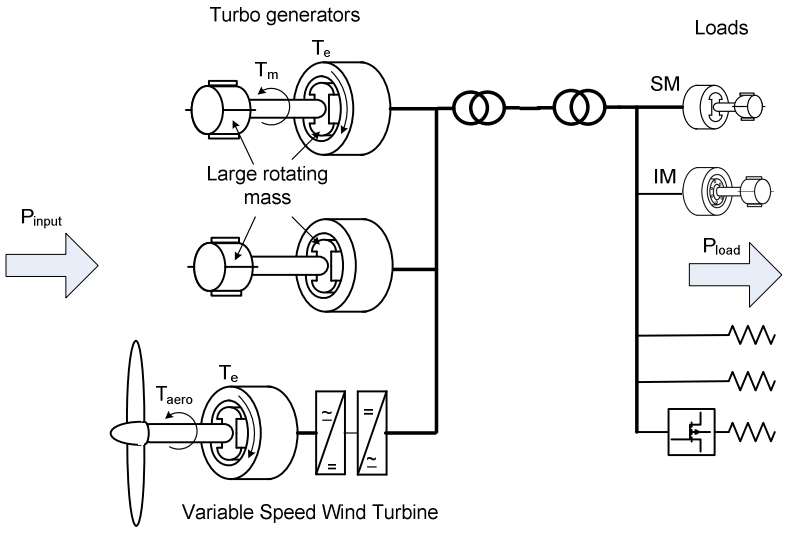

Figure 2.3 – Illustration of electrical machine topology, torque and power imbalance in relation to system inertia.

Rotational Dynamics

An imbalance between prime mover power input P_{input} and power consumed P_{load}, shown in Figure 2.3, will result in a corresponding imbalance between each generator's mechanical input torque T_m and electromagnetic air gap torque T_e. During this imbalance rotor speed and hence system frequency will change according to Eq(2.1) which is known as the 'Swing equation'

$$\sum J\frac{d\omega_r}{dt} = \sum T_{acc} \qquad (2.1)$$

where J is the moment of inertia (kg.m^2) of each generator, ω_r the angular velocity (rad/s) and T_{acc} is the accelerating torque given by T_m-T_e (N.m). Note a negative value of T_{acc} indicates deceleration of rotor speed.

Fundamentally the instantaneous power imbalance is met by changes in the stored rotational Kinetic Energy (K.E) of the system which is given by

$$K.E = \frac{1}{2}J\omega^2 \qquad (2.2)$$

For convenience it is possible to express the inertia of a generator in terms of a dimensionless unit known as the per unit inertia constant H. This is defined as the K.E of the rotating mass divided by its power base and is given in Eq(2.3) where VA_{base} is the rated generator power and ω_{0r} is its rated speed.

$$H = \frac{K.E}{VA_{base}} = \frac{J\omega_{0r}^2}{2VA_{base}} \qquad (2.3)$$

By substituting for J it is now possible to write the swing equation in terms of H thus:

from Eq(2.3)

$$J = \frac{2H\,VA_{base}}{\omega_{0r}^2}$$

and substituting into Eq(2.1) (summation not shown)

$$T_{acc} = \frac{2H\ VA_{base}}{\omega_{0r}^2}\frac{d\omega_r}{dt} = \frac{2H\ T_{base}}{\omega_{0r}}\frac{d\omega_r}{dt}$$

where T_{base} and ω_r are the torque base and shaft speed respectively.

In per unit this can be expressed as:

$$\overline{T_{acc}} = 2H\overline{\frac{d\omega_r}{dt}} \qquad (2.4)$$

Whilst load generation mismatch is kept in check by prime movers equipped with governor speed control loops i.e. providing frequency response services, due to finite response times of governors and plant time constants the initial imbalance is met by changes in the stored K.E of the system. Rearranging Eq(2.4) gives the rate of change of speed of the system

$$\overline{\frac{d\omega_r}{dt}} = \frac{\overline{T_{acc}}}{2H} \qquad (2.5)$$

To obtain rate of change of frequency we divide by 2π. However in p.u Eq(2.5) will be the same as rate of change of frequency in p.u thus

$$\overline{\frac{df}{dt}} = \frac{\overline{T_{acc}}}{2H} \qquad (2.6)$$

For small changes in system frequency the per unit accelerating torque T_{acc} is equivalent to the per unit power system imbalance and hence accelerating power P_{acc} (see 5.2.1). Dispensing with superbar notation for per unit, rate of change of frequency can therefore be written as

$$\frac{df}{dt} = \frac{P_{acc}}{2H_{eq}} \qquad (2.7)$$

Note that P_{acc} is expressed as per unit on the system base S_{sys} and H_{eq} is the equivalent inertia constant of the system given by

$$H_{eq} = \sum_{i=coal,gas,\dots} H_i * \frac{S_i}{S_{sys}} \qquad (2.8)$$

where H_i and S_i are the inertia constant and MVA rating of the different types of plant.

Hence the speed at which system frequency changes is directly determined by the ratio of power imbalance to system inertia.

2.2 Inertial coupling properties of WT generators

The relationship between rotor speed and system frequency for fixed and variable speed turbine topologies is given below along with published models relating to their inertial properties.

2.2.1 Fixed Speed Induction Generator (FSIG)

For the induction generator used in an FSIG turbine, slip s, is the per unit difference between rotor speed ω_r and the rotational speed of the stator field ω_s and is defined as positive for motor action and negative for generator action.

$$s = \frac{\omega_s - \omega_r}{\omega_s} \qquad (2.9)$$

A simplified induction generator circuit model (Kundur 1994) yields the following relationship between slip and electromagnetic torque T_e

$$T_e = 3\frac{p_f}{2}\left(\frac{R_r}{s\omega_s}\right)\frac{V_e^2}{(R_e + R_r/s)^2 + (X_e + X_r)^2} \qquad (2.10)$$

where p_f is the number of poles, V_e, X_e, R_e are the equivalent stator voltage, reactance and resistance respectively and R_r and X_r are the rotor resistance and reactance referred to the stator side. Under normal operation, where values of slip are small (typically 0 to -0.02), Eq(2.10) means that torque will be directly proportional to slip (shown Appendix B1).

During a drop in system frequency, such as after a generation loss, slip will increase and T_e will increase according to Eq(2.10). The speed of the turbine will then reduce until the original torque and slip are restored and the turbine attains a new equilibrium at the lower frequency. With initial slip and post-transient slip the same, Eq(2.9) means that for small changes in ω_s, per unit change in rotor speed ω_r will be approximately equal to per unit change in ω_s; this shows the FSIG to exhibit an inertial coupling whereby rotor speed follows system frequency.

Littler et al. (2005) investigated FSIG inertia for the Irish power system. Field based measurement of a wind farm with FSIG turbines during a frequency event shows an increase in turbine power output as frequency drops before automatic disconnection by ROCOF (Rate of Change of Frequency) relay protection. Simulations with a first order model, Eq(2.1) & (2.9) combined, of the 500kW turbines used on the wind farm (H = 3.0 sec) showed good correlation with the field measurements before the turbines tripped. Comparison of the FSIG response to the expected response from a synchronous machine (Eq(2.7)) indicated similar output from both.

Modelling of FSIG inertial response by Lalor et al. (2005) using a fifth order induction machine model, in contrast to Littler et al. (2005) shows an approximately 50% lower peak in power output response than for the case of a synchronous machine.

2.2.2 Doubly Fed Induction Generator (DFIG)

This topology and the partitioning of its control is illustrated in Figure 2.4. Similar to the FSIG the stator is directly connected to the grid, however rotor field excitation is obtained independently of the stator by use of a 3-phase 'back-to-back' voltage source converter.

The generator converter varies the torque producing component of rotor current according to the torque setpoint, $T_{e\ ref}$, to obtain maximum power extraction. This setpoint, as explained in section 1.2.2, is a function of rotor speed ω_r. The grid converter maintains dc-link voltage $V_{dc\text{-}link}$, constant, by exporting to, or importing from the grid, $P_{r\ gen}$ the power generated or consumed by the rotor circuit. Reactive power control for both converters is implemented as appropriate (not shown in Figure 2.4).

The reference frame needed for vector control for the generator converter is derived from rotor position θ_r and the position of the stator field, the latter obtained via a Phase Lock Loop (PLL). The resulting rotating reference frame enables regulation of the desired i_{dq} components of current independent of rotor speed. The reference frame for the grid converter control is that of the stator field obtained via a PLL. Application of a DFIG vector control scheme is shown in Pena et al. (1996).

Note that at synchronous speed active power flow occurs solely through the stator. At super-synchronous speeds a portion of the total active power P_{grid} is sourced from the rotor via the converters whilst at sub-synchronous speeds rotor power flow is reversed and power is consumed by the rotor (Bose 2002).

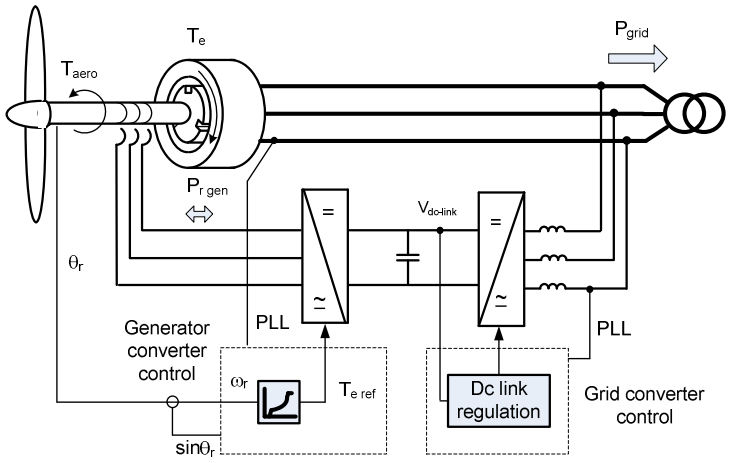

Figure 2.4 – Doubly Fed Induction Generator topology and partitioning of control.

A model of a vector controlled DFIG for use in system frequency studies is derived by A. Mullane & O'Malley (2005) and is shown in Figure 2.5. Electrical torque T_e and magnetizing current i_{qs} (set to zero) are controlled by regulation of q-axis and d-axis rotor currents i_{qr} and i_{dr} respectively. Stator reactive power for the model is set to zero which makes torque solely proportional to the product of the magnetizing flux ψ_{qs} and the rotor d-axis current i_{dr}. The response of the current control loops is adjusted by the proportional and integral gains in the PI controls k_p and k_i respectively. Parameters for the machine are L_s the stator inductance, L_m the mutual inductance and R_r, R_s the rotor and stator resistances. L_α is given by $L_m^2 - L_rL_s$ and k_1 is given by $4L_s/3p_fL_m$ where p_f is the number of machine poles.

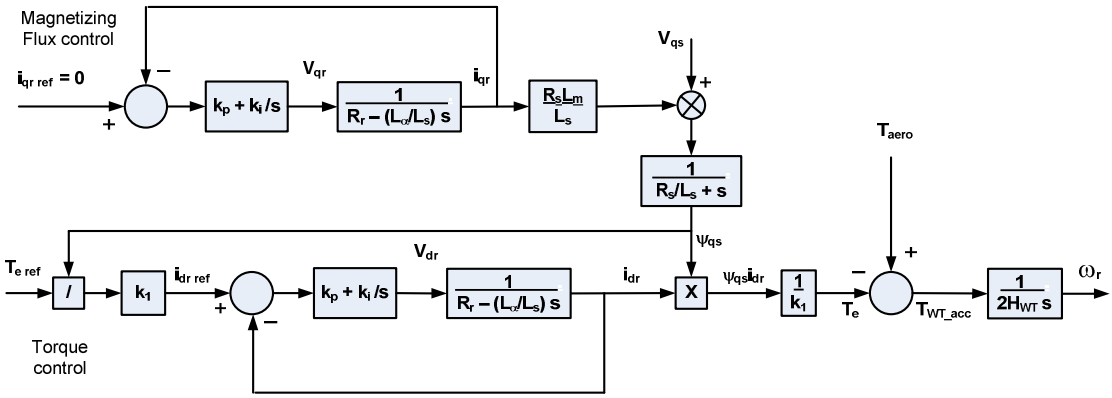

Figure 2.5 – Inertia model for the DFIG (A. Mullane & O'Malley 2005)

Coupling between system frequency and rotor torque occurs through changes in the q-axis stator voltage V_{qs} and the resultant change in the q-axis magnetizing flux ψ_{qs} and therefore torque, given by the product of $\psi_{qs} i_{dr}$.

Using this model Mullane & O'Malley (2005) investigate coupling of DFIG rotor speed to system frequency for a sudden drop in frequency as might occur after a large generation loss. The response obtained from the turbine for different i_{dr} control loop time constants (adjusted by variation of the PI gains) was compared. With a time constant of 0.1 second, no change in turbine torque and speed resulted, hence showing no inertial coupling to exist. With a time constant of 5 seconds the change in rotor speed was shown to be approximately half of that from an equivalent size IG wind turbine (5^{th} order model) and the peak torque approximately a third with a significantly slower rise time.

2.2.3 Full Power Converter (FPC)

The FPC turbine topology, featuring synchronous machine, is illustrated in Figure 2.6. The generator is connected via two voltage source converters connected 'back-to-back' via a dc-link. For a variation on this topology where a diode bridge rectifier replaces the generator converter see Fox et al.(2007).

Generator converter control is similar to that of the DFIG in its regulation of torque, with the exception that stator current is adjusted rather than rotor current. All of the power developed by the generator, $P_{gen,}$ is output via the dc-link. Grid converter operation is again similar to the DFIG with the exception that active power transfer with the FPC topology is always from the generator to the grid. This

power exported to the grid, P_{grid}, is slightly less than P_{gen} due to losses in both converters.

For the FPC topology the vector control reference frame used in the generator converter control, $\sin\theta_r$, is simply obtained from the rotor position θ_r. The grid converter control's vector reference frame is the same as that used with the DFIG i.e obtained via a PLL on the stator voltages.

The de-coupling of rotor speed from system frequency exhibited by the FPC topology is achieved by virtue of the separate control of the converters and the buffering effect of the dc-link capacitor which enables dc-link voltage to remain relatively constant.

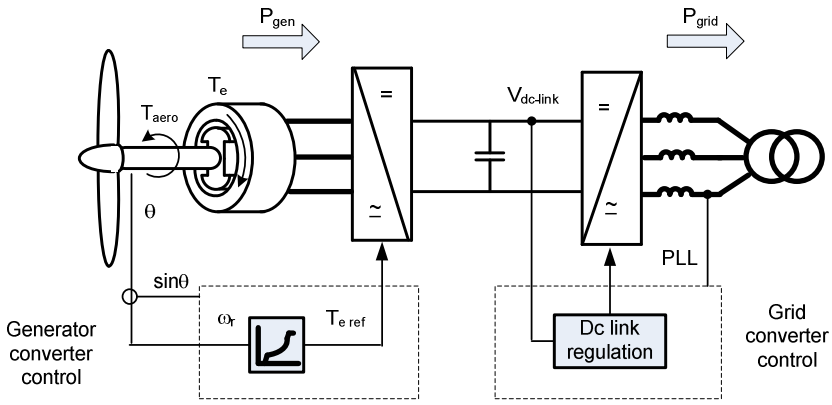

Figure 2.6 – Full Power Converter topology and control partitioning, shown with synchronous machine.

Use of an induction machine instead of synchronous machine results in a similarly de-coupled machine inertia. The principal difference in control of generator torque compared to the synchronous machine is that rotor field position needs to be calculated from rotor position and slip, the latter being firstly calculated from the stator current. Further explanation of vector control of induction machines using the 'indirect' rotor field orientation method mentioned and other methods is given in Novotny & Lipo (1996) and Krause et al.(2002).

A simplified model of an FPC based induction generator wind turbine, with the addition of an inertial response function, is shown in Ekanayake et al. (2008). The model, for use in frequency studies, is shown in Figure 2.7 and represents the torque control implemented by vector control of q-axis stator current i_{qs}; control of flux by

d-axis current is set constant and assumed not to affect the q-axis. Operation on the maximum power extraction curve is achieved by setting the electromagnetic torque reference, $T_{e\,ref}$, equal to the maximum power torque setpoint, T_{Pmax}, with additional torque required to provide inertia response, T_{SI}, introduced at this point. Speed of response of the model's torque control ($T_{e\,ref}$ to T_e) is determined by choice of the current control loop proportional gain k_p. Time constant T_1 and parameter X_2 are derived from machine parameters and L_{rr} and L_m are the rotor self inductance and rotor to stator mutual inductance respectively. The rotating mass of the turbine is represented according to Eq(2.4) where H_{WT} is the inertia constant of the turbine, T_{aero} the aerodynamic torque and T_{WT_acc} the accelerating torque at the turbine.

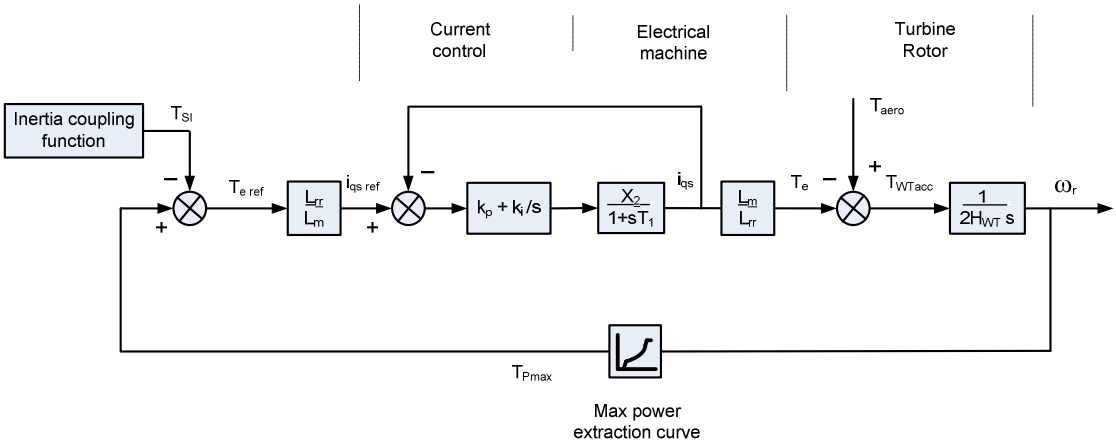

Figure 2.7 – Simplified FPC induction generator wind turbine model for use in frequency studies (Ekanayake et al. 2008)

Comparison of the change in output power between the simplified model and that from a full order machine representation showed "substantial agreement" when inertial response was applied during simulation of system frequency deviation.

2.3 Inertial frequency support methods

Exploitation of stored rotor K.E of the variable speed wind turbine for system frequency support is demonstrated by various authors via essentially two different methods:

- 'Inertia coupling' which attempts to force turbine rotor speed to follow system frequency and restores or increases system inertia, effectively

increasing system damping (Morren et al. 2006), (Lalor et al. 2005), (Kayikci & Milanovic 2009), (Ekanayake et al. 2008), (Conroy & Watson 2008).

- 'Step response' a triggered increase in torque or power to provide an immediate reduction in the system load generation imbalance (Kayikci & Milanovic 2009), (Tarnowski et al. 2009), (Ullah et al. 2008).

The methods are described in the following sections and where appropriate, illustration of their operation uses the model developed in Chapter 6. Note that the constant speed region of the maximum power extraction curve (shown Figure 1.3) is omitted for clarity.

2.3.1 Inertia coupling

Inertia coupling is achieved by applying an accelerating torque to the wind turbine determined by Eq(2.6); the value of the accelerating torque being given by the product of the rate of change of system frequency and double the wind turbine inertia constant H_{WT}. To distinguish synchronous machine accelerating torque T_{acc} Eq(2.1), from the accelerating torque employed to synthesize wind turbine inertia the latter is labeled T_{SI}. Hence for synthesis of inertia :

$$T_{SI} = 2H_{WT}K_c\frac{df}{dt} \qquad (2.11)$$

An increase in the effective size of the wind turbine inertia can be achieved by setting gain K_c above unity. Addition of this inertia coupling 'function' to a DFIG model is shown in Lalor et al. (2005) to provide a change in power output in response to a frequency disturbance similar to that of a synchronously coupled generator (of similar H). Notably a first order filter was applied to the df/dt signal in order to attenuate noise and the model assumed a constant aerodynamic torque and did not include the turbine torque speed control.

To account for attenuation due to the df/dt filter and for scaling of 'coupling' across the possible wide operating speed range, Kayikci & Milanovic (2009) adjust K_c. For frequency deviations of around 1.5 %, simulations demonstrated turbine shaft speed to follow system frequency. These results were obtained by assuming a constant torque setpoint from the torque speed control.

Interaction with maximum power extraction control

Direct summation of the inertia coupling function, Eq(2.11), to the turbine torque speed control is shown in Figure 2.8 where Δf is change in system frequency. Included is representation of the turbine rotating mass and illustration of feedback from rotor speed ω_r. The accelerating torque from the inertia coupling function T_{SI}, is subtracted from the existing torque setpoint T_{Pmax} to give the electrical torque setpoint, $T_{e\ ref}$. A vector control scheme (not shown) will control electromagnetic torque T_e at the machine to match $T_{e\ ref}$. The accelerating torque at the turbine T_{WT_acc}, is given by the electromagnetic torque T_e minus the aerodynamic torque T_{aero}.

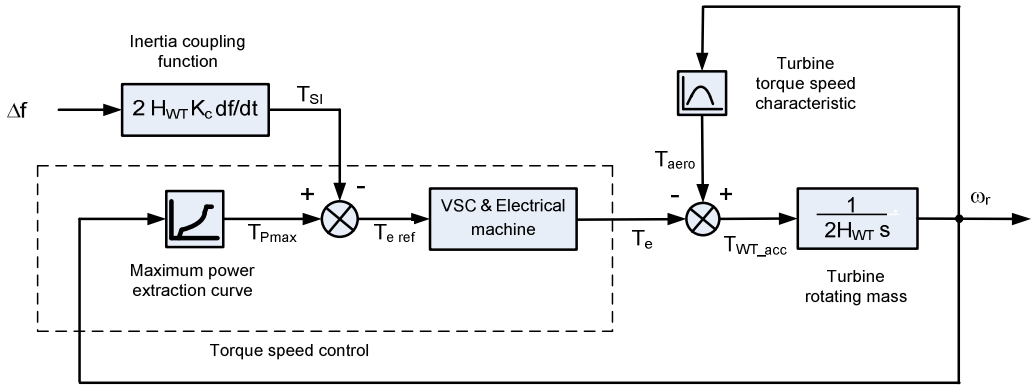

Figure 2.8 - Direct summation of inertia coupling function to turbine torque speed control, turbine rotating mass and feedback from rotor speed.

During a frequency event T_{SI} becomes non-zero and causes rotor speed to change. The values of T_{Pmax} and T_{aero} also depend on rotor speed and changes in these result in T_{WT_acc} no longer being equal T_{SI}. This is more fully illustrated in Figure 2.9 where plot (a) shows the turbine's torque speed curve (magenta), the power curve (blue) and the torque curve , T_{Pmax} (black), corresponding to maximum power extraction. Plot (b), a magnified view, illustrates the application of a step change of accelerating torque T_{SI}, of negative magnitude, as might occur at the beginning of a sudden generation loss. An explanation is given below:

i) At **a**, the turbine is operating at a steady speed determined by the torque speed control shown in Figure 2.8; $T_{e\ ref} = T_{Pmax} = T_{aero}$ and $T_{WT\_acc} = T_{SI} = 0$.

ii) Subtraction of the (negative) accelerating torque T_{SI} from T_{Pmax} results in a step change in $T_{e\ ref}$ from **a** to **b**. At point **b** turbine deceleration torque T_{WT_acc} is equal to T_{SI}.

iii) From **b** onwards, the turbine undergoes deceleration. At **c**, (arbitrarily chosen on the trajectory), the decelerating torque at the turbine is **c – c`** and has reduced in magnitude from in its initial value of T_{SI} due to the increase in aerodynamic torque ΔT_{aero} and the decrease in the maximum power torque setpoint ΔT_{Pmax}.

iv) The turbine decelerates until steady state operation at point **d** is attained. Return of T_{SI} to zero will result in the turbine, by a similar process from i) to iii), but via **e**, returning to steady state operation at point **a**.

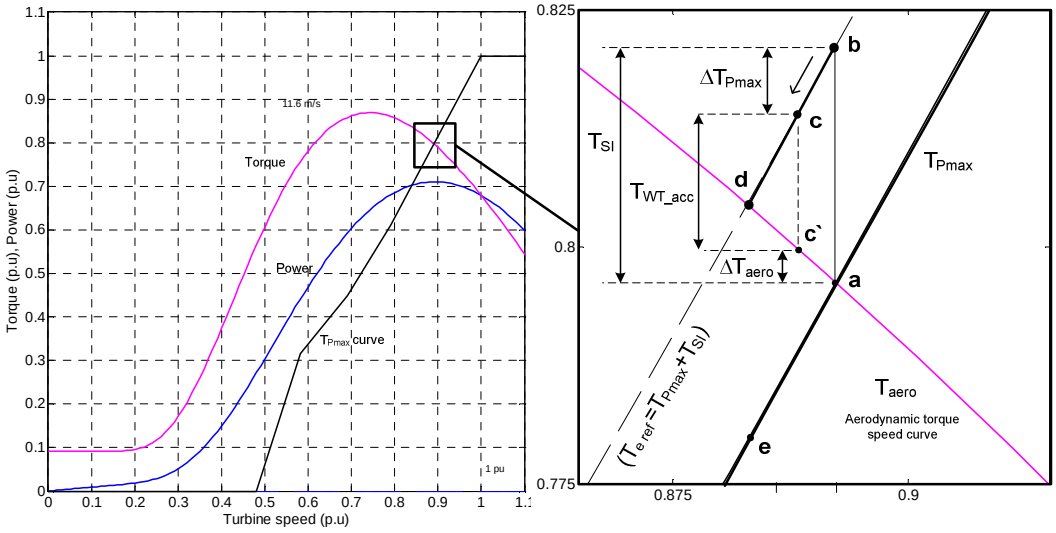

(a) (b)

Figure 2.9 – Reduction in turbine accelerating torque due to speed change for directly summed inertia coupling function. Trajectory of $T_{e\ ref}$ for step change in T_{SI} shown as **abcd**.

From this example it can be seen that with direct summation of the inertia coupling function to the turbine speed control:

- changes in turbine rotor speed reduce the actual accelerating torque.
- summation of a constant value with the torque speed control results in operation of the turbine at a new steady state speed, e.g point **d** (of Figure 2.9), rather than causing a constant acceleration/deceleration as expected.

Illustration of the overall effect on coupling of inertia for an example, step increase with decay to zero of T_{SI}, is shown in Figure 2.10 for an FPC type turbine. The step load generation disturbance occurs at t = 61 sec and no governor response is present. Plot (a) shows the accelerating torque from the inertia coupling function T_{SI}, given by Eq(2.11), and the resulting accelerating torque at the turbine T_{WT_acc}. Plot (b) shows system frequency and (c) rotor speed resulting when using the 'directly summed method' and the required rotor speed for inertia coupling.

Erosion of the accelerating torque due to ΔT_{aero} and ΔT_{Pmax} (shown Figure 2.9), eventually makes the turbine decelerating torque T_{WT_acc}, negative at around t = 67 sec. The turbine then accelerates gradually, returning to its original speed at around t = 120 sec.

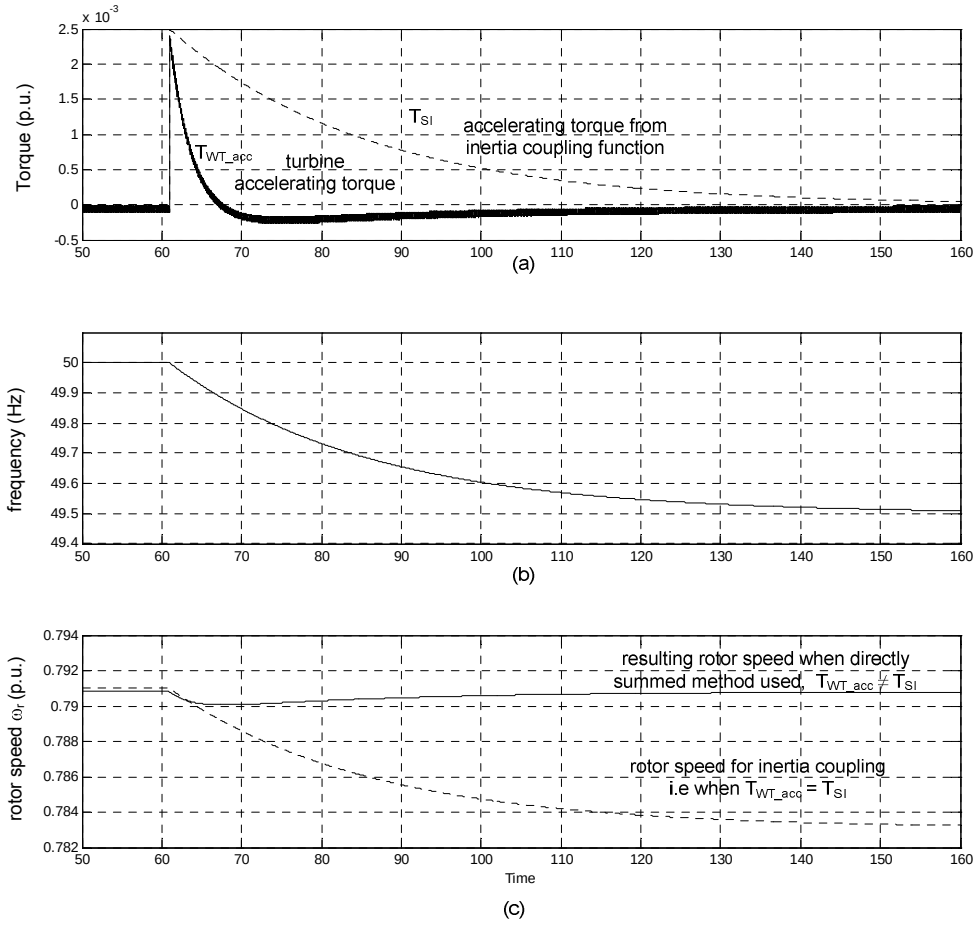

Figure 2.10 - Reduction in turbine accelerating torque due to speed change for directly summed inertia coupling function. Overall effect on coupling of inertia for, step increase with decay to zero, of T_{SI}.

Use of the directly summed method is shown in Ramtharan et al. (2007) and Ekanayake et al. (2008) the latter including an extra differential control term and selection of filter parameters to extend the length of the initial deceleration. Rotor speed is shown to return to its original pre-disturbance speed as df/dt returns to zero, thus returning the turbine to operation at maximum efficiency.

Interaction of the inertia coupling function with the turbine torque speed control, as shown in this section, is highlighted in (Kayikci & Milanovic 2009) but no corrective measures are suggested.

Inertia coupling function with torque compensator

Addition of a compensating control term $K_{T,}$ in proportion to system frequency deviation is shown in Figure 2.11. This acts to cancel out ΔT_{Pmax} and ΔT_{aero} (Figure 2.9) which otherwise decrease the net accelerating torque as rotor speed drops.

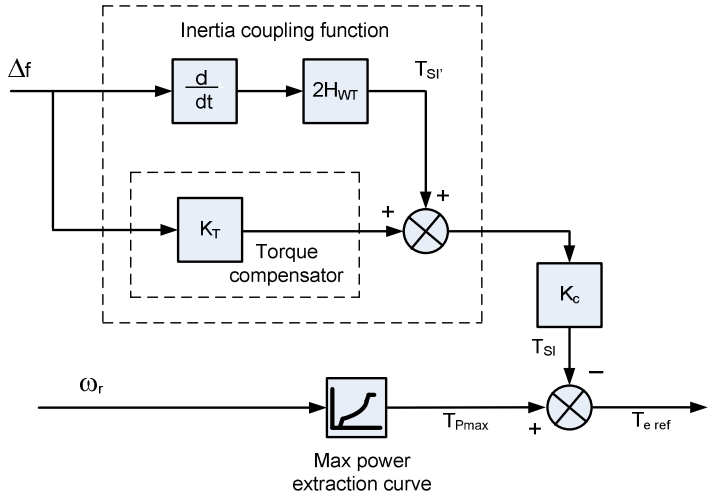

Figure 2.11 – Inertia coupling function with addition of torque compensator.

By suitable choice of gain K_T, the turbine is subject to the desired accelerating torque given by $T_{SI'}$. For large changes in rotor speed this compensator may not be accurate, however it can be seen from Figure 2.9a) & b) that for changes up to 0.1pu in rotor speed, where ΔT_{aero} and ΔT_{Pmax} will be approximately linear functions of speed the compensator will function as intended for the turbine.

The compensatory nature of this additional control term and its facilitation of rotor to system frequency tracking (i.e inertia coupling) is recognized and shown in Ramtharan et al. (2007). Use is also made in Conroy & Watson (2008) where it is

referred to as a ‘droop’ control, similar to that found on conventional generating plant. A side-by-side comparison of the inertial coupling function and a ‘droop’ function (implemented via power rather than torque control) is done in Morren et al. (2006). It could be argued however, that in combination with the inertia coupling function and the turbine torque speed control, the torque compensator and its effect should not be likened to governor droop.

Adjustment of the inertia response is demonstrated in Conroy & Watson (2008). Reduction in magnitude of the output from the df/dt component is shown to reduce the size of the initial output peak. Increasing the relative size of K_T is shown to increase the K.E extracted by reducing the final (steady state) speed of the turbine. Using this latter adjustment, and forcing turbine speed ω_r down from 0.93 to 0.77p.u, a visible drop in final steady state turbine power output occurs. Conroy & Watson (2008) present a scheme for implementing turbine re-acceleration whilst system frequency remains below nominal.

2.3.2 Step response

Step response methods may be classified into those which use a step increase in torque (Kayikci & Milanovic 2009) and those which use a step increase in power, (Ullah et al. 2008), (Tarnowski et al. 2009), in order to implement frequency support.

An instantaneous step is presented in each case by the above authors. This step increase can be maintained according to different strategies as desired. In Ullah et al. (2008) it is maintained for a pre-determined time length, in Kayikci & Milanovic (2009) it is held until a defined point on the maximum power extraction curve is reached and in Tarnowski et al. (2009) is set to end at a lower turbine speed limit.

The step response methods in the cited literature directly control the turbine torque setpoint. Thus their output is independent of interaction with the turbine torque speed control during their operation or from further changes in system frequency after they are initially triggered unlike the inertia coupling functions.

At the end of the support period provided by the step output, a recovery/re-acceleration phase, where the turbine output power is less than the aerodynamic torque, is needed to return the turbine back to maximum operating efficiency and also to restore support capability.

Step torque

A step torque function is illustrated in Figure 2.12. Comparator 1 monitors system frequency, f, and when the trigger frequency f_{trig} is reached, enables the step change in torque output T_{step}. At the same time the sample and hold circuit is activated which keeps the torque setpoint T_{Pmax} constant during the frequency event. Comparator 2 monitors rotor speed ω_r and disables the step output and sample & hold circuit once a desired minimum speed limit ω_{min} is reached.

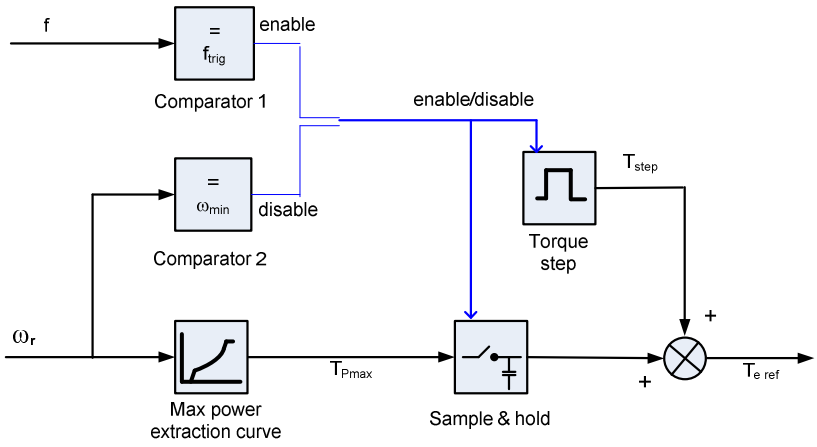

Figure 2.12 – Example of 'Step response' inertial function using torque.

Operation of the function with T_{step} set to 0.1p.u and ω_{min} set to 0.8p.u for the turbine operating at 11.6m/s wind speed is illustrated in Figure 2.13 and is explained below:

i) At point **a** aerodynamic torque T_{aero} is equal to the generator electrical torque setpoint $T_{e\ ref}$ and the turbine is operating at a steady speed; $T_{aero} = T_{e\ ref}$ (= T_{Pmax}).
ii) A generation loss occurs such that the trigger frequency is reached. The step change in output T_{step} is added to the sampled and held value of the existing torque setpoint T_{Pmax} which results in the generator electrical torque setpoint moving from **a** to **b**.
iii) An initial controlled deceleration (of gradually reducing magnitude) occurs from point **b** until point **c** where the minimum speed limit ω_{min} selected for the function is reached.
iv) Reduction of T_{step} to an intermediate magnitude indicated at point **d** will result in steady state operation at this lower speed (Kayikci & Milanovic 2009 use point **e**).

Alternatively reacceleration to the original speed is achieved if T_{step} is returned to zero; reacceleration beginning initially, with $T_{e\ ref}$ located at the intersection of the T_{Pmax} curve and the vertical line **cd** (located off the bottom of the figure).

Note that while the electrical torque setpoint is held constant, **b** to **c**, output power will drop due to operation away from the optimum location on the maximum power extraction curve.

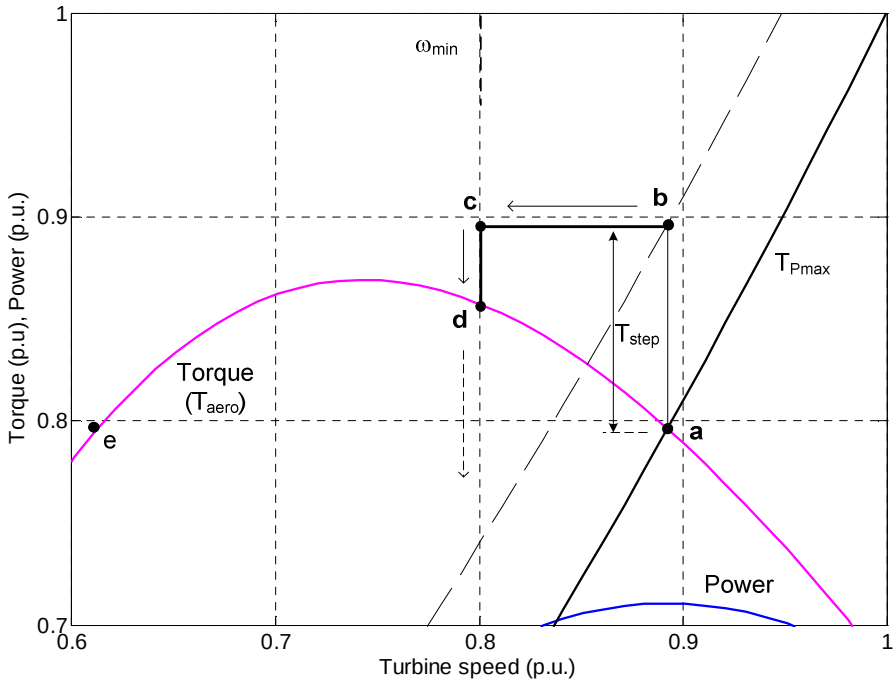

Figure 2.13 – Example operation of torque step method for 0.1pu torque step. Torque speed curve (magenta), power curve (blue) and T_{Pmax} curve (black).

Step power

A step power function is illustrated in Figure 2.14. Similar to the torque step function comparator 1 monitors system frequency, f, and upon reaching a trigger threshold f_{trig}, enables the step change in power. The required torque step, which in fact becomes a ramp as speed changes, is calculated by dividing the desired power step, P_{step}, by the rotor speed ω_r. This equivalent torque is summed with the existing torque setpoint, T_{Pmax}, from the sample and hold circuit. Comparator 2 monitors rotor speed ω_r and disables the step output and sample & hold circuit once a desired minimum speed limit ω_{min} is reached.

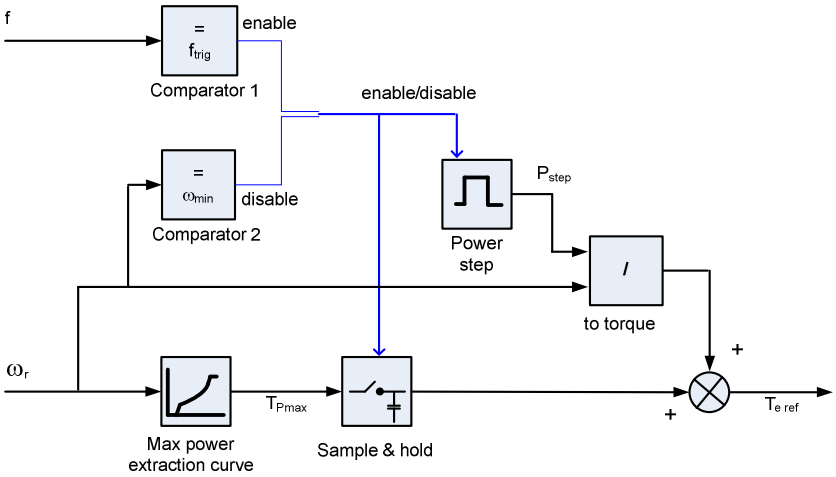

Figure 2.14 - Example of step power inertial function (re-acceleration logic not shown)

Operation of the function with P_{step} set to 0.05p.u and ω_{min} set to 0.8p.u for the turbine operating at a wind speed of 11.6m/s is illustrated in Figure 2.15. Similar to the torque output for the torque step method, shown in Figure 2.13, the power output increases from its pre-disturbance steady state value at **a** to its new value **b** due to the addition of the desired step (0.05 p.u power in this case). A period of controlled deceleration follows, this time of increasing magnitude, until point **c** is reached where ω_r is equal to ω_{min}. Reacceleration of the turbine begins when the power step, P_{step}, is dropped to a value slightly (0.1p.u in this case) below the output power of the turbine, **c** to **d**. As the turbine speeds up this value of P_{step} is increased to maintain constant reacceleration, until at point **e**, the power step is returned to zero and the turbine operates at its original speed and power output. This reacceleration technique/method is used in Tarnowski et al. (2009).

In the Figure, points **A**, **B**, **C**, **D** and **E** are the values of torque corresponding to **a**, **b**, **c**, **d** and **e**.

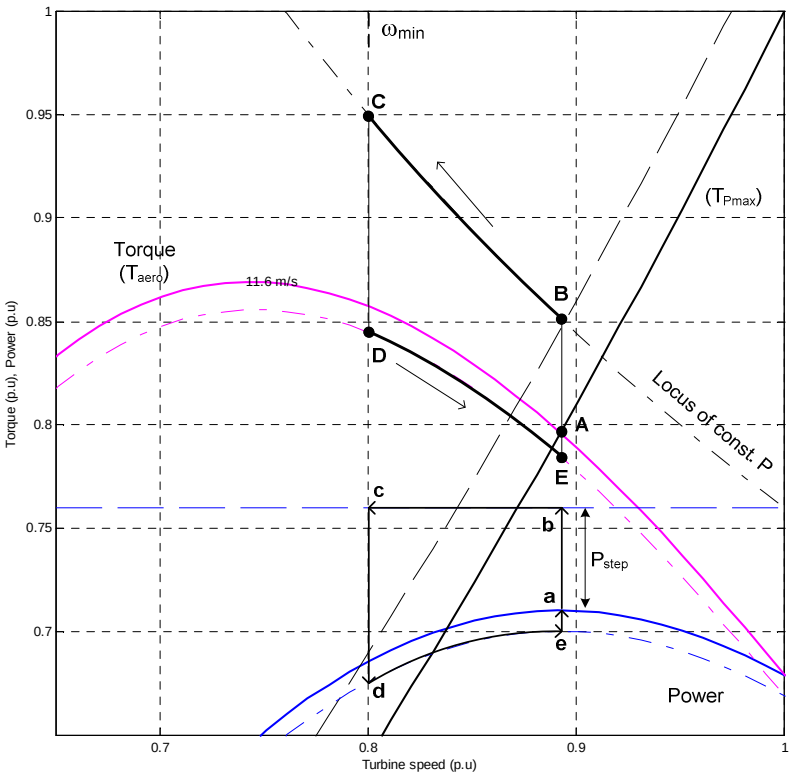

Figure 2.15 – Example operation of step power method for 0.05p.u power step. Torque speed curve (magenta), power curve (blue) and T_{Pmax} curve (black).

Turbine support capability

Kayikci & Milanovic (2009), Tarnowski et al. (2009) and Ullah et al. (2008) present the step method as a means of extracting the maximum possible amount of K.E from the wind turbine and achieve this by selecting a minimum rotor speed limit as low as possible. The maximum duration of a 0.05p.u power step is shown in Table 2.2 for various wind speeds.

In Ullah et al. (2008) a turbine based on the GE 3.6MW DFIG model (Miller et al. 2003) is used this having an inertia constant of 5.19 seconds. A minimum speed limit of 0.7p.u was chosen. Power step times of 28 and 61 seconds are obtained for wind speeds of 7.5 and 10.1 m/s respectively. For higher than 10.5 m/s and up to rated wind speed, support duration starts reducing being 53 seconds at 10.5m/s and only 45 seconds at the 11.2m/s wind speed.

Tarnowski et al. (2009) assesses support duration capability of the step power function method to vary between 7.5 seconds at 7.5m/s wind speed up to a maximum of 34 seconds at 11 m/s. Reduction in support duration, due to operation in the constant speed region of the maximum power extraction curve, begins near

this point with the support duration at 12m/s (rated wind speed) being only 26 seconds.

Table 2.2 – Support duration capability of the step power method with 0.05p.u step (Ullah et al. 2008) and (Tarnowski et al. 2009).

Wind speed (m/s)	**Support duration (sec) Ullah / Tarnowski**	**Comment**
7.5	28 / 7.5	
10.1	61 / --	start of constant speed region[7] / --
10.5	53 / --	
11.0	-- / 34	
11.2	45 / --	rated wind speed / --
12.0	-- / 26	-- / rated wind speed

Regarding overall operation of the step power function, (Tarnowski et al. 2009) investigates tradeoffs between re-acceleration power, length of recovery and lost energy. For slow re-acceleration, the net power lost due to operating away from the maximum turbine efficiency is larger. For higher wind speeds support duration is longer and again net energy loss is larger. Ullah et al. (2008) investigates the sensitivity of support duration to the shape of the C_p curve and as might be expected a flatter C_p curve gave a longer support time.

2.3.3 System frequency support performance

Measures of frequency support performance are illustrated using the frequency profile in Figure 2.16 for an example a load generation imbalance. Steady state response of the system is indicated by the settling frequency. Typically for large disturbances a transient component of response will occur and can be quantified by the minimum frequency and the 'overshoot' which is the magnitude of the frequency deviation beyond the steady state value.

[7] The operating range of a variable speed turbine is divided into regions as explained in section 1.2.3.

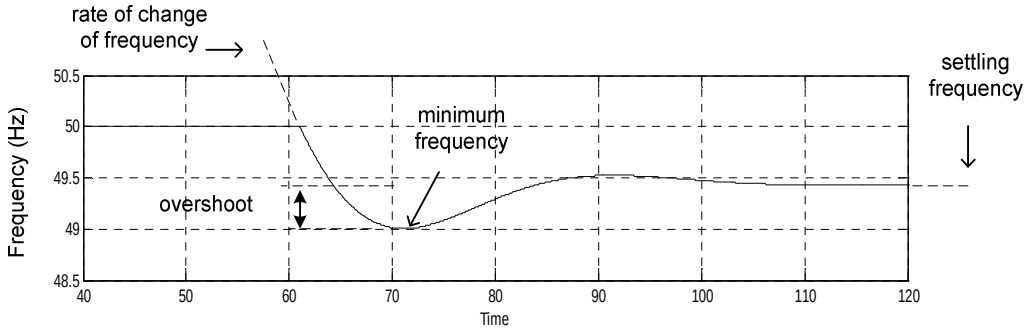

Figure 2.16 – Frequency profile during a step load generation imbalance showing measures of performance

The detrimental effect on system frequency due to introduction of wind plant and remediation by wind turbine inertia response is shown in Lalor et al. (2005). FSIG response and DFIG response with and without inertia coupling is modelled for the Irish power system, peak capacity 6100MW. For the minimum summer demand with 2GW of DFIG based turbines operating, and using an in-feed loss of 422MW, results show a higher rate of change of frequency (0.44 increased to 0.69Hz) and a lower minimum frequency (49.4 decreased to 49.3Hz). Application of the inertia coupling function to the DFIG turbines restores rate of change of frequency to within statutory limits (0.5Hz/sec) and the minimum frequency to a similar value to the no wind turbine case. For the case of FSIG based wind turbines, rate of change of frequency increases to a similar extent as with the 'inertia-less' DFIG turbines but minimum frequency remains unaffected.

Comparison of the inertia coupling method (without torque compensator) and the step torque method set for maximum power extraction is given in Kayikci & Milanovic (2009). The power system modeled consists of a single 8MVA diesel generator in combination with a 1.5MW DFIG turbine. In this example, operation of the DFIG does not degrade system performance by displacing inertia as may happen in larger systems. Inertial response is used to provide an improvement in system frequency response performance compared to the no wind turbine case. Improvement in rate of change of frequency and the minimum frequency is shown to occur for both the inertia coupling method and the step torque method, for the latter a near 50% reduction in the minimum frequency is obtained. Although the step method substantially improves the minimum frequency, the method has the effect of

prolonging recovery of frequency to the steady state value as compared to the case of no support or support via inertial coupling.

Frequency support performance is demonstrated for the inertia coupling function with torque compensator in Conroy & Watson (2008), the gain K_T (Figure 2.11) being set high enough to provide rotor speed to system frequency coupling greater than unity. The system modelled consists of a 120MW FPC based wind farm, six synchronous generators totaling 320MW and sudden loss of one unit as the load generation imbalance. Clamping of maximum output from the inertia coupling function results in a step increase in output from the turbine similar in profile to the torque step method used in Kayikci & Milanovic (2009). Displacement of system inertia by the wind turbines causes an increase in rate of change of frequency and a drop of the minimum frequency of approximately an extra 1/3rd compared to the case without the wind farm. Application of the turbine inertia support results in a minimum frequency similar to the case without the wind farm. The turbine model included a two mass representation of the drivetrain which showed large oscillations (magnitude 10%) on application of the step increase in torque.

Application of the step power function to a hydro dominated system is demonstrated in Ullah et al. (2008) and is proposed in order to help mediate the negative power surge characteristic of hydraulic turbines (Kundur 1994) which limits their effective response after a frequency event. Simulation of a large generation loss of 0.1p.u showed a very large overshoot with a minimum frequency of 48Hz and a maximum rate of change of frequency of 1Hz/sec. Addition of DFIG wind generation at 20% penetration lowers the minimum frequency. Application of the step function returns a 0.5Hz improvement in the minimum frequency compared to the case of DFIG turbine with no inertia. A large temporary frequency drop of 0.5Hz is shown to occur 10 seconds after the initial disturbance, this being due to re-acceleration of the turbine.

2.4 Grid code requirements

2.4.1 Overview

All transmission system operators have specific technical requirements, sometimes referred to as grid codes, which any connected generator must adhere to. This helps facilitate safe, efficient and economical operation of the electrical transmission system. The grid codes typically state the following requirements:

- Voltage and frequency ranges
- Active power frequency response
- Reactive power and voltage control
- Fault ride through (including fast acting voltage control)
- Islanding, black start and other ancillary services.
- Data communication and documentation (including simulation models)
- Capability testing and voltage quality
- Operational procedures and division of responsibilities

Scope

Only active power frequency response and frequency ranges are reviewed here and where present or proposals exist, synthetic inertia. The grid codes chosen, listed in Table 2.3, pertain to generators or groups of generators connected to the transmission system and are chiefly those from Western European countries which have a large quantity of wind capacity integrated and hence specific requirements for connection of wind plant exist. For the UK and Germany (Central Corridor) the complete grid codes are reviewed, for the other countries only grid code annexes relating to wind farms are reviewed.

The new European generator grid connection code is also included which has been published in draft by the 'Network of Transmission System Operators for Electricity' (entso-e). This generic grid code is an attempt to harmonise standards as part of efforts to improve cross-border electricity trading and market access across the European Union. A wider review of grid code technical requirements relevant to wind integration is given in Moore (2011).

Table 2.3 – Grid code documents reviewed for active power frequency response and frequency range

Company / Country	Document Reviewed	Issue & Date
National Grid / UK	The Grid Code, balancing code and connection code sections (National Grid 2010b)	Issue 4 Rev 5, 31/12/2010
EON-Netz / Germany (Central Corridor)	Grid Code – High and extra high voltage (EON-Netz 2006) Requirements for Offshore Grid Connections in the E.ON Netz Network (EON-Netz 2008)	Status 1, 04/2006 1/04/2008
Eltra / Western Denmark	Wind Turbines Connected to Grids with Voltages above 100 kV(EON-Netz 2008)	3/12/2004
EIR / Ireland	Controllable Wind Farm Power Station Grid Code – WFPS1 (EirGrid 2009)	30/01/2009
entso-e / Europe	Requirements for Grid Connection Applicable to all Generators (Entso-e 2010)	Working Draft, 19/08/2010
Hydro-Quebec / Canada	Technical requirements for connection of power plants to the transmission system, 14.4 , inertial response (Hydro - Quebec 2009)	02/2009

Terminology

Standard terminology across the grid codes does not exist hence to preserve intended meaning, terminology from the original grid codes where appropriate is indicated in single quotation marks ‘thus’. Longer quotations from the relevant grid codes, appear in double quotation marks “thus”.

2.4.2 Frequency response

All large generating plant, and groups of smaller generators (such as wind farms), are normally required to have capability to participate in frequency control by supplying an increase in power if frequency drops below and a decrease in power if frequency increases above a nominal frequency. This is achieved by operation at less than maximum available output in order to provide ability to regulate power production upwards. Generators which do not operate to provide this governor type response will normally still need to provide a high frequency response where active power is gradually reduced above a certain frequency. During low frequency no increase in active power is required, in fact an allowed reduction in power is specified to account for technology dependant characteristics (see 2.1.4) of output power verses frequency for certain types of plant.

National Grid

For the UK grid, generating plant above 50MW in size including dc converter and Power Park Modules[8] "must be fitted with a fast acting proportional frequency control device (or turbine speed governor) and unit load controller or equivalent control device to provide frequency response". Frequency ranges for 'plant and apparatus' requires continuous operation between 47.5 and 52 Hz and operation for a period of at least 20 seconds between 47.5 and 47.0 Hz after which they may disconnect. The frequency control device (or speed governor) is required to be operated and designed to a European specification or commonly used European standard and have a droop of between 3 and 5% and deadband of ±15mHz.

Control of frequency via this plant is achieved by instruction to operate in either one of two modes:

'Frequency Sensitive Mode (FSM)' - This mode provides the primary and secondary response for negative frequency excursions as illustrated in Figure 2.2. Generators in this mode must also have capability to provide 'high frequency' response. The minimum required responses for FSM are shown in Figure 2.17. The rate of change of output for high frequency response is set by an ancillary service agreement with National Grid.

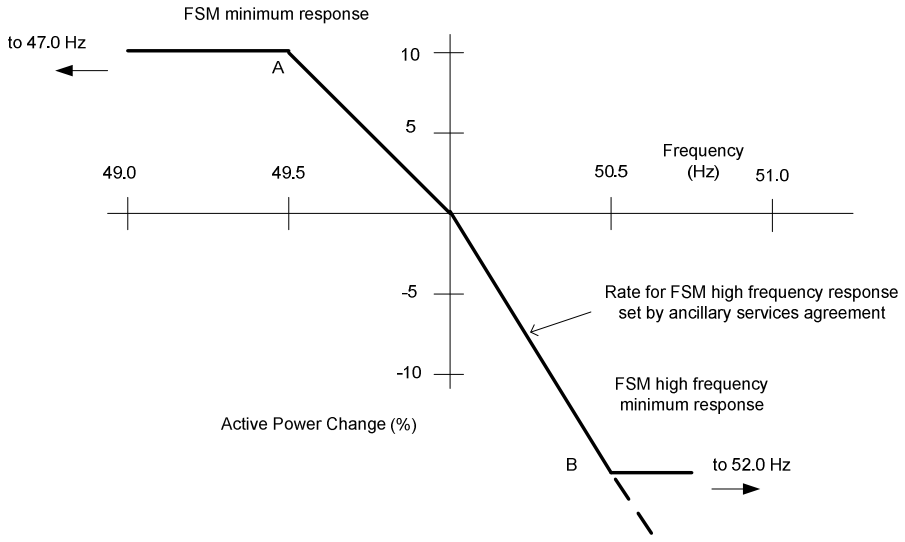

Figure 2.17 – National Grid primary/secondary and high frequency response active power verses frequency requirements for plant operating in Frequency Sensitive Mode (FSM).

[8] A power park module is a collection of generators, powered by an intermittent source, which utilise a common connection point (National Grid 2010b).

For the low frequency response the effective ‘droop’ in the proportional band between point A and 50Hz is:

Droop (%) = 100% x (p.u change in freq)/(p.u change in power)

= 100% x (0.5/50) / (0.1) = 10 %

‘Limited Frequency Sensitive Mode (LFSM)’ - This mode has high frequency response capability only, the minimum required response and the required maintenance of active power during low frequency within this mode is shown in Figure 2.18. Generators should maintain normal active power between 49.5 and 50.4Hz. Above this a proportional high frequency response of 2% change in output per 0.1Hz deviation above 50.4Hz is required (equivalent to 10% droop). Below 49.5Hz proportional reduction of active power output is allowed up to a maximum of 5% at 47.0Hz (equivalent droop of -100%). For Combined Cycle Gas Turbines disconnection is allowed if frequency remains below 48.8Hz for more than 5 minutes. Some types of plant such as “existing gas cooled reactor plant” are exempt from FSM capability and operate only in LFSM.

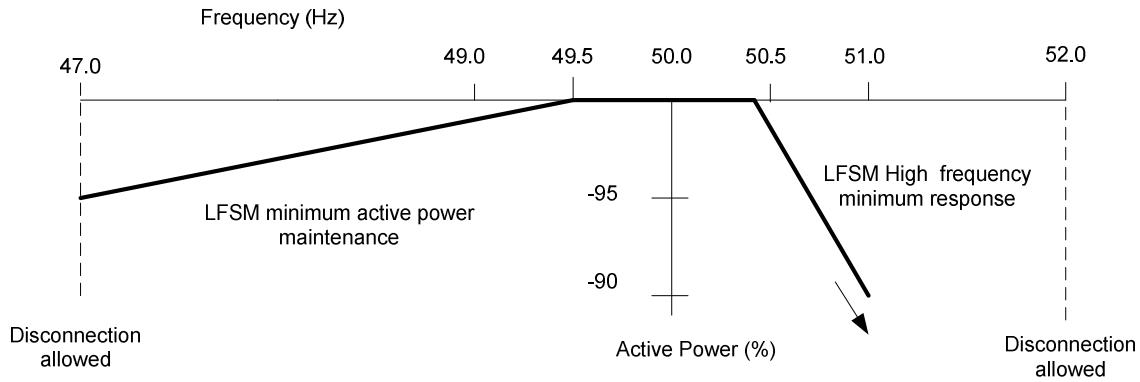

Figure 2.18 – National Grid requirements for high frequency response and maintenance of active power during low frequency for plant operating in LFSM.

Reduction of required response capability due to plant loading for primary/secondary and high frequency response is shown in Figure 2.19. The figure corresponds to operation at point A or B on Figure 2.17. For low frequency (i.e primary/secondary) response the full minimum increase in output (10% of registered capacity) is required between 55 and 80% loading with a proportional reduction allowed until loading reaches 100%. For high frequency response the full reduction in response (set in ancillary service agreement) is required at loadings between 70 and 95%. Generators must have a high frequency response capability when operating at the minimum generation level (65%), this capability being indicated by a requirement to operate down to the Designed Minimum Operating Limit (DMOL) at 55% (or if feasible below).

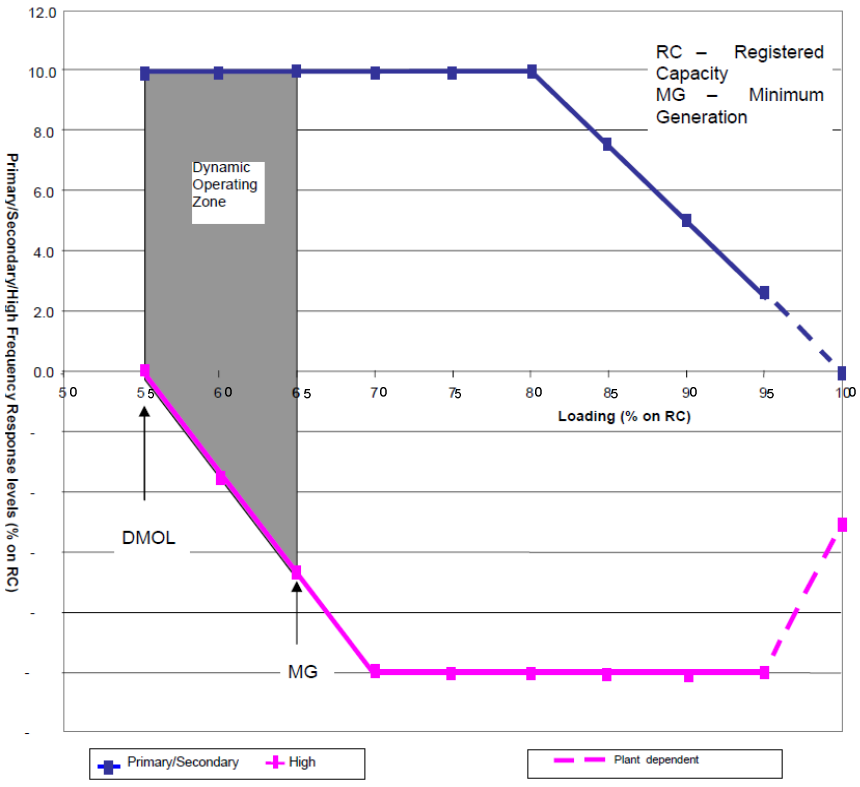

Figure 2.19 – National Grid generator frequency response verses loading for 0.5Hz deviation (National Grid 2010b)

Delivery of the active power increase for low frequency response is shown in Figure 2.20. It is required that “output should be released increasingly with time over the period of 0 to 10 seconds from the time of the start of the frequency fall.” Capability for reactivation of the response is required within 20 minutes. Figure 2.20 also shows the method of testing of frequency response by injection of a test frequency (upper plot) and the measurement of response delivered. For primary response this is the minimum sustained increase in output over the 10 to 30 second time period (in this case point P) and for secondary response the minimum sustained increase in output over the 30 second to 30 minute time period (point S).

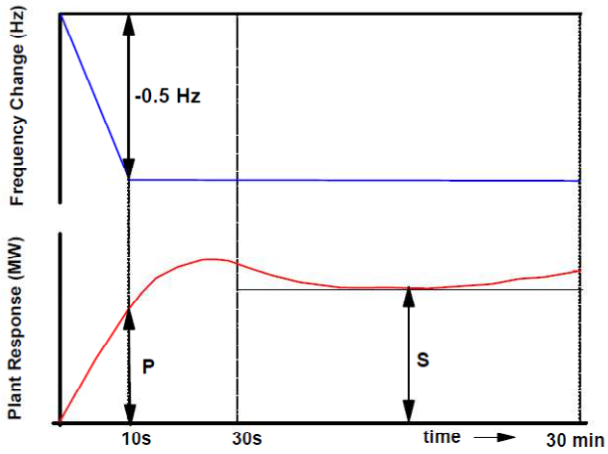

Figure 2.20 – National Grid primary/secondary response. Measurement (lower) and frequency injection test stimulus (upper) (National Grid 2010b)

EON-Netz

Frequency response capability is required from all generators above 100MW, this response capability being termed ‘primary control’ (see 2.1.3). Continuous operation of generating plant is required between 49.0 and 50.5Hz. Operation outside these limits, down to 47.5 and up to 51.5Hz, is required but only for between 30 and 10 minutes whereafter they may disconnect. Offshore wind generators have an extended short term operating region for 10 seconds duration between 46.5 and 47.5Hz and between 51.5 and 53.5Hz.

Governor droop is specified as adjustable with a deadband of less than ±10mHz. The active power range capability must be a minimum of ±2% of rated power and the response delivered must be activated within 30 seconds and supplied for a

minimum of 15 minutes. Reactivation capability is required within 15 minutes of return to nominal frequency.

Minimum requirements for ‘overfrequency’ are a reduction in active power at rate of 5% droop beginning at 50.5Hz. For onshore generators which are subsidized via the German ‘Renewable Energy Act’ the reduction in frequency begins at 50.2Hz. For offshore wind generators the droop is 2% and the threshold frequency 50.1Hz.

For ‘underfrequency’ minimum requirements are that active power must remain constant down to 49.5Hz and below this not drop below an equivalent droop of -10%. The EON grid code in addition to including a diagram similar to Figure 2.18 includes specification for maintenance of active power during a short-term frequency event. This is reproduced in Figure 2.21 and specifies that no change in active power is allowed above the thick red line shown.

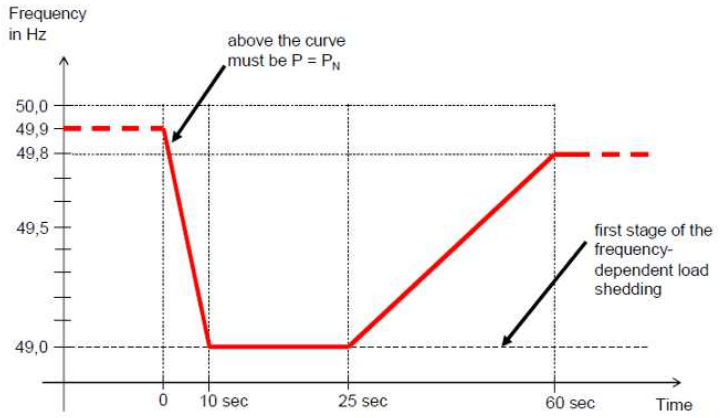

Figure 2.21 – EON active power maintenance requirement for short term frequency deviation (EON-Netz 2006)

entso-e

The European draft code requires ‘active power frequency response’ capability from all generators (synchronous and non-synchronous) according to Figure 2.22 where power is indicated on the y-axis and frequency on the x-axis. Generators operating in ‘frequency sensitive mode’ are required to operate according to droop characteristics 1 and 2 (thick red line).

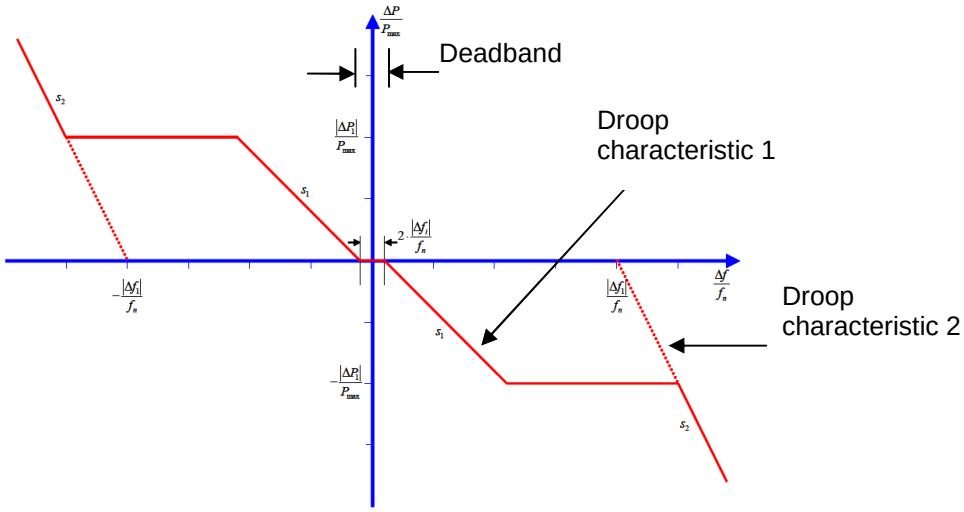

Figure 2.22 – entso-e ‘frequency sensitive mode’ and ‘limited frequency sensitive mode’ active power verses frequency requirements (Entso-e 2010)

When not operating in this mode generators should operate in ‘limited frequency sensitive mode’ where they are only required to change active power according to droop characteristic 2 (thick and dotted thin part of red line). Ranges of active power, deadband, and minimum response times are also specified.

Eltra

Continuous operation of wind turbines are required between 49.5 and 50.5Hz. Outside these limits, reductions in power are possible, disconnection is allowed at 47.5 and 53.0Hz.

All wind turbines are required to have ‘automatic frequency regulation’ capability and similar to the entso-e grid code a frequency verses active power diagram is included (see Figure 2.22). Droop and deadband are specified as adjustable and active power range is required to be variable between 20 and 100%. Delivery of response must be adjustable between 1 and 10% of rated power per second.

EIR

Frequency range requirements dictate that wind farms must operate at normal output between 49.5 and 50.5Hz. Either side of this central band they must remain connected for 60 minutes or for 20 seconds if between 47.0 and 47.5Hz.

A ‘frequency response system’ is specified for wind farms above 5MW and 10MW in size. Similar to the entso-e grid code a frequency verses active power

diagram is included to illustrate the requirements. For wind farms between 5 and 10MW, high frequency response capability is required and for low frequency, active power is required to be maintained at 100% of that available. For wind farms greater than 10MW low and high frequency response is required. Values for droop and deadband where applicable are specified in agreement with EIR. The response rate of each turbine is required to be a minimum of 1% of rated capacity per second.

2.4.3 Synthetic inertia requirements

Specification of inertial response from non-synchronous generators appears in the Canadian grid code and the draft generator requirements published for consultation by entso-e.

Hydro-Quebec

An 'inertial response' from wind turbines is required to act during 'major frequency deviations' in order to help restore system frequency :

> "To achieve this, the (frequency control) system must reduce large, short-duration frequency deviations at least as does the inertial response of a conventional synchronous generator whose inertia (H) equals 3.5s. This target performance is met, for instance, when the system varies the real power dynamically and rapidly by at least 5% for about 10 s when a large, short-duration frequency deviation occurs on the power system."

entso-e

An active power response, from Power Park Modules (PPM[9]), above an agreed size, is required of the form shown in Figure 2.23 "in order to limit the rate of change of frequency following a sudden generation loss". Full delivery must occur within 200ms and "the initial injected active power supplied to the network shall be in proportion to the rate of change of network frequency". The transmission system operator is required to define the support duration period where the response (now exponentially declining) must remain of a positive magnitude and similarly define a suitable recovery period.

[9] Power Park Modules are "Multiple interconnected Generating Units which are not synchronous and have a common [Point of Common Connection] to the Network" (Entso-e 2010).

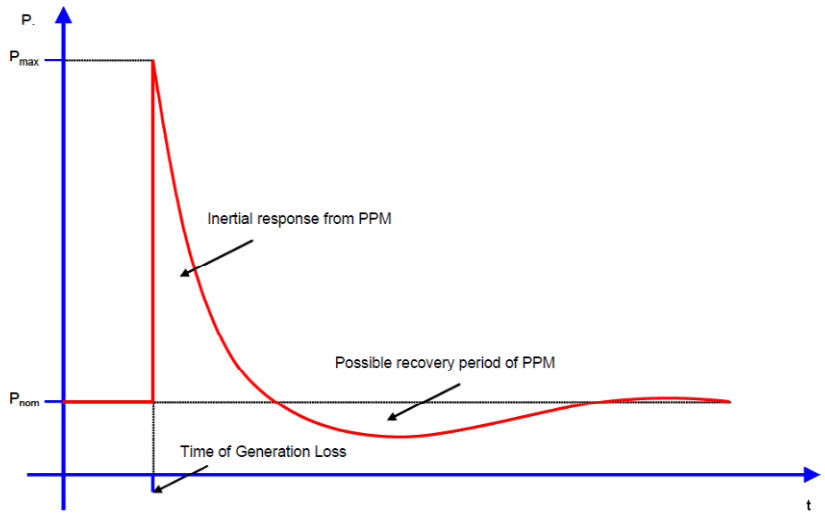

Figure 2.23 – entso-e non-synchronous inertial response (Entso-e 2010)

This synthetic inertial capability must operate when the plant is in Limited Frequency Sensitivity mode (see 2.4.2 entso-e). Operation in combination with active power response during frequency sensitive mode is desirable but not compulsory. The control system which provides the synthetic inertia must have an adjustable rate of change of frequency deadband and a method to "limit the bandwidth of the output" to remove the possibility of exciting torsional oscillations in other generating plant.

2.5 Discussion

Response from generators over various time frames makes up the principal method of regulating frequency for an electrical power system. For the UK system, response from generators is sufficiently important for the service to be divided into two distinct periods. This is in contrast to larger power systems such as those in mainland Europe. System inertia is principally held in large rotating generators and their attached machinery such as steam turbines. During a frequency disturbance K.E is exchanged between these large rotating masses and the electrical system. This additional exchange of power from a synchronous machine during a disturbance acts to slow down the change in system frequency and is proportional to the rate of change of frequency.

This inertia response is instantaneous and is currently provided by default due to large synchronous generators being predominant on the system. However inertia

response is not currently provided by variable speed wind turbine topologies and is also not a part of commercial balancing services.

Inertia coupling properties of wind turbine generators

Field based measurement and modelling of the FSIG turbine shows an inertial response to occur with this topology. The response is fundamentally related to slip velocity rather than rotor angle as is the case of the synchronous machine and thus a slightly lower peak power output is to be expected. Rotor speed change and K.E exchange when frequency changes, from one steady state value to another steady state value, will be close to that from a similarly sized synchronous machine. Contradiction in FSIG response between models by (Lalor et al. 2005) and (Littler et al. 2005) indicate that use of higher order machine models may be appropriate. A general review of the inaccuracies of reduced order induction models is given in Thiringer & Luomi (2001).

The de-coupling of the DFIG topology is due to separate excitation of rotor current via an electronic power converter. The speed of the control loop is shown to affect the extent of the de-coupling (A. Mullane & O'Malley 2005). However it might be argued that requirements for reactive power regulation for grid code compliance and control of turbine torque for avoidance of resonance will demand fast control of real and reactive current. Hence coupling between torque and system frequency, to any significant degree, will not be present in a typical DFIG turbine.

The FPC turbine conversely shows clear de-coupling courtesy of its topology. A simplified model of an FPC turbine equipped with induction generator, suitable for use in system frequency studies, demonstrates the 'synthesis' of an inertia response by addition of a function to the torque speed control loop (Ekanayake et al. 2008).

Inertial frequency support methods

Two distinct methods were found in the literature. Firstly, the inertia coupling method, which produces a response essentially similar to that from a synchronous machine, Eq(2.6). Direct summation of the inertia coupling function, Eq(2.11), with the torque speed control loop, however, does not provide the expected coupling of torque to frequency. This was illustrated to be due to change in turbine aerodynamic torque and change in the torque setpoint from the torque speed control loop. Inclusion of an additional control signal in proportion to frequency deviation is used

by a number of authors to provide the necessary compensation for synchronous-like coupling. The ability to achieve a higher torque and thus speed change, to extract extra energy from the turbine by adjustment of the inertia coupling function was also demonstrated (Conroy & Watson 2008).

The second distinct method was that using a step increase in output of either torque or power. Significantly the step methods both control turbine torque directly and independently of system frequency apart from their initial triggering at a frequency threshold. The step methods are typically presented configured for maximum possible K.E extraction. Due to the large change in rotor speed when configured as such, a distinct reacceleration of the turbine is implemented at a suitable point after the initial frequency deviation. As an example of the support capability for the turbines modelled, using a 0.05pu power increase, duration of support was shown to vary from 7.5sec at low wind speed up to 61sec at high wind speed.

The regulation of system frequency following a load generation disturbance can be assessed by the value of minimum frequency reached, the ensuing steady state value of frequency and the rate of change of frequency. Modelling of the Irish system (Lalor et al. 2005), a single diesel generator (Kayikci & Milanovic 2009) and a small multi-generator system (Conroy & Watson 2008) illustrate how introduction of variable speed wind turbines can deteriorate frequency regulation and additionally how the inertia support methods, inertia coupling and step torque can restore or improve performance.

The step method was shown to be particularly helpful when applied to a hydro dominated power system; the capability to supply a large quantity of energy in the first few seconds of a load generation imbalance to counteract slow initial response from hydro governors.

Grid codes

Two complete grid codes, that of the UK's National Grid company and E-ON's network code in Germany were reviewed for requirements of frequency response and frequency ranges. The review additionally included annexes relating to the connection of wind generators for two other European countries and a draft European grid code which is part of moves to standardize grid codes in Europe.

Basic requirements for frequency response capability apply according to the size of power generating station whether this be a single large synchronous unit or a collection of smaller non-synchronised generators which form a ‘power park’ (National Grid and entso-e term). Capability to be instructed to operate in one of either two modes is commonly required. The first is a fully responsive mode (e.g Figure 2.17) where a governor action provides appropriate variation in active power as frequency changes. The second is a mode which has no active power increase requirement as frequency drops but retains a ‘high frequency’ response where active power is reduced as frequency rises (e.g Figure 2.18). A noticeable difference between the National Grid code and the E-ON code is the level of detail, the National Grid code including requirements for minimum increase/decrease in output at different loadings and detail of the measurement of delivery of response.

Regarding range of frequency for operation, the capability for wind turbines to remain connected over a wider frequency range than conventional generating stations is indicated in short term requirements to operate down to 46.5 and up to 53.5Hz in the EON offshore connections code.

Inertia response from wind turbines is a requirement in the current grid code of the Canadian Hydro-Quebec company, the power system being 42GW in size and consisting of mainly hydro-electric generating stations. The inertia response required approximates to the step function as described in 2.3.2. As mentioned above this type of system benefits from a step type inertia response. Insight into the draughting of this requirement is given in (Brisebois et al. 2011). The European entso-e draft code in contrast specifies an inertial response similar to that which occurs from synchronous generators; an increase in power in proportion to the rate of change of frequency, rapidly delivered and having a (typically) exponential declining profile (Figure 2.23). This required response is clearly identifiable with the inertia coupling function described in 2.3.1.

2.6 Conclusion

Review of published literature including generator connection requirements from system operators shows the following:

- The inherent inertia response provided by large synchronous machines is not present by default in variable speed wind turbines; the FSIG turbine provides a form of inertia response, the DFIG exhibits torque to frequency coupling which is eliminated via suitable control of its rotor power converter and the FPC turbine is inherently decoupled.
- Synthesis of an inertia response can be achieved via addition of a suitable function added to a variable speed turbine's torque speed control loop.
- Two basic methods are to be found in the published literature. Firstly inertia coupling which provides a response similar to synchronous machines i.e in proportion to rate of change of system frequency. Secondly a step method which controls turbine output directly and can be used to extract maximum K.E from the turbine.
- Remediation and improvement of system frequency is demonstrable through modeling of system response using turbines equipped with inertia response. A simplified model of the DFIG and the FPC induction generator based turbine has been published.
- Introduction of inertial response requirements for the UK will be of particular significance, due to the existing high importance of UK frequency response services compared to mainland Europe.

To further investigate the provision of wind turbine inertia response, for the UK mainland system, the following work is undertaken:

- Development of a simplified model of the FPC turbine equipped with synchronous machine (Chapter 3).
- Evaluation of use of the two basic inertia response methods in conjunction with a frequency model of the UK system (Chapter 5).
- Experimental testing of an inertia coupling function (Chapter 6).

3 Synchronous machine modelling and vector control

3.1 Introduction

Chapter 2 identified the need to model the synchronous machine based Full Power Converter wind turbine. A basic outline of synchronous machine theory is given along with the fundamental principles of vector control applied to the synchronous machine. A first order simplified model of the synchronous machine is derived for use in the wind turbine model of Chapter 5.

3.1.1 Rotating reference frame

Figure 3.1 shows the orientation of rotor and armature[10] magnetic fields for a 2-pole, 3-phase synchronous machine and the location of the three phase windings, aa`, bb` and cc`.

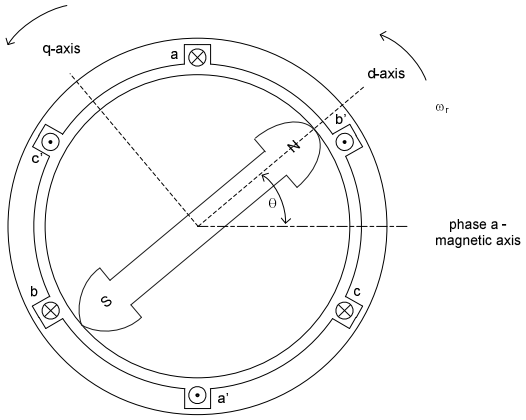

Figure 3.1 – Orientation of stator and rotor fields for a (2 pole) 3-phase synchronous machine and location of rotating dq reference frame (Kundur 1994).

Flow of 3-phase sinusoidal currents in the stator will result in a (net) rotating stator field of constant magnitude and rotation of the rotor in synchronism with this (net) field. Stator and rotor quantities can be referred to a rotating reference frame located along the magnetic axis of the rotor. This rotating reference frame is indicated in Figure 3.1 by the (direct) d-axis, and an orthogonal (quadrature) q-axis which leads the d-axis by 90 degrees. The speed of rotation of the reference frame is the same as

[10] For 3-phase rotating machines *armature* is used synonymously with *stator*, where the second indicates the armature is non-rotating. This is in contrast to brushed dc machines where the main current (non-field) winding is wound on the rotor.

the rotor speed ω_r. The position of the d-axis ahead of the stationary magnetic axis of phase a is indicated by θ.

Conversion of quantities in the stationary reference frame to those in the rotating reference frame is achieved by use of Eq(3.1) to (3.3) these applying to current

$$i_d = k_d \left[i_a \cos\theta + i_b \cos\left(\theta - \frac{2\pi}{3}\right) + i_c \cos\left(\theta + \frac{2\pi}{3}\right) \right] \qquad (3.1)$$

$$i_q = k_q \left[i_a \sin\theta + i_b \sin\left(\theta - \frac{2\pi}{3}\right) + i_c \sin\left(\theta + \frac{2\pi}{3}\right) \right] \qquad (3.2)$$

$$i_0 = \frac{1}{3}(i_a + i_b + i_c) \qquad (3.3)$$

Similar equations apply when converting flux linkage or voltage. The value of the constants k_d and k_q are chosen to give desired scaling between the resulting dq quantities and the sinusoidal quantities. Use of $k_d = k_q = 2/3$ results in the magnitude of the dq quantity being equal to the peak value of the sinusoidal quantity, use of $k_d = k_q = \sqrt{2/3}$ results in a power invariant transform (Kundur 1994).

3.2 Synchronous machine stator and rotor equations (Kundur 1994)

The behavior of the synchronous machine, under balanced operating conditions[11], is described by the following equations[12] in terms of voltages which are developed due to changes in flux linkage, and flux linkages which occur due to the flow of current. All quantities are in per unit and per phase and are transformed to the d-q axis reference frame; the suffix d and q indicating these axis quantities respectively. The equations apply to a machine with a sinusoidal flux distribution i.e. a non-salient pole machine. Damper windings are included.

3.2.1 Voltages

The terminal voltage of the machine is given by Eq(3.4) & (3.5) where e_d and e_q are the direct and quadrature components of voltage, $p\lambda$ is the rate of change of flux

[11] The zero sequence components of current and voltage are zero; $i_0 = e_0 = 0$.

[12] Flux linkage is denoted by the symbol λ in keeping with most textbooks on electrical machine theory. In Kundur (1994) ψ is used to denote flux linkage to avoid confusion with Eigenvalue notation.

linkage, pθ is the rate of change of the d-axis position with respect to the stator field, R_a is the per phase resistance of the armature and i is current.

$$e_d = p\lambda_d - \lambda_q p\theta - R_a i_d \qquad (3.4)$$
$$e_q = p\lambda_q - \lambda_d p\theta - R_a i_q \qquad (3.5)$$

The field voltage e_{fd} is located entirely in the d-axis and is given by

$$e_{fd} = p\lambda_{fd} + R_{fd} i_{fd} \qquad (3.6)$$

Damper windings for the machine in the q-axis and d-axis are represented by Eq(3.7) & (3.8) where k is a number denoting a particular damper winding of which there may be many. These windings are short circuited and hence for the case of balanced currents, no voltages are developed across them.

$$e_{kd} = 0 = p\lambda_{kd} + R_{kd} i_{kd} \qquad (3.7)$$
$$e_{kq} = 0 = p\lambda_{kq} + R_{kq} i_{kq} \qquad (3.8)$$

3.2.2 Flux linkages

The d-axis flux linkage λ_d (Eq(3.9)) is determined by the armature d-axis mutual inductance L_{ad}, the leakage inductance L_l and the d-axis stator, field winding and damper winding currents, i_d, i_{fd} and i_{kd}. The q-axis flux linkage λ_q (Eq(3.10)) is determined by the armature q-axis mutual inductance L_{aq}, plus L_l (similar for both axis) and the respective q-axis currents i_q and i_{kq}.

$$\lambda_d = -(L_{ad} + L_l) i_d + L_{ad} i_{fd} + L_{ad} i_{kd} \qquad (3.9)$$
$$\lambda_q = -(L_{aq} + L_l) i_q + L_{aq} i_{kq} \qquad (3.10)$$

The inductances associated with the total flux linkages due to i_d and i_q respectively are denoted as L_d and L_q where $L_d = L_{ad} + L_l$ and $L_q = L_{aq} + L_l$. Thus Eq(3.9) & (3.10) may be written as

$$\lambda_d = -L_d i_d + L_{ad} i_{fd} + L_{ad} i_{kd} \qquad (3.11)$$

$$\lambda_q = -L_q i_q + L_{aq} i_{kq} \qquad (3.12)$$

The d-axis flux linkage in the field winding, λ_{fd}, is determined by the d-axis currents and the field self-inductance L_{ffd}, the field to d-axis damper winding mutual inductance L_{fkd} and the d-axis mutual inductance L_{ad} according to

$$\lambda_{fd} = L_{ffd} i_{fd} + L_{fkd} i_{kd} - L_{ad} i_d \qquad (3.13)$$

Flux linkage in the d-axis damper windings λ_{kd} is determined by currents in the d-axis and the d-axis damper winding self inductance L_{kkd}, the d-axis mutual inductance L_{ad} and the field to damper winding mutual inductance L_{fkd}. Flux linkages in the q-axis damper windings λ_{kq} are determined by currents in the q-axis and the q-axis damper winding self inductance L_{kkq} and the q-axis mutual inductance L_{aq}.

$$\lambda_{kd} = L_{kkd} i_{kd} - L_{ad} i_d + L_{fkd} i_{fd} \qquad (3.14)$$
$$\lambda_{kq} = L_{kkq} i_{kq} - L_{aq} i_q \qquad (3.15)$$

3.2.3 Speed voltages and transformer voltages

Since the rate of change of position $p\theta$ is equal to the rotational speed of the rotor ω_r, Eq(3.4) & (3.5) may be rewritten as

$$e_d = p\lambda_d - \lambda_q \omega_r - R_a i_d \qquad (3.16)$$
$$e_q = p\lambda_q - \lambda_d \omega_r - R_a i_q \qquad (3.17)$$

The terms $\lambda_d\omega_r$ and $\lambda_q\omega_r$ are known as the speed voltages and the terms $p\lambda_d$ and $p\lambda_q$ as the transformer voltages. The transformer voltages occur “due to flux changes in time” and the speed voltages occur “due to flux change in space”. Under steady state conditions the transformer voltages are zero which leaves the speed voltages to constitute the main components of stator voltage.

3.3 Vector control of the synchronous machine

3.3.1 Power and torque (Kundur 1994)

Terminal power P_t can be expressed as the product of voltages and currents

$$P_t = \frac{3}{2}\left(e_d i_d + e_q i_q\right) \qquad (3.18)$$

Substituting for voltage using Eq(3.16) & (3.17) and rearranging results in an expression for power in terms of "rate of change of armature magnetic energy", "power transferred across the air-gap" and "armature resistance loss". The component of power associated with torque, the air gap power is

$$P_{air-gap} = \frac{3}{2}\left(\lambda_d i_q - \lambda_q i_d\right)\omega_r \qquad (3.19)$$

To obtain torque T_e, the air-gap power is divided by the mechanical speed of the rotor ω_{mech} giving Eq(3.20). Division of electrical speed by mechanical speed simplifies to give Eq (3.21) where p_f is the number of field poles.

$$T_e = \frac{3}{2}\left(\lambda_d i_q - \lambda_q i_d\right)\frac{\omega_r}{\omega_{mech}} \qquad (3.20)$$

$$T_e = \frac{3}{2}\frac{p_f}{2}\left(\lambda_d i_q - \lambda_q i_d\right) \qquad (3.21)$$

3.3.2 Control of torque and flux

Torque

From Eq(3.21) it is seen that torque is proportional to the cross product of stator flux with stator current i.e the difference between the products of d-axis flux with q-axis current and q-axis flux with d-axis current. Substituting for flux linkages λ_d and λ_q Eq(3.11) & (3.12)

$$T_e = \frac{3}{2}\frac{p_f}{2}\left(i_q(L_{ad} i_{fd} - L_d i_d + L_{ad} i_{kd}) - i_d\left(L_{aq} i_{kq} - L_q i_q\right)\right) \qquad (3.22)$$

$$T_e = \frac{3}{2}\frac{p_f}{2}\left(i_q L_{ad} i_{fd} + i_d i_q\left(L_q - L_d\right) + \left(i_q L_{ad} i_{kd} - i_d L_{aq} i_{kq}\right)\right) \qquad (3.23)$$

Eq(3.23) shows torque to be composed of three components (Novotny & Lipo 1996). Firstly the excitation or reaction torque, secondly the saliency/reluctance torque and the thirdly the damping torque. Control of torque is obtained, via the first term, through regulation of q-axis current, with in the case of a salient pole machine an additional adjustment made for d-axis current.

A special case occurs when i_d is regulated to zero; orthogonal orientation of the excitation flux to the armature flux (torque angle equal to 90 degrees). This results in control of torque entirely via the q-axis and also maximization of the torque to current ratio (Novotny & Lipo 1996). Operation of the machine is now analogous to the operation of a dc-machine where armature current directly controls torque. Note that the machine operates at lagging power factor under this condition.

Flux

Control of the field of the machine is obtained via regulation of d-axis current to achieve one of three aims; operation at a desired power factor, control of machine terminal voltage, or as explained above, orientation (of the field) to obtain direct control of torque (Rashid 2001). At high speeds 'field weakening' may be necessary to limit terminal voltage. Multi-mode operation such as this can be used to optimize the combination of machine and converter (Gallegos-Lopez et al. 2005).

3.4 Simplified model for use in frequency studies

For modelling of system frequency, where transients are not important and also multiple instances of machines may be required, it is useful to derive a simplified model of the synchronous generator. This model is utilised within the wind turbine model of chapter 5.

3.4.1 Simplifying assumptions

The following assumptions are made:

- Damper winding currents are zero (a) – Damper windings are designed to produce a restraining torque to reduce oscillations in rotor angle during disturbances. For relatively slow changes in torque which would occur via a

turbine's torque controller, no currents would be expected to flow in these damper windings.

$$i_{kd} = i_{kq} = 0 \qquad (3.24)$$

- Saliency small and d-axis current regulated to zero (b) – A round rotor construction is assumed as opposed to a salient pole machine. Along with regulation of d-axis current to zero this ensures no contribution from the saliency torque, the middle component of Eq(3.23).

$$L_d = L_q \text{and } i_d = 0 \qquad (3.25)$$

- Rotor field current constant (c) – The rotor field current i_{fd} is held constant by a suitable excitation control system.

$$i_{fd} = \text{constant} \qquad (3.26)$$

3.4.2 Realisation of torque and flux control

Control of torque and flux is obtained via output of an appropriate terminal voltage at the generator's voltage source converter, further explanation being given below.

Torque

Torque is controlled through regulation of q-axis current (3.3.2). Taking Eq(3.17) and replacing p with d/dt and substituting for λ_q (where $i_{kq} = 0$, assumption (a)), the rate of change of i_q is determined by

$$e_q = -\frac{d}{dt} L_q i_q - \lambda_d \omega_r - R_a i_q \qquad (3.27)$$

where $\lambda_d \omega_r$ is the speed voltage component of the q-axis terminal voltage e_q due to the magnetizing flux. Note that when the machine is open circuited, e_q is measurable at the terminals and is known as the internal voltage.

Given assumption (b) and substituting for λ_d in Eq(3.27), the relationship between i_q and the applied voltage e_q and field current i_{fd} is

$$e_q = -\frac{d}{dt} L_q i_q + L_{ad} i_{fd} \omega_r - R_a i_q \qquad (3.28)$$

This shows a first order relationship to exist between q-axis terminal voltage e_q and q-axis current i_q and thus torque.

Flux

Control of flux is obtained through regulation of d-axis current (3.3.2). By a similar process to that shown for control of torque above, given assumption (a) ($i_{kd} = 0$), rate of change of i_d is determined by

$$e_d = -\frac{d}{dt} (L_d i_d + L_{ad} i_{fd}) - \lambda_q \omega_r - R_a i_d \qquad (3.29)$$

where $\lambda_q \omega_r$ is the speed voltage component of the d-axis terminal voltage e_d due to the q-axis current.

Given assumption (c) and substituting for λ_q in Eq(3.29), the relationship between i_d and the applied voltage e_d is

$$e_d = -\frac{d}{dt} L_d i_d + L_q i_q \omega_r - R_a i_d \qquad (3.30)$$

Again similar to torque, this shows a first order relationship to exist, this time between d-axis terminal voltage e_d and d-axis current i_d and hence magnetizing flux.

For the vector control scheme chosen via assumption (c), where i_d is assumed regulated to zero, e_d in steady state will be solely determined by i_q as below

$$e_d = L_q i_q \omega_r \qquad (3.31)$$

Illustration of vector control

A phasor diagram[13] illustrating the variation of terminal voltage, current and flux for a synchronous generator, given the stated assumptions (a) to (c), is shown in Figure 3.2. Phasor quantities in the stationary reference frame are indicated by capitals; E_{int} the internal voltage of the machine, E_T the terminal voltage, I_T the current and X_s the impedance (which in per unit equals L_d and L_q). dq quantities are indicated by lower case. Flux linkages are located 90 degrees behind their corresponding voltages and out of phase with their respective currents; field flux linkage λ_{fd}, stator flux linkage λ_s (= λ_{dq}), and armature reaction flux linkage λ_a.

Three steady state operating points are shown. Point 1 indicates open circuit operation where the internal voltage of the machine is measureable at the terminals. Points 2 and 3 show, with accompanying blue and red phasors respectively, the machine generating. Point 3 indicates a doubling of i_q compared to point 2 and hence a doubling of the torque. The changes in the components of q-axis and d-axis voltage Δe_q and Δe_d can be seen to be due to the resistance R_a and the reactance of the machine X_s respectively.

Points 1', 2' and 3' show the corresponding flux linkages. Note that with the d-axis component of current equal to zero, the torque angle δ_T, the angle between the armature reaction flux λ_a and the field flux λ_{fd} is always 90 degrees.

Control of the machine in steady state is achieved by setting the d-axis voltage e_d proportional to the q-axis current according to Eq(3.31) and setting the q-axis voltage according to Eq(3.28), the internal voltage minus the voltage drop across the resistance.

[13] An explanation of phasor representation of dq quantities is given in Appendix B1.

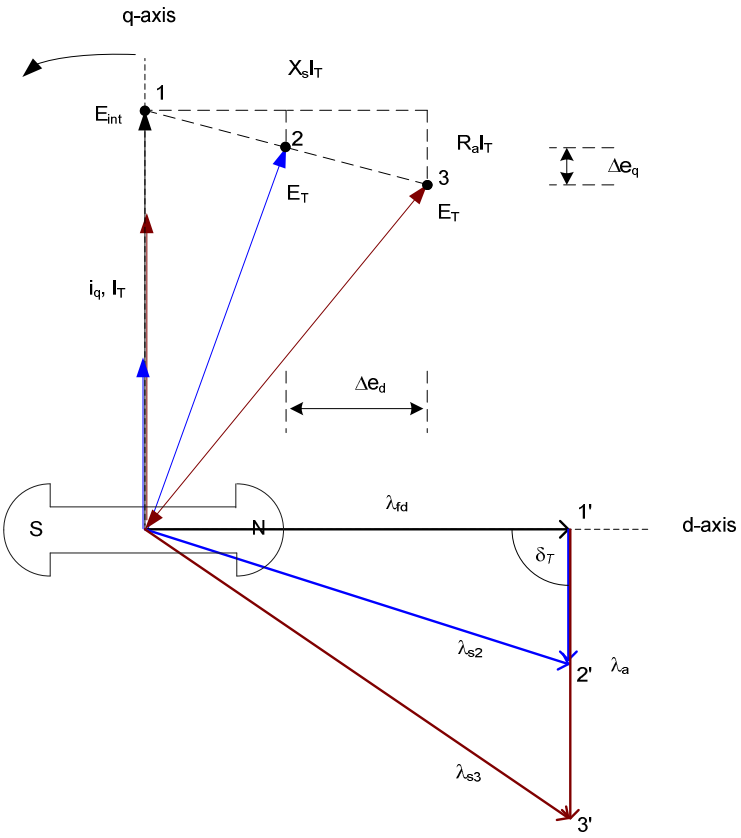

Figure 3.2 – Phasor diagram for the synchronous generator illustrating change in steady state terminal voltage for a doubling of torque (operating point 2 to 3).

3.4.3 Conversion to s-domain

The differential equation describing the simplified generator, Eq(3.28), is converted into the s-domain as below:

Collecting the input terms (the applied voltage) and the output terms (i_q) Eq(3.28) becomes

$$e_q - L_{ad} i_{fd} \omega_r = -\frac{d}{dt} L_q i_q - R_a i_q \qquad (3.32)$$

Taking the Laplace transform of Eq(3.32) and denoting the internal voltage of the machine $L_{ad} i_{fd} \omega_r$ as e_{int} and the control component of the applied voltage $e_q - e_{int}$ as $e_{q\text{-}int}$ gives

$$e_{q-int}(s) = -s i_q(s) L_q - R_a i_q(s) \qquad (3.33)$$

The transfer function G(s) which describes the behavior of the system represented by Eq(3.33) is given by the ratio of the Laplace transform of the output variable to the Laplace transform of the input variable (Bolton 1998). Hence

$$G(s) = \frac{i_q(s)}{e_{q-int}(s)} \qquad (3.34)$$

$$= \frac{i_q(s)}{-si_q(s)L_q - R_a i_q(s)} \qquad (3.35)$$

$$= -\frac{1}{(L_q s + R_a)} \qquad (3.36)$$

$$= -\frac{1/R_a}{\left((L_q/R_a)s + 1\right)} \qquad (3.37)$$

In steady state Eq(3.37) has a gain of $1/R_a$ and a time constant of L_q/R_a.

3.4.4 Simplified model

The simplified model of the synchronous machine consists of a control loop for torque via q-axis current, plus the transfer function of the electrical machine in terms of e_q and i_q, Eq(3.36). Assumption (b) obviates the need to include modelling of the d-axis current control. The q-axis current control is implemented, as is common practice, by a PI compensator and negative closed loop feedback. The resulting model is shown in Figure 3.3 where k_2 is the ratio of q-axis current to torque.

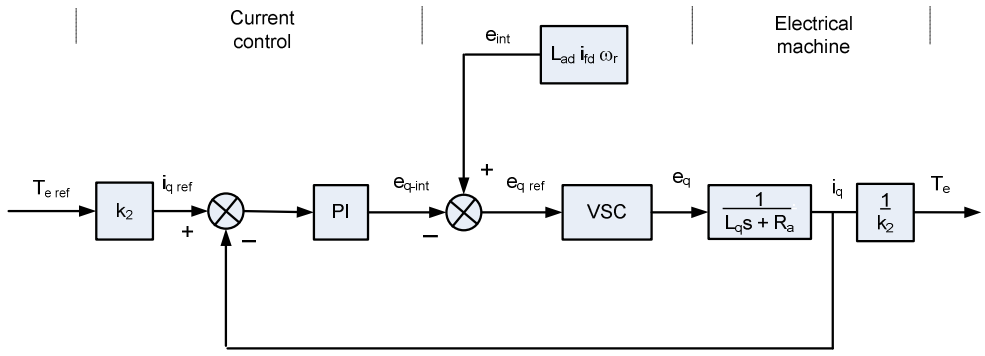

Figure 3.3 – Simplified model of the synchronous generator.

Further simplification is obtained by assuming that the VSC under normal operation behaves as a linear amplifier (Y. Ming et al. 2004) and that the internal voltage of the machine e_{int} will remain constant since ω_r will be slow to change due to the inertia of the rotor and turbine. This results in the model shown in Figure 3.4 where k_p and k_i are the equivalent PI gains.

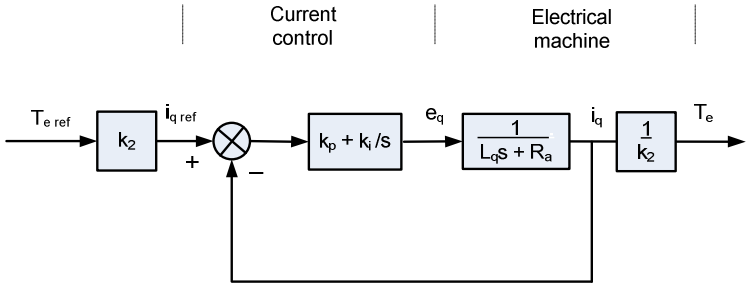

Figure 3.4 – Simplified model of the synchronous generator suitable for frequency studies

3.5 Summary

The following was undertaken :

- Governing equations of the synchronous machine in the rotating reference frame were given.
- Control of torque and flux was shown possible via regulation of q-axis and d-axis currents respectively.
- Assumptions were made in order to obtain a simplified model of the synchronous machine: (a) damper winding currents are zero, (b) d-axis current regulated to zero and saliency small and (c) rotor excitation current held constant.
- Control via the terminal voltage components e_d and e_q was illustrated, in steady state, with d-axis current regulated to zero.
- An s-domain transfer function was obtained describing the dynamics of the q-axis current in the machine.
- A simplified model suitable for use in frequency studies was presented. This is comprised of the electrical machine transfer function and a PI control loop for q-axis current.

The simplified model of Figure 3.4 is used within the wind turbine model in Chapter 5. The time constant for the electrical machine L_q/R_a is experimentally measured in Chapter 4.

4 Laboratory wind turbine test rig

4.1 Introduction

Research into wind turbines, their generators and control systems, invariably makes use of laboratory based test rigs[14]. A brief account of published work is given below, and following this, an overview of the wind turbine test rig constructed by the candidate.

4.1.1 Experimental testing of wind turbines

Description of the design of two wind turbine test rigs, a 4kW DFIG based system and a 3kW interchangeable IG and PM based system are described in Rabelo & Hofmann (2002) and in Chinchilla et al. (2004). The first gives detail of filter design, controller gain calculations, measurement of machine parameters and practical insights into the overall development and commissioning of a test rig. Inclusion of a multi-mass model of the drive train in combination with wind data and a model of turbine's power characteristics enabled emulation of drive train dynamics (Rabelo et al. 2004). Inclusion of other effects such as tower shadow and wind shear are presented in Chinchilla et al. (2004). Whilst most test rigs utilize a machine size of between 2 and 4kW, the Norwegian University of Science and Technology use a 55kW machine which is stated to be more representative of full-scale turbines due to the p.u values of the machines being similar (Molinas et al. 2005).

Examples of areas of investigation which have utilized a wind turbine test rig are:

- Comparison of energy yield between a stall regulated IG and a pitch regulated variable speed PM turbine (Chinchilla et al. 2004).
- Demonstration of control and operation of a PM FPC turbine including control of d-axis current for optimum efficiency (Chinchilla et al. 2006).
- Experimental testing of inverter active and reactive power limits for a PM FPC turbine (Chinchilla et al. 2005).
- Fault Ride Through capability of the grid inverter on an IG FPC turbine (Molinas et al. 2005).

[14] Also referred to in a number of publications as Wind Turbine Emulators.

- Gain scheduling of a stall controlled variable speed IG FPC turbine (Bourlis 2009).
- De-loading for primary frequency control using fuzzy logic control of pitch and torque (Courtecuisse et al. 2008).

4.1.2 Overview of the wind turbine test rig

For the research described in this thesis, a test rig was constructed consisting of a 0.8kW 3-phase synchronous generator, driven directly by a dc drive. The synchronous generator was connected to the grid via an FPC type arrangement, two identical converter bridges connected back-to-back via a dc-link. To emulate the torque produced by the rotor of a wind turbine, the dc drive's torque reference was calculated by using a model of the turbine's power characteristics (the same model that is described in Chapter 5). Control of the complete system was implemented on a rapid prototyping embedded control system[15]. This consists essentially of hardware, a controller board with master processor and slave DSP[16], and software, a PC based user interface and a development platform for coding and graphical input of the control design via MATLAB Simulink®.

The components of the test rig are shown in the schematic of Figure 4.1 and are broadly divided into the hardware and software blocks indicated. The hardware components consist of the electrical machines (A, B), power electronics (C), grid connection (D) and the embedded controller platform (E). The software components consist of the control system (F) which is implemented on the embedded controller platform and the user interface (G) which is located on a dedicated PC. Sensors are indicated on the schematic along with (major) signals between the blocks. Further detail of each block is given in the following sections, 4.2 to 4.5.

[15] Rapid prototyping embedded control systems are typically used in industry to develop and implement a control system at the design stage. Finalisation of the control system design, onto to a specific (and lower cost) hardware platform, then follows.

[16] A Digital Signal Processor (DSP) is a processing device optimised to perform mathematical calculations and is commonly found in high-performance motor/generator control applications.

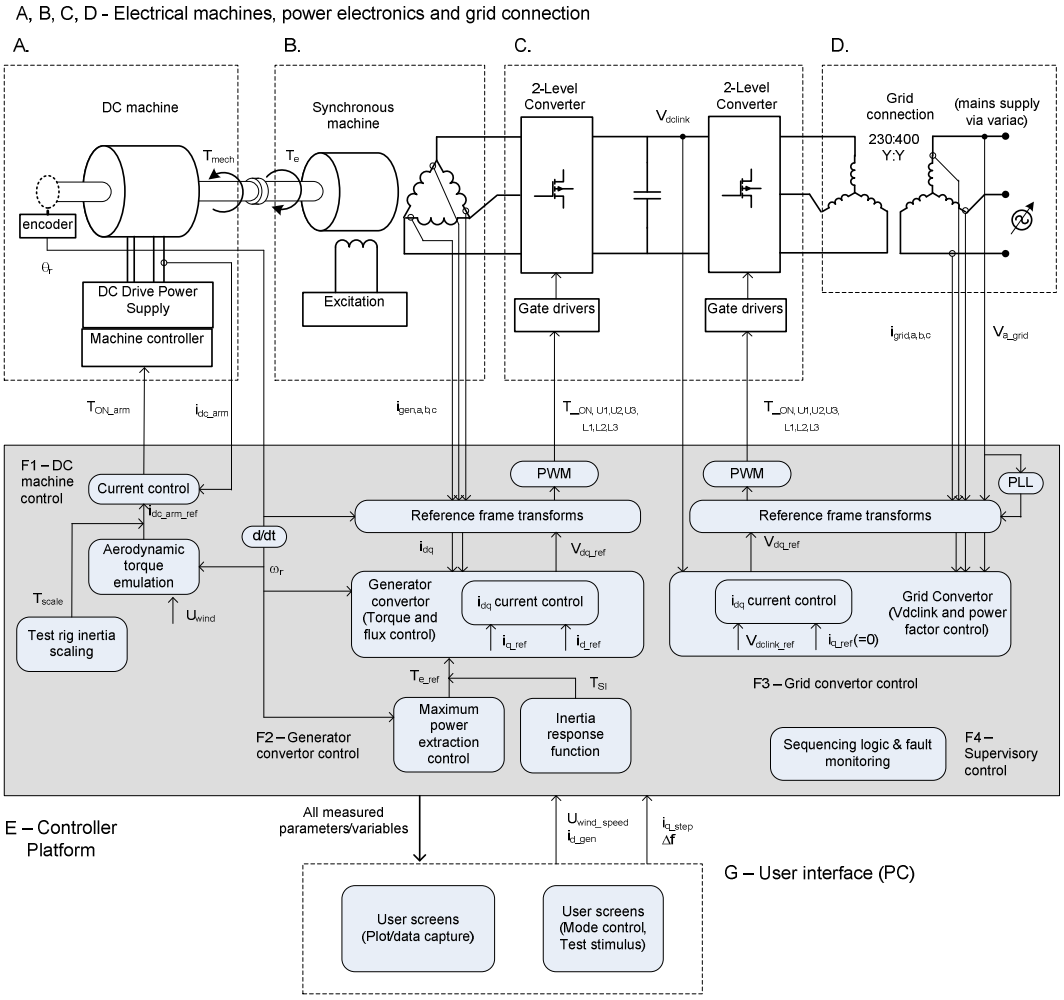

Figure 4.1 – Schematic of the wind turbine test rig showing functional blocks and major signals and measurements.

4.2 Electrical machines, power electronics and grid connection

The main items of hardware are described in this section except for the controller platform (E) and sensors which are described in 4.3.

4.2.1 dc drive (A)

The dc drive and its power supply and controller are shown in Figure 4.2 and are explained below.

dc machine

The dc machine is of the shunt wound type and has a rating of 1kW at 1500rpm and 2kW at 3000rpm. The armature current has a maximum rating of 8.5A and the field current a maximum rating of 0.7A.

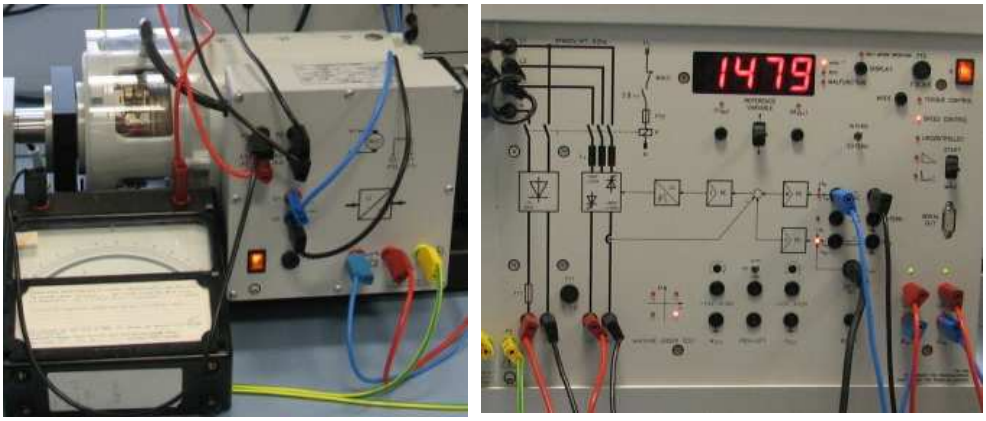

Figure 4.2 - dc machine (left) and drive power supply and machine controller (right).

dc drive power supply and machine controller

The dc drive power supply consists of a 3-phase thyristor based rectifier to provide armature current and an uncontrolled single phase rectifier to supply a constant voltage to the field. Incorporated in the power supply unit is a machine controller. Although torque and speed control is possible using the machine controller an external control mode was utilized which gives direct control of the duty cycle of the armature thyristors via the external signal $T_{\_ON\_arm}$. This signal was provided via an external current control loop implemented on the platform controller, block E1.

4.2.2 Synchronous machine (B)

Synchronous machine and excitation

The 3-phase synchronous machine is of 4-pole, wound rotor construction (non-salient) with damper windings and is shown with its excitation supply in Figure 4.3. Name plate ratings for the machine give operation at 400/230 Volts, 1.52/2.66A in Y and delta configuration respectively at 50Hz and 0.8kVA at power factor of ±0.8. Maximum allowable excitation current for the machine is 1.6A and maximum excitation voltage 220V. The machine windings were configured in delta to allow operation of the dc-link at a reasonably low voltage (i.e less than 500Vdc).

Excitation for the machine was provided by a single phase thyristor controlled rectifier with current externally adjustable via a duty cycle input signal.

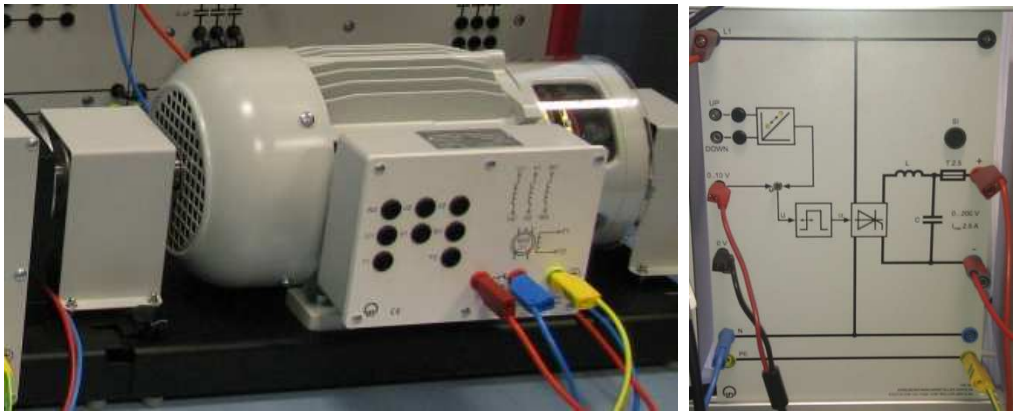

Figure 4.3 – Synchronous generator (left) and excitation unit (right).

4.2.3 Power converter (C)

The power converter consists of a pair of identical 6-pulse[17] converter bridges arranged in back to back configuration and connected via a dc-link equipped with a capacitor. Units such as these where connected to a capacitor are also known as Voltage Source Converters (VSCs). The arrangement of the power switching devices is shown in Figure 4.4 along with the gate drive circuitry which was necessary for interfacing to the embedded controller.

A brief explanation of the converter bridge units and the gate driver board and their development follows. Full schematic diagrams for the bridge and gate driver boards are located in Appendix A2.

Development

An initial version of the test rig made use of converter bridges which were made up by interconnecting individual switching units. These units consisted of a single MOSFET plus some minor additional components, located on its own individual PCB. However, stray inductance associated with inter-unit wiring and PCB tracking lengths was suspected of causing emission of unwanted noise and mal-operation of the converters. The 6-pulse converter bridges, located on a single circuit board and described below, were developed to remedy this problem.

[17] A 6-pulse converter uses 6 switching devices arranged in pairs, one pair for each phase, to either 'invert' a dc supply and create 3-phase alternating current output or 'rectify' an ac supply to create a dc current output.

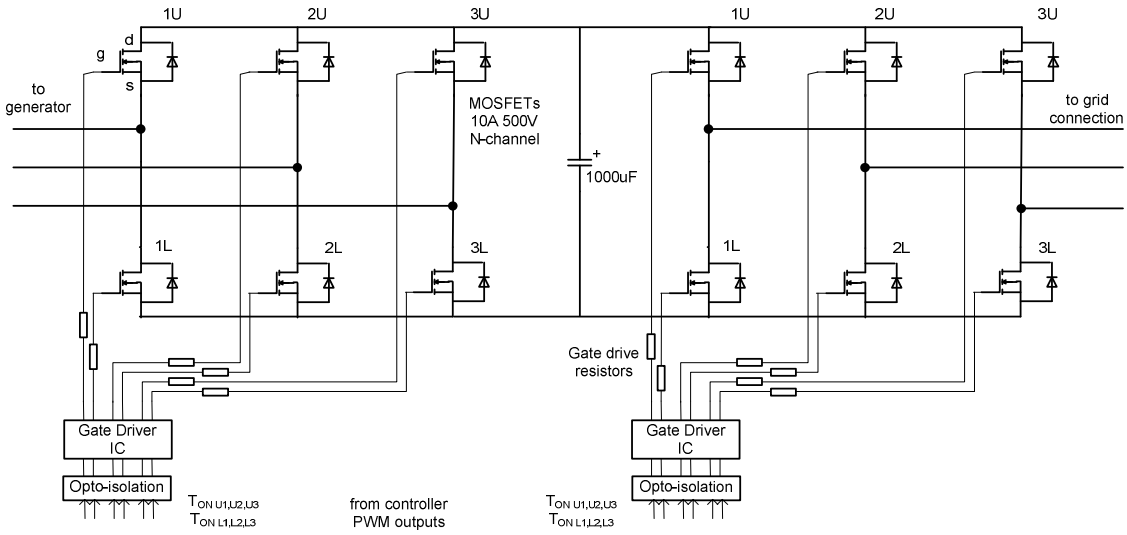

Figure 4.4 – Power converter schematic showing the MOSFET switches[18], dc link, capacitor and connection to embedded controller via gate drive circuitry.

Converter bridges

MOSFET devices were selected for use as power switches for the test rig which is nominally rated at 800W at 220V. The MOSFET device chosen was deemed of a suitable rating after checking its characteristic Safe Operating Area (SOA) chart[19].

Additional local capacitors and varistors (not shown in Figure 4.4) are connected across each bridge leg (e.g 1U and 1L), between the upper MOSFET device's drain pin 'd' and the lower device's source pin 's'. The capacitor serves to reduce noise from switching transients and the varistor provides overvoltage protection for the two MOSFET devices in the bridge leg. One of the two converter bridges is shown in Figure 4.5 (right) connected to its gate driver board.

[18] The discrete diodes indicated in the figure are in fact an integral part of the MOSFET device and are known as 'body' diodes.

[19] Voltage and current ratings for a power switching device are subject to duty cycle and pulse length limitations. These rating capabilities are expressed in a SOA chart supplied by the manufacturer. An overview of how to interpret an SOA chart is given in (Raychem n.d.).

Gate Drivers

A number of requirements exist for the correct and efficient switching of MOSFET devices which are used in a VSC (International Rectifier n.d.). These relate chiefly to the signal applied to the gate pin (indicated 'g' in Figure 4.4):

- A minimum voltage amplitude of 10 to 15V.
- For the upper devices (indicated 'U' in Figure 4.4) the voltage must be 10 to 15V above the dc-link voltage.
- Logic interfacing capability and a number of other protective requirements relating to abnormal operation and prevention against failure of the bridge components.

To meet these requirements whilst at the same time reducing part count and development time, an Integrated Circuit (IC) was used. Additional isolation between the high voltage/current circuitry of the converter bridges and the controller platform was achieved via use of opto-isolators. This minimises noise interference and also ensures catastrophic failure of the converter bridges does not cause damage to the controller platform.

The gate driver board additionally features a PIC microcontroller to assist in (sequential) interfacing between the gate drive IC and the controller platform. The PIC was also used on the generator side gate driver board to derive the complimentary[20] gate drive signals for the lower devices (indicated 'L' on the left bridge in Figure 4.4); this being due to a limitation in available outputs on the controller platform. Note that for simplicity, the schematics in this chapter depict the grid and generator gate driver circuits as being identical and having the full complement of input signals from the controller platform.

The values of the gate drive resistors were experimentally selected to give a relatively slow gate voltage rise time. This was done to reduce the size of the transients which occur when each MOSFET device starts to conduct. For an

[20] Except when the bridge is de-energised (all switches are off), the lower devices are always driven with the inverse logic value of the upper devices and vice-versa, these lower drive signals being known as the 'complimentary' of the upper drive signals. A 'dead-time' (or 'blanking') period does in-fact exist where both switches are held in the off state to ensure avoidance of a short circuit of the bridge. Note that the gate driver IC that was used, incorporates its own dead-time protection (of 200nsec) regardless of the gate drive logic inputs at the device.

illustration and explanation of changes in current and voltage across the respective terminals of a MOSFET device during switching see Mohan et al. (2003).

Figure 4.5 – Gate driver board (left) and 6 pulse MOSFET converter (right) forming one half of the back to back bridges, developed by the candidate and constructed at Cardiff University.

4.2.4 Grid connection (D)

Transformer

The 3-phase transformer shown Figure 4.6, rating 364VA per phase, was used to connect the power converter to the mains. This was configured in YY, and due to the particular winding ratio provided on the transformer, results in a stepping up of the converter voltage from 220 to 400V enabling interfacing to the mains supply. Since the YY connection results in the generation of 3rd harmonic voltages (Chapman 2005) a set of tertiary windings are utilised in delta which allows the flow of circulating currents which suppress the 3rd harmonic components.

A 3-phase variac was used at the mains connection point in order to provide controlled energisation of the dc-link and facilitate operation of the grid converter at a lower voltage if needed.

Note that the transformer additionally provides the series inductance needed for the grid side converter control scheme which measures the phase shift between the current and voltage, output to the grid.

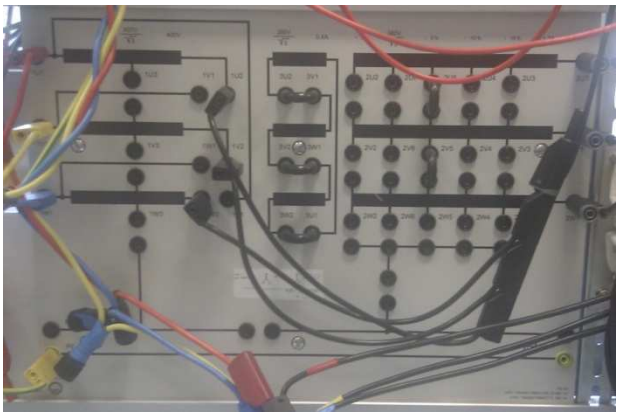

Figure 4.6 – Transformer used to connect the power converter to the mains supply.

4.3 Controller platform and sensors (E)

4.3.1 Controller platform

The controller platform used was a dSPACE® DS1103PPC and its architecture is shown in Figure 4.7. The platform essentially consists of a main processor and a slave DSP (indicated) with respective analogue and digital I/O interfaces. Additional Analogue to Digital Converters (ADCs) and Digital to Analogue Converters (DACs) are provided on the platform along with an incremental encoder interface and a number of internal and external communication interfaces, one of which is to the PC. All of the control functions indicated in Figure 4.1 and described in section 4.4 run on the controller platform. The controller was programmed via entry of a the control design in MATLAB Simulink®. Compilation of the design into code which runs on the platform controller was again done on the PC, within the dSPACE® and MATLAB® development environment, and then downloaded to the platform controller.

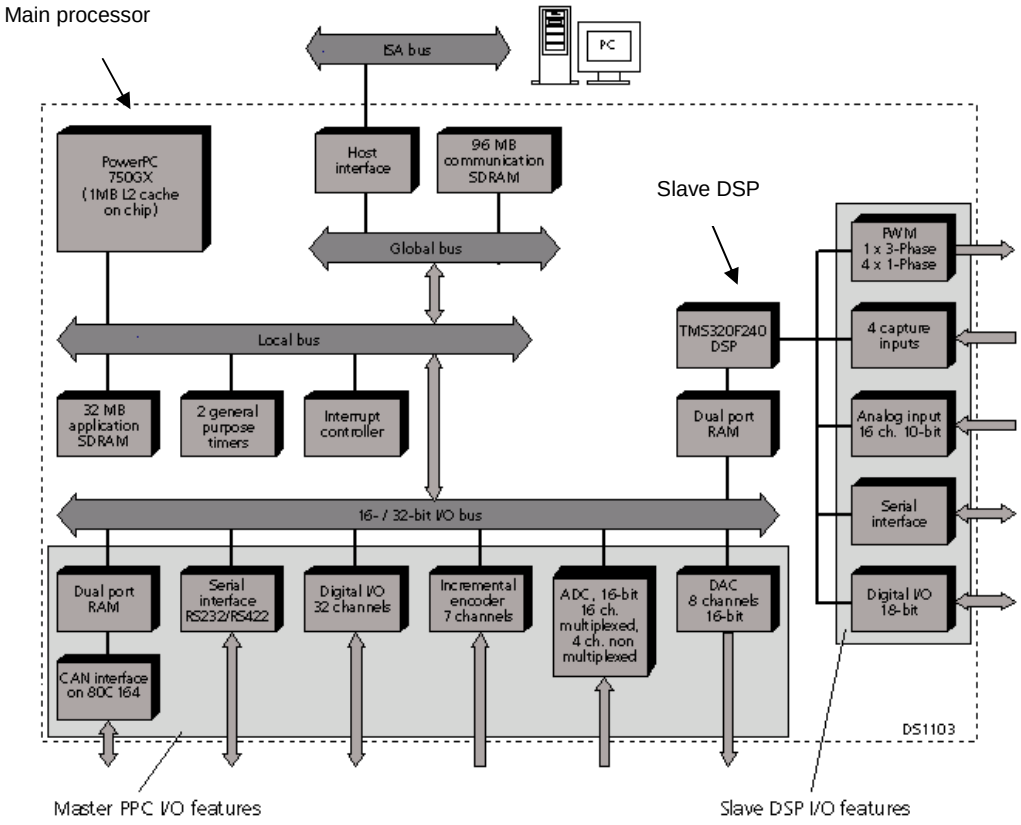

Figure 4.7 – Hardware architecture of the controller platform showing main processor, slave DSP and internal and external interfaces (dSPACE 2009).

4.3.2 Sensors

Sensors were connected via the breakout panel supplied by dSPACE® shown in Figure 4.8.

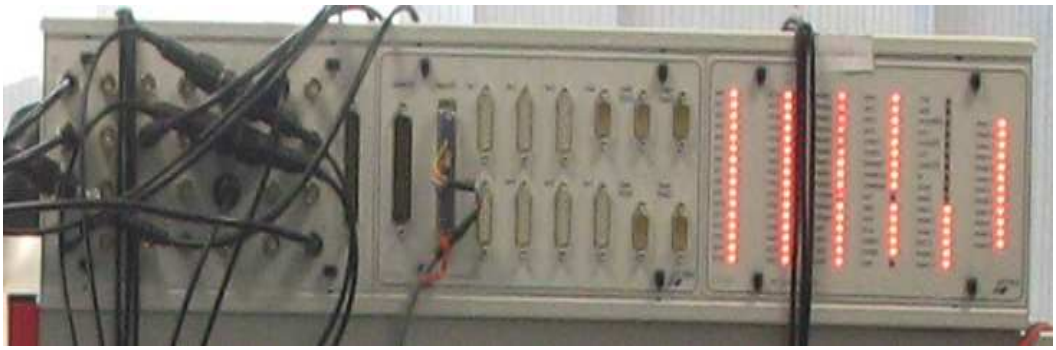

Figure 4.8 – Breakout panel for connection of sensors and digital I/O, including status LEDs for the digital I/O.

Analogue signals were connected using co-axial cabling and digital signals were connected via twisted pair screened cabling. Appropriate advice on cabling methods for the avoidance noise emission and interference is given in Williams (1991).

The principal sensors necessary to operate the test rig are shown in Figure 4.1 and are explained below. Note additional voltage and current sensors were used to obtain measurements of extra signals as and when necessary for use within the controller platform. Use was also made of a 4-channel oscilloscope for monitoring and measurement purposes independent of the controller platform.

Voltage and current measurement

The measurement of voltage was obtained using modular devices which employ Hall effect sensors and closed loop compensation to give a measurement output which is isolated. An assembled measurement unit is shown in Figure 4.9 (left) along with its PCB.

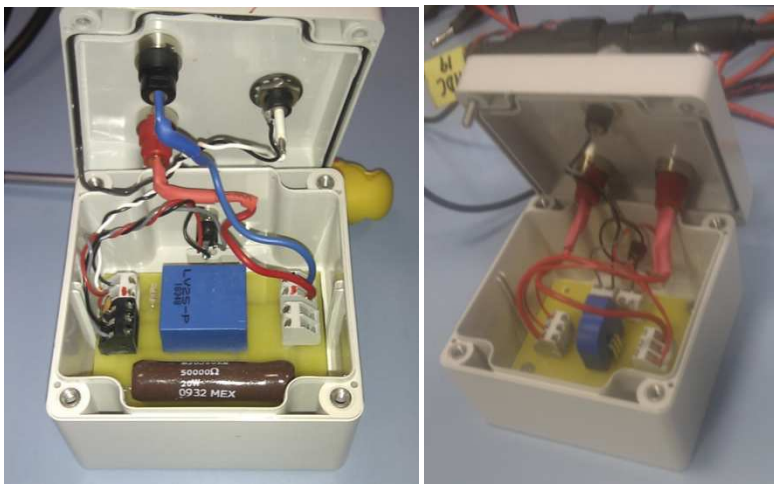

Figure 4.9 - Voltage measurement unit (left) and current measurement unit (right).

Similarly for the measurement of current, modular devices are employed which use the Hall effect and an assembled unit is shown in Figure 4.9 (right). Information about the operation and characteristics of both these isolated voltage and current sensors is given in (LEM n.d.).

Encoder

The encoder used was of the incremental type and is shown in Figure 4.10. It has three channels, the first two generating rectangular pulse waveforms, 1024 per revolution which are 90 degrees offset from each other. The third channel generates a single pulse per revolution which is used as a reference.

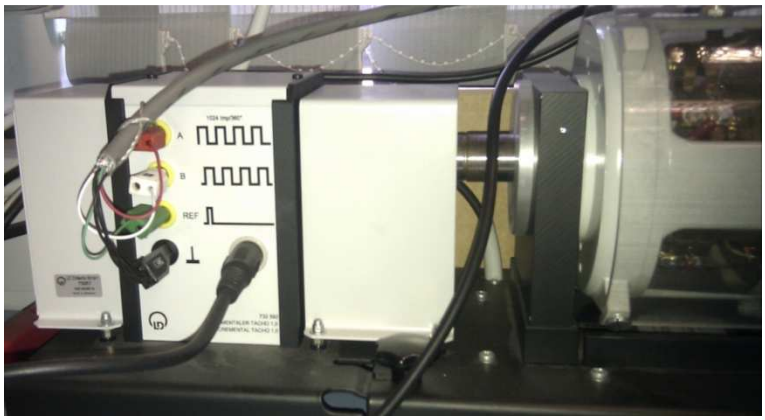

Figure 4.10 – Encoder used for the measurement of rotor position and speed, shown connected to the dc machine.

4.4 Control scheme (F)

The control scheme for the wind turbine test rig can be divided into three separate areas. Firstly control of the dc machine which emulates aerodynamic torque, secondly control of the power converter which is divided into the generator converter control and the grid converter control, and lastly supervisory control of the test rig as a whole. The functioning of these are described below.

4.4.1 DC machine control (F1)

The control of the dc machine is shown in Figure 4.11 and is divided into a further three functions, current control, aerodynamic torque emulation and test rig inertia scaling. Note an additional function, manual speed control, was included for run-up of the test rig.

Current control

Control of the armature current for the dc machine was implemented by a PI controller. Some non-linearity was found between the dc machine controller's input

and the actual value of armature current. Hence extra compensation was added (not shown) which consisted of level shifting and rate adjustment depending on the value of the duty cycle, T_{ON_arm}, output from the PI block.

Aerodynamic torque emulation

Emulation of the aerodynamic torque produced by the turbine was implemented using the Matlab Simulink® 'wind turbine' block. This consists of a mathematical function (see Appendix B2) which gives the value of torque according to the wind speed input, U_{wind}, and the turbine rotor speed ω_r. The same block with identical parameters is used in the wind turbine model of Chapter 5.

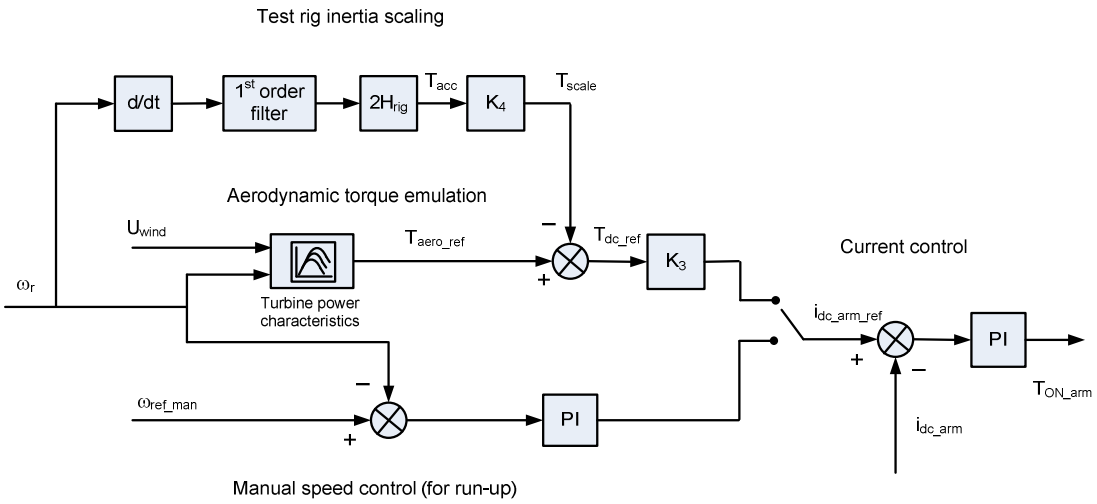

Figure 4.11 – dc machine control scheme consisting of current control, aerodynamic torque emulation, test rig inertia scaling and an additional manual speed control function.

Test rig inertia scaling

This function artificially increases the effective inertia of the test rig itself. Small rotating electrical machines have a comparatively low inertia (discussed 2.1.5), a 5kW induction machine for example having a per unit inertia constant of 0.06 sec compared to between 2 and 7 sec for typical MW size variable speed wind turbines.

For a small electrical machine the energy exchange[21] between the rotating mass and the grid due to a change in speed is too small to accurately measure.

The scaling operates by subtracting a component of torque, T_{scale}, from the dc machine's torque reference, which represents the additional shaft torque needed to accelerate or decelerate an additional rotating mass. Conceptually this is equivalent to adding an extra rotating mass to the test rig but applying its associated accelerating/decelerating torque via the dc machine's rotor rather than a mechanical coupling.

The scaling component of torque T_{scale} is determined by firstly calculating the accelerating torque, T_{acc}, corresponding to the real rotating mass using Eq(2.4). This value is then multiplied by the desired scaling factor, K_4. The resulting effective test rig inertia, H_{eff}, is given by

$$H_{eff} = H_{rig} (K_4 + 1) \qquad (4.1)$$

where H_{rig} is the real inertia constant of the test rig due to its physical rotating mass. Since a differentiator is used to obtain the rotor acceleration, a first order filter is included to reduce noise. Conversion between p.u output of the dc machine and p.u current on the synchronous generator is accounted for by K_3.

4.4.2 Converter control (F2 & F3)

Generator converter

Control of generator torque was achieved by regulation of q-axis current using a PI controller and is shown in Figure 4.12. The torque reference T_{e_ref} was supplied via the maximum power extraction curve block (see later). The current reference was derived from Eq(3.22) where p_f is the number of poles of the machine. The current error, i_{q_error}, was converted via the PI term into a q-axis voltage, V_q, applied to the generator terminals by the VSC. (Derivation of the coupling between V_q and i_q is shown in 3.4.2).

Control of flux was implemented in a similar way to control of torque, however in the case of flux, d-axis current i_d was regulated and coupling was via V_d. As

[21] The inertia constant, H, is the K.E of the rotating machine at rated speed, divided by the VA rating of the machine (Eq(2.3)). Hence for the example 5kW induction machine, given that K.E is proportional to the square of shaft speed (Eq(2.2)), a change in speed from 1.0 to 0.9p.u over 1 second corresponds to a change in terminal output power of $0.06 * (1^2 – 0.9^2) = 0.01$p.u, for a period of 1 second.

explained in 3.3.2, the d-axis current can be set to zero to maximize the torque to current ratio of the generator and give direct torque control of the machine. For the test rig, field weakening, ($i_d > 0$), was used to reduce terminal voltage.

Cross-coupling terms due to speed voltages (3.2.3) were included. For the q-axis, the speed voltage, cross decoupling term (V_{q_speed}), has a component $L_{ad}i_{fd}\omega_r$, due to the magnetizing flux from the rotor excitation current in addition to the term, $i_dL_d\omega_r$, due to current in the d-axis (Eq(3.11) & (3.17)). For the d-axis the speed voltage, cross decoupling term (V_{d_speed}), is $i_qL_q\omega_r$ (Eq(3.12) & (3.16)).

For the test rig, it was assumed that the saliency component of torque (3.3.2), $i_di_q(L_q-L_d)$, was significantly smaller than the excitation torque component, $i_qL_{ad}i_{fd}$, and hence only a small reduction in accuracy of the torque control will occur when operating with i_d at a non-zero value.

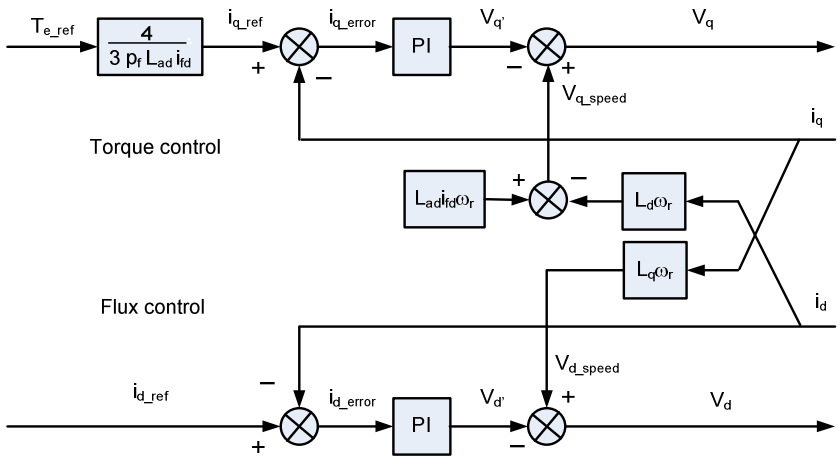

Figure 4.12 – Implementation of generator converter control scheme for torque and flux.

Grid converter

The grid converter was connected to the grid via a transformer as indicated in Figure 4.1. This connection can be represented by a series impedance, $R+j\omega_eL$. Defining current flow as positive towards the grid, the relationship between the voltage at the VSC terminals, V_{dq}, and the voltage on the grid side of the inductances and resistances, V_{dq_grid}, is (Pena et al. 1996)

$$V_d = V_{d\_grid} + L\frac{di_d}{dt} + Ri_d - \omega_e Li_q \qquad (4.2)$$

$$V_q = V_{q\_grid} + L\frac{di_q}{dt} + Ri_q + \omega_e Li_d \qquad (4.3)$$

The grid converter reference frame was obtained from a Phase Lock Loop (PLL) on the grid side of the inductance/resistance. Reference frame alignment was chosen such that V_d leads V_q by 90 degrees and hence V_{q_grid} will be equal to zero and Eq(4.3) simplifies to

$$V_q = L\frac{di_q}{dt} + Ri_q + \omega_e Li_d \qquad (4.4)$$

The control of the respective dq-axis currents was derived from Eq(4.2) & (4.4) similar as to that which was done for the generator side. However this time due to the reference frame alignment being reversed, active power was controlled via i_d and V_d and reactive power was controlled via i_q and V_q. This led to the control scheme implementation shown in Figure 4.13, the upper half showing reactive power control and the lower half active power control.

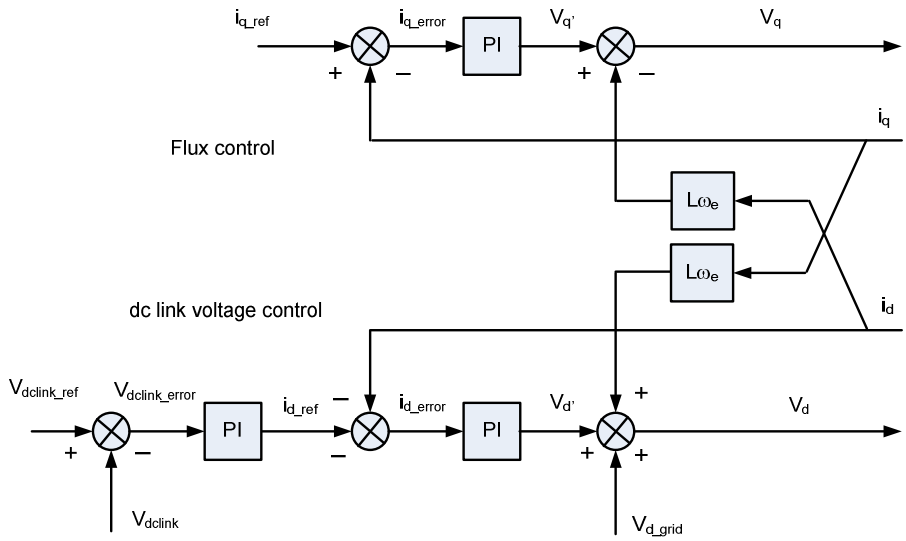

Figure 4.13 – Implementation of grid converter control scheme for reactive power and dc link voltage.

Regulation of dc link voltage [22] was achieved via the (outer) PI loop which determines the active power reference i_{d_ref}.

Reference transformations and PWM

The conversion between stationary reference frame variables and rotating reference frame variables for both the generator and converter control schemes is indicated in Figure 4.14. For the generator control scheme, V_q was chosen to lead V_d; Eq(3.1) & (3.2) were used for the conversion (its inverse transform is shown Appendix A1). The quantities sinθ and cosθ were obtained from the rotor position encoder. A phase shift was necessary for the inverse reference frame transformation to account for the 30 degree displacement between phase currents and line voltages in the delta configured synchronous machine.

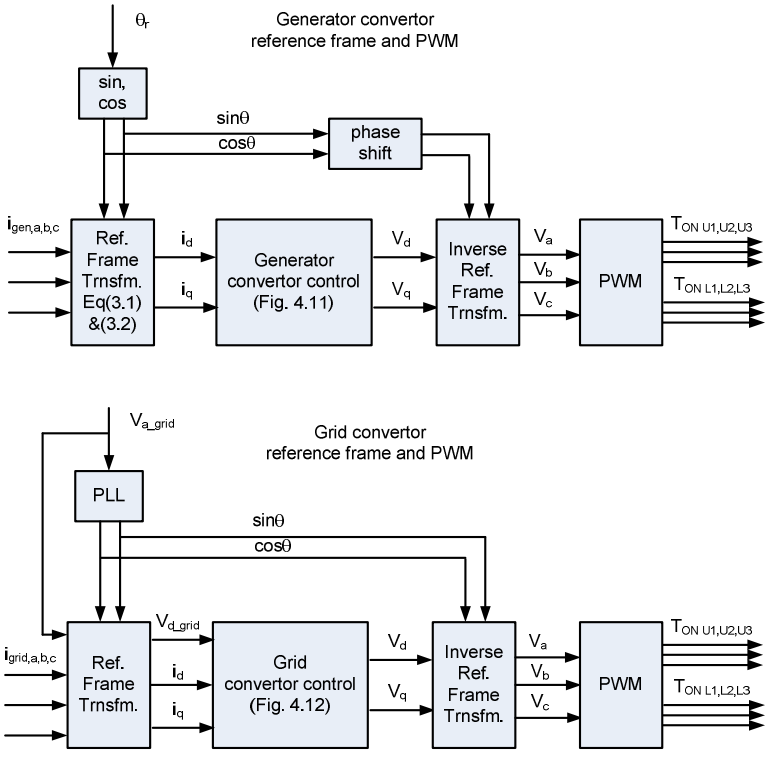

Figure 4.14 – Reference frame transformations and PWM for the generator and grid converter control schemes.

[22] The relationship between dc link voltage, V_{dc_link}, grid converter power output to the grid, P_{grid}, generator active power output to the bridge, P_{gen}, and the capacitance, C, is given by $V_{dc\_link} = \sqrt{\frac{2}{C}\int(P_{gen} - P_{grid})dt}$ (Anaya-Lara et al. 2009).

For the grid converter control scheme a Phase Lock Loop (PLL) provides the sinθ and cosθ quantities. In contrast to the choice of alignment for the generator converter control, the grid control uses V_d leading V_q.

The PWM blocks both functioned similarly for the generator controller and the grid controller in converting the required VSC terminal voltages V_{abc} into three-phase sinusoidal Pulse Width Modulated (PWM) drive signals. These signals U1, U2, U3 and L1, L2, L3 (the logic inverse of the upper gate signals) were routed via the gate driver boards to the appropriate bridge switches. Functioning of sinusoidal PWM is explained in (Mohan).

Maximum power extraction control

The torque reference for the generator T_{e_ref} (Figure 4.12) was derived from the turbine's T_{Pmax} curve and rotor speed input (explained 1.1). This curve was implemented as a look up table and is shown in Figure 4.15.

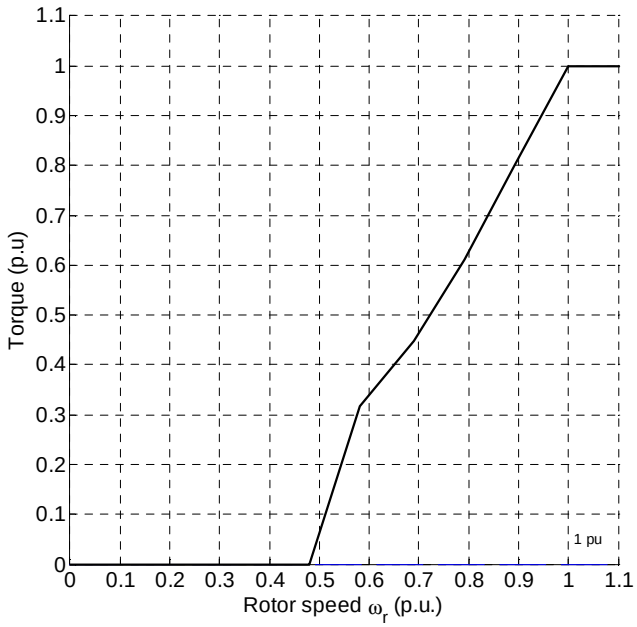

Figure 4.15 – T_{Pmax} curve used to derive torque reference from rotor speed.

The breakpoints for the curve were obtained from plots of power and torque verses rotor speed for wind speeds between 6 and 13m/s using the model contained in the turbine power characteristics block of Figure 4.11. Maximum torque for the generator was set to occur at 1p.u rotor speed. The minimum speed for the machine

was implemented by reducing torque gradually as rotor speed, ω_r, went below 0.582, the value of the torque reference becoming zero when rotor speed was 0.481pu.

4.4.3 Supervisory control (F4)

Supervisory control of the test rig is shown by the state transition diagram of Figure 4.16. Each box describes a state in which the test rig was operating, transition between each state as indicated by the arrow, occurred when the statements located next to the bar on the arrow, became true. The state machine was implemented via a 'case' statement type programming structure within MATLAB Simulink®.

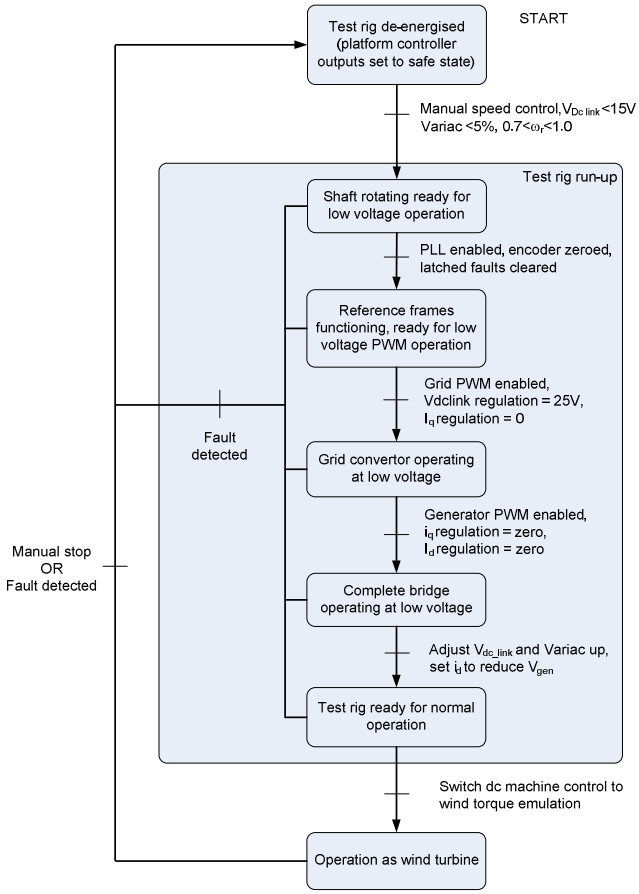

Figure 4.16 – State transition diagram for the test rig

To guard against mal-operation or failure of any of the components, a number of important input signals were monitored. These were rotor speed, grid and generator converter currents, dc link voltage and a gate drive fault signal from the gate driver board. If these exceeded pre-determined limits then the signal 'Fault detected'

became true and as indicated in Figure 4.16, the test rig immediately returned to the de-energised state.

4.4.4 Configuration of controller program code

The controller platform had the capability to schedule the running of separate parts of the program code at different rates and with different priorities, this being a common feature of what are known as real-time operating systems. Additionally, certain hardware interfaces present on the platform (DSP PWM, ADCs and encoder of Figure 4.7) were also configurable in their exact timing of data capture and data output. Introduction of an offset between the alignment of the input sampling and the PWM output transition enabled the reduction of noise on the input signals; this is utilized in a power electronic converter application by selecting the offset so the sampling occurs after the switching operation in an individual bridge leg has fully completed.

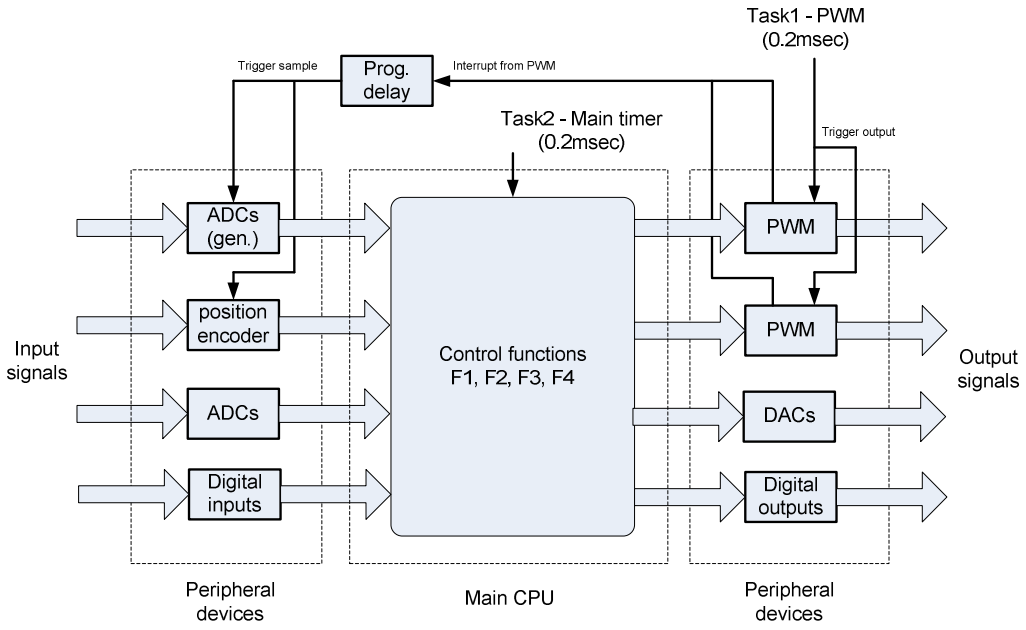

Figure 4.17 – Configuration of program execution and timing of data capture and PWM output for the test rig.

The configuration of program execution and the timing of data capture and PWM output for the test rig is shown in Figure 4.17. The highest priority task[23], Task1,

[23] A task is a collection of one or more parts of the program code which are chosen to be executed together. Different tasks have different priorities, higher priority tasks interrupting lower priority

triggered the output from the PWM blocks. This in turn generated an interrupt signal which after a programmable delay, triggered sampling on the ADCs indicated (for measurement of the generator current) and the position encoder inputs. When Task1 completed, Task2 ran, this task containing all of the control functions F1 to F4 (shown Figure 4.1). Both tasks were configured to run at 5kHz.

4.5 User interface (G)

The user interface, located on the PC, consisted of a number of control screens. All signals which appear in the functional blocks F1 to F4 (Figure 4.1) were available for monitoring in a control screen either via a digital display or within a plot format. Modification of constants or gains was possible via a suitable screen control. As an example the main control screen (Figure 4.18) is described in the following section.

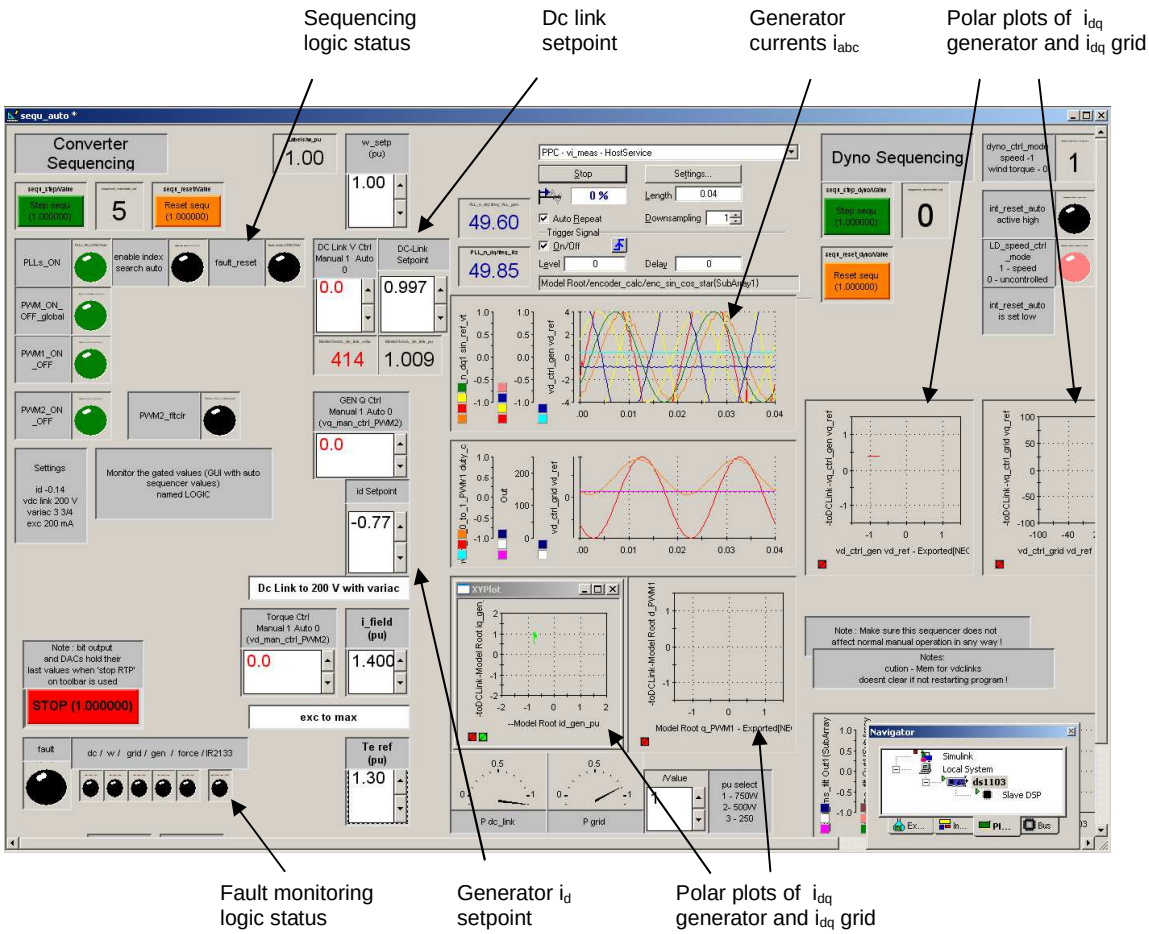

Figure 4.18 – Main control screen for the test rig

tasks when necessary. For an overview of the functioning of real-time operating systems see Cedeno & Laplante (2007).

4.5.1 Main control screen

The main control screen is shown in Figure 4.18 and illustrates a number of user interface controls. The left hand side of the screen corresponds to the sequencing logic shown in the state machine of Figure 4.16. Control of relevant setpoints such as the dc link voltage and i_d and i_q currents for the converters is shown alongside (right) with the status of the fault monitoring logic shown lower left. In the centre of the screen are real-time plots of the generator currents i_{abc} and the corresponding V_{dq} output from the control loop. Polar plots of V_{dq} and i_{dq} also feature (right).

4.6 Commissioning

After assembly of the test rig a number of tests were performed which are described in the following sub-sections. Determination of the synchronous machine parameters and those of the transformer are recorded in Appendix A3.

4.6.1 Measurement and scaling of test rig inertia

The inertia of the test rig, consisting of the dc machine coupled to the synchronous machine, was measured and a test rig inertia scaling factor, K_4 (Figure 4.11), selected appropriately, the overall process being described below. An initial test was also performed to determine the torque to current scaling for the dc machine.

dc machine torque to current scaling

Under normal operation the measurement of dc machine torque on the test rig is achieved by measuring the armature current of the dc machine and applying a scaling ratio to this current. An initial test was performed to obtain the ratio between torque and current by using a torque sensor attached to the dc machine. The torque sensor operated by allowing the body of the machine to rotate against a sprung steel plate to which a strain gauge sensor was attached. After suitable signal processing (part of the dc machine controller unit) a readout of torque was provided. Driving the synchronous machine at its rated output, 800W, the dc armature current i_{dc_arm} was 5.25A and the torque reading 6.0Nm. Allowing approximately 0.4A for friction (evident in the next section also) the torque per ampere characteristic for the dc machine was calculated to be 1.24Nm/A.

Procedure for inertia measurement

The dc machine was placed in speed control mode with the synchronous generator open circuited i.e. with no load. Saturation of the speed control input occurred such that a (relatively) constant step change in current was applied to the armature of the dc machine and thus a constant accelerating/decelerating torque applied to the rotating mass. The dc machine current, torque (calculated from current) and the resulting change in speed is shown in Figure 4.19. Three step decreases in commanded speed of 0.4p.u were applied followed by one step increase of 1.2p.u at t = 16.5 sec.

Figure 4.19 – Measurement of test rig inertia. Rotor speed (red), armature current (yellow) and calculated torque (green). Vertical grid line (dotted) in div. of 1/ 16^{ths}.

Calculation of inertia

From Figure 4.19 it is noted that a current was required to overcome friction (approximately 0.4A) and also at zero speed an offset current in the dc machine flowed (-0.3A). Hence for the inertia calculation, the current required to accelerate the machine was calculated using the difference between the current during acceleration, t = 16.5 to 19.5 sec, and the current at steady state after the acceleration, t > 20 sec. The inertia is calculated as below:

From Figure 4.19 the accelerating time

$$t_{acc} = 19.5 - 16.5 \text{ sec} = 3.0 \text{ sec}$$

The accelerating current, i_{acc}, is the current reading during acceleration minus the reading after acceleration

$$i_{acc} = (0.5 + (10/16)) - (0.5 - (1/16))$$

$$i_{acc} = 1.125 - 0.438 = 0.69A$$

The torque per ampere characteristic of the dc machine is 1.24Nm/A, therefore T_{acc} the accelerating torque, applied from 0 to 1800rpm, is

$$T_{acc} = 1.24 * 0.69 = 0.86Nm$$

Rearranging Eq(2.1)

$$J = \frac{T_{acc}}{d\omega_r/dt}$$

$$\frac{d\omega_r}{dt} = (1800 * 2\pi/60) = 62.83 rads^{-2}$$

therefore

$$J = \frac{0.86}{62.83} = 0.014 kgm^{-2}$$

Using Eq(2.3)

$$H = \frac{J\omega_0^2}{2VA_{base}} = \frac{0.014\left(\frac{1500 * 2\pi}{60}\right)^2}{2 * 800} = \frac{0.014 * 157.08^2}{1600} = 0.22 \text{ sec}$$

Selection of test rig inertia scaling factor

To provide representative simulation of the effects of inertia from a MW sized turbine, a test rig inertia scaling factor, K_4 = 12.5 was chosen. This resulted in an effective test rig inertia, Eq(4.1), of

$$H_{eff} = (K_4 + 1) * H_{rig} = (12.5 + 1) * 0.22 = 2.97 \text{ sec}$$

4.6.2 Tuning of controller gains

All of the PI controllers for the test rig were tuned experimentally using the zone-based technique given in Ellis (2004). Although the use of design techniques to tune the controllers is commonly reported (Rabelo & Hofmann 2002), (Pena et al. 1996), an experimental tuning method may be considered appropriate here; the test rig was electrically noisy and this is likely to have been the limiting factor in performance as opposed to limitations due to stability criteria such as gain and phase margins (Ellis 2004).

Procedure

The zone based tuning technique utilises the fact that the proportional gain k_p and the integral gain k_i are individually dominant over different regions. The tuning technique used was as follows (Ellis 2004):

- Set k_i to zero. Set k_p low.
- Apply square wave input signal of a large amplitude but avoiding saturation.
- Raise k_p so a small amount of overshoot occurs (<5%). k_p is now set.
- Increase k_i until approximately 10% overshoot occurs, k_i is now set.

For the PI loops which were contained inside an outer loop, the inner loop was tuned first e.g the current control loop of Figure 4.11. However for the inner d-axis current control of Figure 4.13 this needed to be tuned whilst the outer loop was functioning in order to maintain control of the dc link. This was achieved by temporarily inserting a square wave oscillator and modulating the reference signal, i_{d_ref}, so that the PI controller could be tuned whilst the average value of voltage remained the same.

4.7 Summary

A laboratory based wind turbine test rig was constructed to the following specification:

- Dc machine to emulate aerodynamic torque, controlled via a model of turbine characteristics.
- 0.8kW 3-phase synchronous wound rotor machine used as the turbine generator.
- Full Power Converter (FPC) constructed using MOSFETs.
- Converter control implemented using vector control and sinusoidal PWM.
- Control implemented using a rapid prototyping system incorporating a DSP and control program description via MATLAB Simulink®.
- Additional (scaling) function to modify the dc machine electrical torque in order to increase the effective inertia of the test rig rotating mass.

A photo of the complete test rig is shown Figure 4.20.

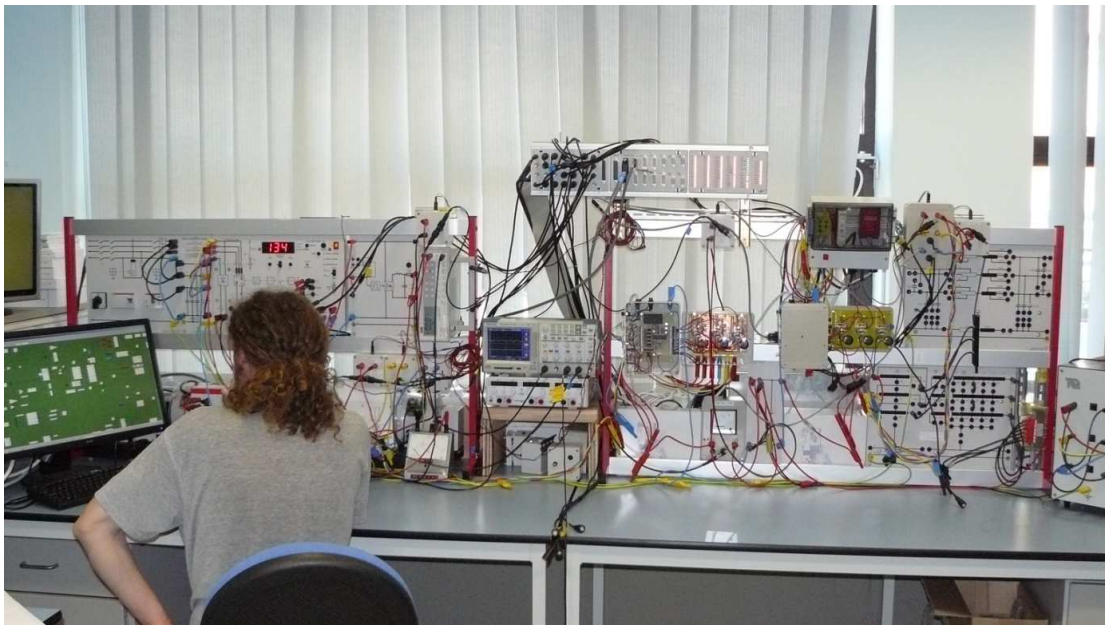

Figure 4.20 – Laboratory based wind turbine test rig.

5 Modelling of system frequency and WT inertial response

5.1 Introduction

Application of WT inertia response to support system frequency during load generation imbalances is investigated. A simple lumped mass model is presented including a wind turbine model with inertia response functions from chapter 2 implemented.

The effects of wind speed and the constant speed region of the T_{Pmax} curve on inertia response performance is evaluated. The wind turbine electrical machine and voltage source converter is represented by the simplified torque model developed in Chapter 3.

The effect of high wind capacity on the quantity of synchronous plant needed for primary response for cases with and without inertia response is shown including the effect of an increase in the maximum credible generation loss to 1800MW.

5.2 Modelling for frequency studies

5.2.1 System model

The system model is a representation of the large rotating synchronous generating plant and the power imbalances due to changes in load or prime mover input which causes increase or decrease in system frequency.

Power swing equation

For load-frequency studies the preferable quantities to analyse are power and frequency as opposed to torque and frequency. Conversion from torque to power is done as follows (Kundur 1994):

Power is the product of torque T and rotational speed ω_r and for a deviation Δ from an initial value (indicated by subscript $_0$) and with all values in p.u the torque, rotational speed and power P is given by

$$T = T_0 + \Delta T \quad (5.1), \quad \omega_r = \omega_0 + \Delta\omega_r \quad (5.2), \quad P = P_0 + \Delta P \quad (5.3)$$

Combining Eq(5.1, 5.2, 5.3)

$$P_0 + \Delta P = (\omega_0 + \Delta\omega_r)\,(T_0 + \Delta T)$$

and assuming that the product of $\Delta\omega_r$ and ΔT is comparatively small then

$$\Delta P = \omega_0\,\Delta T + T_0\,\Delta\omega_r$$

Also since $\omega_0 = 1$ and if $\Delta\omega_r$ is small then

$$\Delta P = \Delta T \qquad (5.4)$$

Hence for small speed deviations we can express the swing equation, Eq(2.4), in terms of power as

$$P_{acc} = P_{input} - P_{load} = 2H_{eq}\frac{d\omega_r}{dt} \qquad (5.5)$$

where the accelerating torque has been replaced by an accelerating power P_{acc} given by the difference between system power input P_{input} and system load P_{load}.

Lumped mass model

A model was implemented as illustrated in Figure 5.1 using a single lumped mass to represent the synchronous generating plant.

Many studies use single bus electrical models for simulating system frequency (Lalor et al. 2005), (Pearmine et al. 2007a), (Kayikci & Milanovic 2009). Here it is assumed that voltage is unaffected by frequency and that changes in electrical power consumed or supplied will result in proportional changes in current and hence where appropriate torque and mechanical power as given by Eq(5.4).

Changes in electrical power external to the synchronous generation consist of the net change in load ΔP_{load} and the wind turbine response $\Delta P_{WT.}$ Change in load is due to the load disturbance and the load damping constant D (set to 2%, see 2.1.4). Subtraction of the wind turbine response from the net load change gives the change in power ΔP_{term} at the electrical 'terminals' of the lumped mass synchronous machine.

Changes in mechanical power input to the synchronous generation are the response from synchronous governors P_{gov}, and the change of power due to a generator disturbance (e.g generator disconnection). Summation of these two power input changes minus the change in electrical output of the machine results in an accelerating power P_{acc} applied to the synchronous machine as per Eq(5.5).

The system block diagram can be reduced by removing the load damping loop such that the load damping constant D appears in the denominator of the rotating mass transfer function (Kundur 1994). Whilst investigating the synthesis of inertia it is useful to see the power flow associated only with the inertia itself (P_{acc}) hence this reduction is not done.

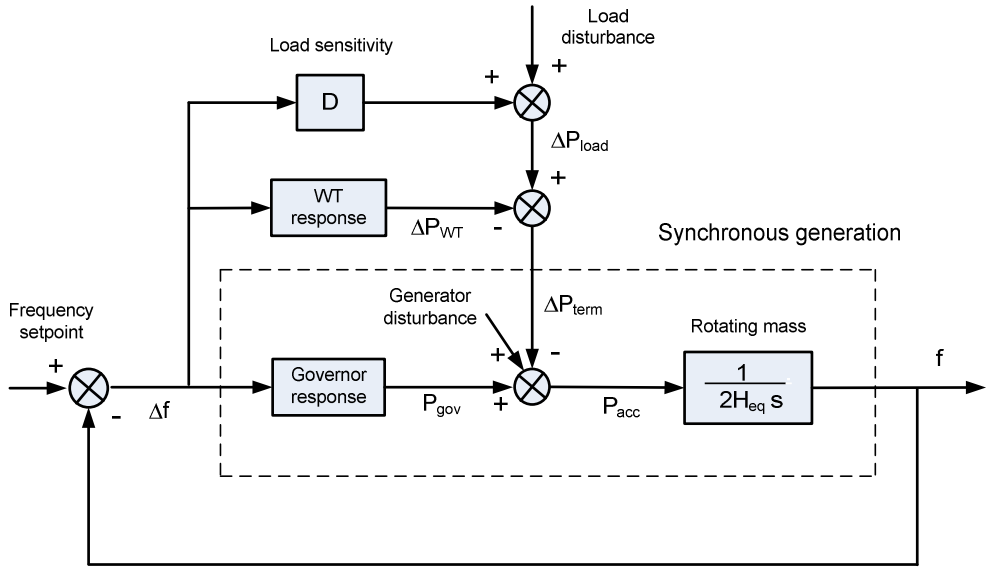

Figure 5.1 - Simulation of system frequency using lumped mass model.

Calculation of system inertia

Equivalent system inertia H_{eq} for a synchronous power system is determined by Eq (2.8). For simplification of the model the following assumptions are made

- Individual synchronous plant have the same inertia constant, H_i = 4.5 sec, regardless of plant type.
- Increased output from wind plant causes a pro-rata decrease in connected synchronous capacity.

- Increased contribution to inertia due to de-loading of synchronous plant is ignored

Thus equivalent system inertia for the model is

$$H_{eq} = \frac{\text{Demand} - \text{Wind Output}}{\text{Demand}} * 4.5 \text{ sec} \quad (5.6)$$

where the numerator is the total (post-disturbance) capacity of synchronous plant connected and the denominator, demand, is system base.

5.2.2 Governor response model

In the UK primary response has been predominantly provided by coal fired steam turbine plant, with more recently, CCGT plant becoming increasingly utilized (Pearmine et al. 2007a). Performance of plant models and real plant for both CCGT and coal fired plant are compared by Pearmine, Song & Chebbo (2007a) along with the development of a model to represent CCGT response. Since the coal-fired steam turbine model is significantly simpler, this type of plant is chosen to model the entire frequency response provided by synchronous generators.

Steam turbines convert thermal energy to rotating mechanical power for input to an electrical generator. A simplified model of a steam turbine (Kundur 1994) is shown in Figure 5.2 and is used to model the 'Governor Response' block in Figure 5.1.

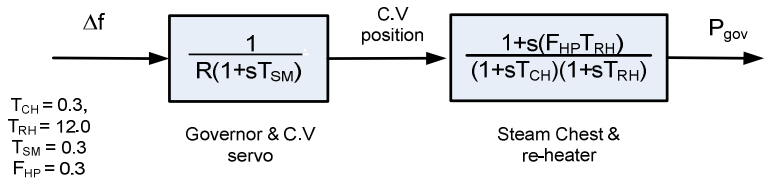

Figure 5.2 – Steam Turbine 'Governor Response' Transfer function (Kundur 1994)

The first transfer function represents the governor and Control Valve (C.V) dynamics where T_{SM} is the servo motor time constant and R is the droop. The second transfer function represents the steam chest and re-heater dynamics with time

constants T_{CH} and T_{RH} and additionally the high pressure turbine fraction F_{HP}. A schematic of the turbine is included in Appendix B3.

5.2.3 WT Response model & inertia functions

The WT model used to implement the 'WT response' block in Figure 5.1 is described below along with its constituent parts.

WT response model

Aggregate WT response is modelled as shown in Figure 5.3. Turbine speed control is achieved using the torque speed loop explained in 1.4 (WT torque speed control). Integration of the inertia functions is achieved, as explained in 2.3, by suitable summation with the maximum power torque setpoint T_{Pmax}. Similar to the system model, speed is determined by the swing equation using the turbine inertia constant H_{WT} and the difference between T_e and aerodynamic torque T_{aero}. Changes in the aerodynamic torque due to variation of rotor speed and different steady state wind speeds is modeled by the block indicated 'turbine power characteristics'.

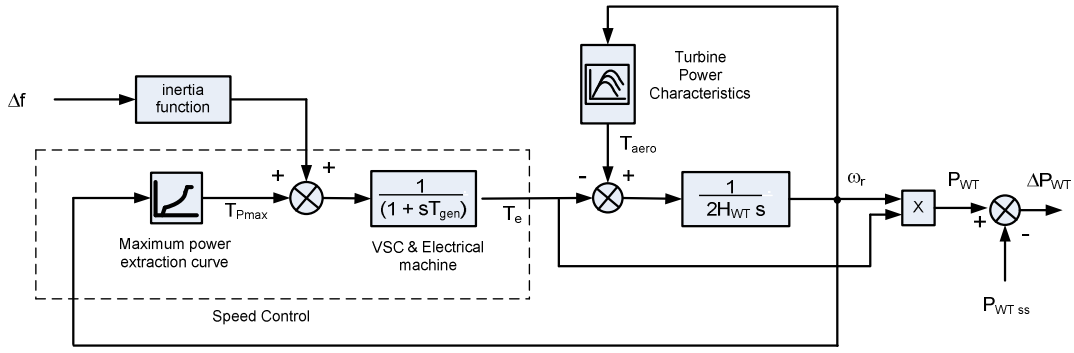

Figure 5.3 – WT response model showing turbine speed control and calculation of response output power

The turbine power response ΔP_{WT} is given by the difference between the output power during the disturbance P_{WT} and output power at steady state before the disturbance occurred $P_{WT\,ss}$ (taken from Table 5.1).

An inertia constant H_{WT} of 3.0 seconds is used which is a recommended value for use when modelling a GE 1.5/3.6 DFIG turbine (Miller et al. 2003).

VSC and electrical machine

Derivation of a suitable model to represent the combined electrical machine, VSC and vector control scheme for a variable speed FPC synchronous machine based turbine is shown in 3.4 (machine modeling & vector control Chapter). A time constant of 20ms is used for T_{gen} in the block shown Figure 5.3.

Turbine power characteristics

Turbine power output for different steady state wind speeds and variation of aerodynamic power due to changes in rotor speed are modelled using a mathematical function. Adjustment of the function parameters enables the approximation of a particular wind turbine's coefficient of performance and thus power output (Heier 2006). The 'wind turbine' block supplied in MATLAB Simulink® is utilised, its function and the parameters used are included in Appendix B2.

During each simulation wind speed is assumed constant and only one of three different speeds is chosen. These are listed in Table 5.1 along with their corresponding values of speed and torque for maximum power. For the purposes of the simulations the three wind speeds are designated as Low, Medium or High with the latter corresponding to rated speed and power.

Table 5.1 – Corresponding steady state values of torque, speed and power for the 3 different wind speeds used in the simulations

Wind Speed (Designation) m/s	**Torque p.u**	**Speed p.u**	**Power p.u**
(Low) 10.2	0.610	0.791	0.483
(Med) 11.6	0.797	0.891	0.710
(High) 13.0	1.000	1.000	1.000

Maximum power extraction curve

A plot of torque speed for the three wind speeds and the T_{Pmax} curve for the turbine is shown in Figure 5.4 a). The minimum turbine speed was set to 0.481p.u and maximum torque set to 1.0 p.u at 1.0 p.u speed. Operation of the turbine in a region

where speed is constrained (explained in 1.2.3) is modelled by curve b). Implementation of the constant speed region as a vertical section is avoided in order to prevent large oscillations in torque occurring in the simulation. Since turbine speed control may in reality be implemented using a PI type control (explained section 1.2.4) for dynamic operation, this 'near constant' maximum power extraction may be a reasonable approximation. However steady state control of speed will be inaccurate.

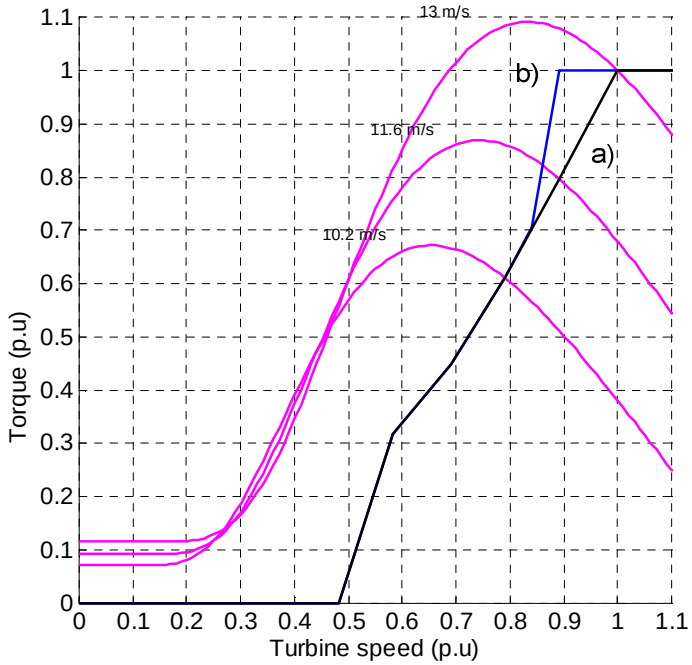

Figure 5.4 – Torque speed characteristics (magenta) for the turbine and (a) T_{Pmax} curve (black) and (b) T_{Pmax} curve with addition of near constant speed region (blue).

Inertia functions

The inertia functions implemented in the WT model are illustrated in Figure 5.5 a-i) for inertia coupling, a-ii) for inertia coupling without torque compensator, b) for step torque and c) for step power. Basic functioning is explained in Chapter 2 (Literature review). For the inertia coupling functions a filter is applied to the differentiator input with time constant T_{dif}.

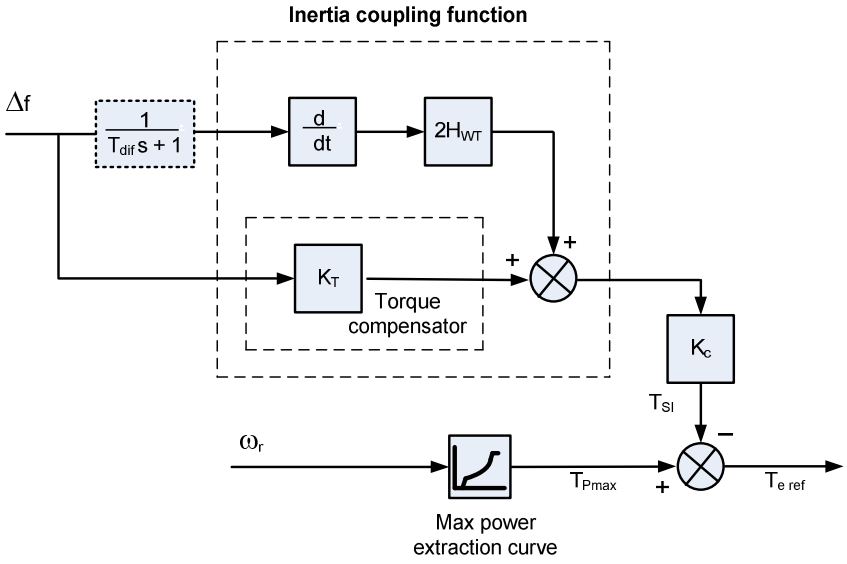
Inertia coupling function
Δf
1
T_dif s + 1
d
dt
2H_WT
K_T
Torque
compensator
+
+
K_c
T_SI
−
ω_r
T_Pmax
+
T_e ref
Max power
extraction curve

a-i)

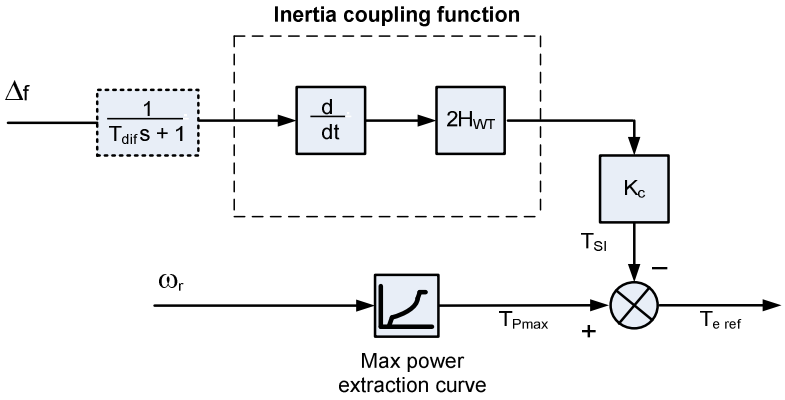
Inertia coupling function
Δf
1
T_dif s + 1
d
dt
2H_WT
K_c
T_SI
−
ω_r
T_Pmax
+
T_e ref
Max power
extraction curve

a-ii)

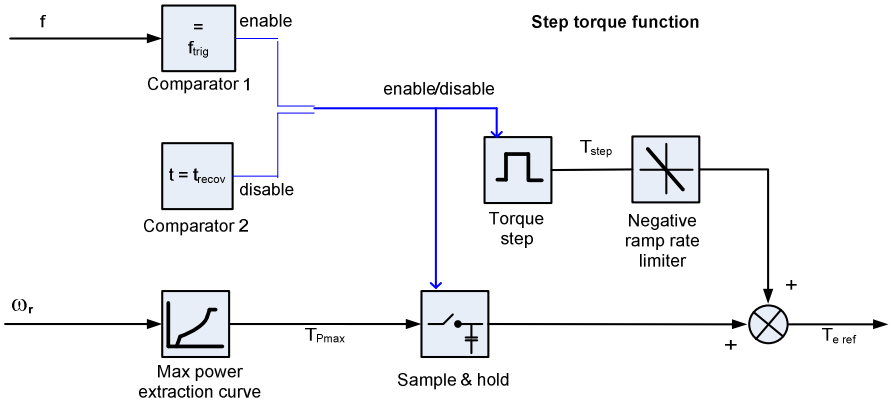
f
=
f_trig
enable
Comparator 1
Step torque function
enable/disable
t = t_recov
disable
Comparator 2
T_step
Torque
step
Negative
ramp rate
limiter
+
ω_r
T_Pmax
+
T_e ref
Max power
extraction curve
Sample & hold

b)

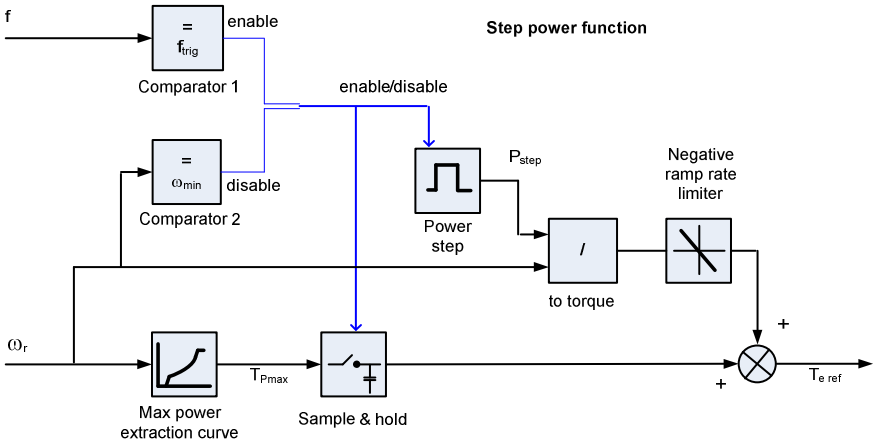

c)

Figure 5.5 – Inertia functions a-i) inertia coupling a-ii) inertia coupling without torque compensator, b) step torque and c) step power.

The step functions include the addition of a negative ramp rate limiter to smooth the change in torque which occurs when the step increase in power or torque ends.

5.3 Inertia function evaluation

Simulations are undertaken of the inertia response functions in Figure 5.5 initially for the purpose of basic evaluation. The inertia coupling function is then selected for further evaluation by parameter tuning and observation of the effects of operation with different wind speeds and use of a maximum power extraction curve which includes a constant speed region.

System setup

Plant capacities, governor response and wind turbine setup are shown in Table 5.2. The disturbance applied is a 1320MW generation loss. Responsive synchronous plant is sized such that the steady state frequency limit is just met with governor droop set as per the National Grid specification (section 2.4.2).

Table 5.2 – System setup for inertia function evaluation

Item	Setting
System	Demand 30 GW, Wind capacity 20 GW
Governor	Sync response plant 10GW, Governor droop R = 10%
Turbine	Wind speed medium, Wind output 14.2 GW Maximum power extraction curve Figure 5.4 a) unless stated otherwise as b)

5.3.1 Basic comparison

The inertia functions of Figure 5.5 were simulated with parameter settings as shown in Table 5.3.

Table 5.3 – Parameter settings for inertia functions in the basic comparison

Inertia Function (from Figure 5.5)	Parameters
(a-i) Inertia coupling	$K_T = 2.7$, $K_c = 1$
(a-ii) Inertia coupling without torque compensator	$K_c = 1$
Step Functions	$f_{trig} = 48.8$Hz
(b) Step torque	$T_{step} = 0.05$(machine p.u), $t_{recov} = 30$ sec
(c) Step power	$P_{step} = 0.025$(machine p.u), ω_{min} = -5% of steady state

For the step power function, accelerating power at the end of support is set to 10% of the power step size $P_{step.}$ Calculation of the torque setpoint for summation with T_{Pmax}, by division of P_{step} with rotor speed, uses the value of turbine shaft speed ω_r occurring at the beginning of the disturbance.

Results

Basic characteristics of the inertia functions are illustrated in Figure 5.6 plot i) to iii) after application of the generation loss at t = 0 sec. Plot i) shows turbine power response, ii) turbine rotor speed and iii) system frequency.

i)

ii)

iii)

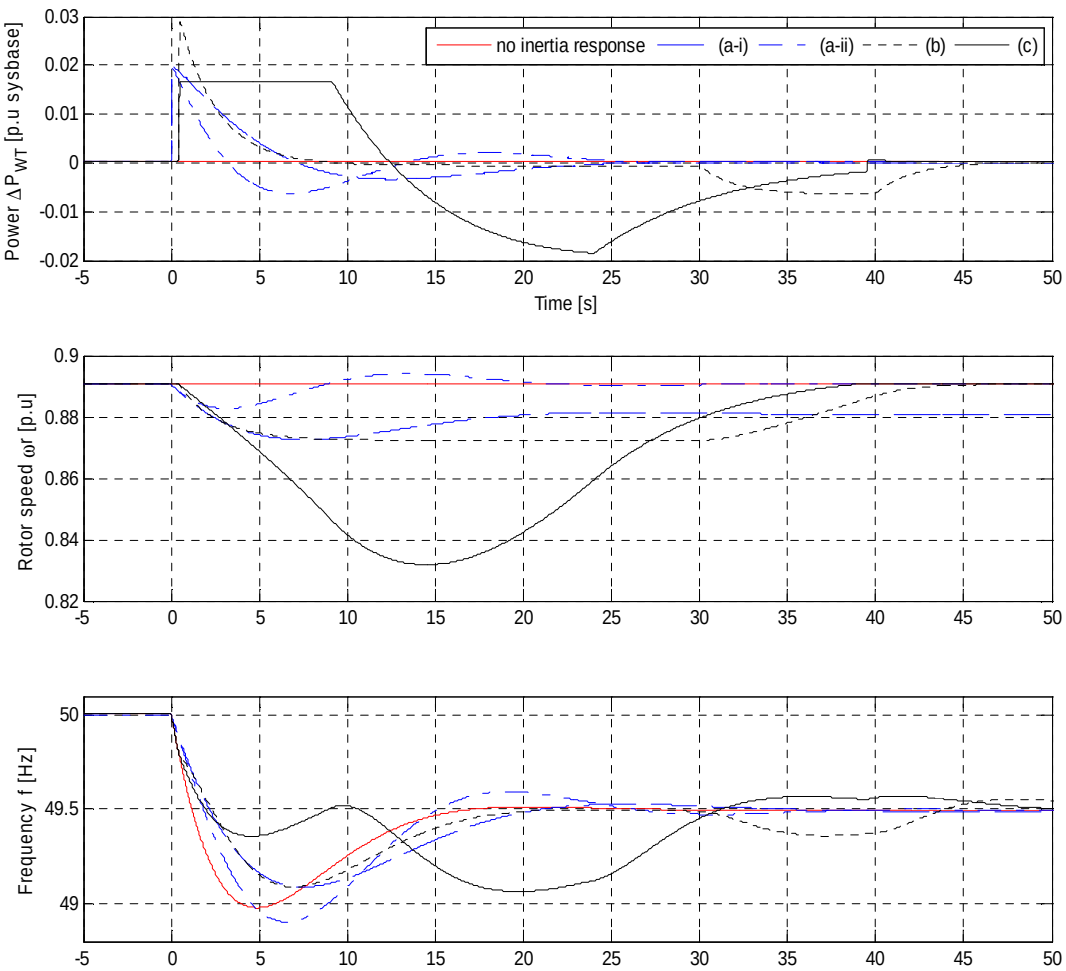

Figure 5.6 – Basic comparison of inertia functions. Wind turbine power response ΔP_{WT} (i), rotor speed (ii) and system frequency (iii) for no inertia response, (a-i) inertia coupling, (a-ii) inertia coupling without torque compensator, (b) step torque, and (c) step power functions.

The results are explained below:

Red line - No inertia response implemented, no change in turbine power occurs.

(a-i) Inertia coupling - Turbine power response, plot i), is proportional to rate of change of frequency and becomes negative at t = 7 sec when minimum frequency occurs. This function forces p.u rotor speed to closely follow p.u system frequency (shown later in Figure 5.7 ii)).

(a-ii) Inertia coupling without torque compensator - Immediately after the generation loss, turbine power is similar to (a-i), however output power rapidly drops as rotor speed drops due to the reducing maximum power extraction setpoint and reducing aerodynamic torque (explained in 2.3.1). After the disturbance has settled, (rate of change of frequency equals zero), turbine speed returns to its pre-disturbance value at t = 25 sec.

(b) Step torque - This function applies a step increase in torque which results in an initial step increase in power output. However power output immediately drops due to reducing aerodynamic torque as rotor speed decreases (explained in 2.3.2). A permanent change in rotor speed occurs similar to the inertia coupling function. Return of rotor speed to its pre-disturbance value commences when the torque step is removed at t = 30 sec.

(c) Step power – This function applies a step increase in torque which increases in magnitude as rotor speed decreases. This results in a step change in power output which is maintained constant as rotor speed changes. Similar to the step torque function the step power function shows a delay in commencement compared to the inertia coupling functions because it is triggered on frequency deviation (f_{trig} = 49.8Hz). Ending of the support phase of the step power function and recovery of turbine speed occurs when the lower speed limit is reached (speed change of -5%).

System frequency support performance can be observed in plot iii). With no inertia response (red line) minimum system frequency is 48.98Hz and the settling frequency 49.5Hz, thus exceeding the UK statutory limit for the minimum frequency by 0.22Hz (Table 2.1).

The inertia coupling function (a-i) and step torque function (b) improve the minimum frequency, plot iii), by approximately 0.11 Hz compared to the no inertia response case. A slight deterioration of 0.08Hz occurs for the inertia coupling function without torque compensator (a-ii). The step power function (c) shows a significant change in the initial minimum to 49.40Hz. This however is followed by a ‘secondary’ minimum which is as severe in magnitude as the case with no inertia response and occurs 20 seconds after the disturbance. This secondary minimum is a result of termination of the power step support and commencement of turbine

acceleration[24]. A similar but less severe 'secondary' minimum occurs for the step torque function (b) approximately 37 seconds after the disturbance.

Rate of change of frequency with the inertia coupling function (a-i) reduces from 0.37 to 0.22Hz/sec, the function without inclusion of the torque compensator (a-ii) performing slightly worse at 0.27Hz/sec. The step functions reduce rate of change of frequency to 0.18 and 0.16Hz/sec for step torque (b) and step power (c) respectively, this reduction does not occur however until after a delay of 0.6 seconds.

For time to minimum frequency the inertia coupling (a-i) and step torque functions (b) both show improvement compared to the case with no inertia response, the time to minimum being extended from 5 to 7.5 seconds. The inertia coupling function without torque compensation (a-ii) shows a small extension of 1.5 seconds to the time to minimum.

Support performance for the inertia functions in this basic comparison is summarized in Table 5.4 including overshoot which is the percentage deviation of the minimum frequency past its steady state post disturbance value.

Table 5.4 – Inertia function frequency support performance

Function	**Rate of change of frequency - initial 2 sec (Hz/sec)**	**Minimum frequency (Hz)**	**Overshoot (%)**	**Time to minimum (sec)**
No inertia response	0.37	48.98	104	5
(a-i) Inertia coupling	0.22	49.09	82	7.5
(a-ii) Inertia coupling without torque compensator	0.27	48.90	120	6.5
(b) Step torque	0.37, 0.18	49.09	82	7.5
(c) Step power	0.37, 0.16	49.40 /49.06	20/88	4.5/20

5.3.2 Further evaluation

Adjustment of the inertia coupling function by variation of its parameters is undertaken. The effect of different wind speeds and the use of a maximum power extraction curve which includes a near constant speed region is also investigated.

[24] The change in output power on termination of the step power function and re-acceleration of the turbine is unavoidable (see Figure 2.15 points **c** to **d**). A negative ramp rate limiter was added to the turbine power output to reduce the impact on system frequency which occurs during the termination and re-acceleration period (Figure 5.5c).

Parameter adjustment

The inertia coupling function, Figure 5.5 a-i), was adjusted using three parameters, K_c the coupling gain, T_{dif} the differentiator filter time constant and K_T the torque compensator gain. Each parameter was varied in turn (highlighted in bold) as shown in Table 5.5 except for case (t) where both K_c and K_T are changed.

Table 5.5 – Parameter adjustments for Inertia Coupling function

Description	Parameters
No inertia response	$K_c = 0$, $T_{dif} = 0$, $K_T = 2.7$
'Base case'	$K_c = 1$, $T_{dif} = 0$, $K_T = 2.7$
Filter applied to differentiator	$K_c = 1$, $T_{dif} = \mathbf{5.0}$, $K_T = 2.7$
Inertia coupling gain doubled	$K_c = \mathbf{2}$, $T_{dif} = 0$, $K_T = 2.7$
Shape adjustment	$K_c = \mathbf{0.33}$, $T_{dif} = 0$, $K_T = \mathbf{2.7*3}$

Inertia coupling function performance is shown in Figure 5.7 plot i) to iii) after application of the generation loss at t = 0 sec. Plot i) shows turbine power response, ii) turbine rotor speed and iii) system frequency. The five cases in Table 5.5 are explained below:

No inertia response - No change in turbine power occurs.

Base case – To facilitate comparison this case uses the inertia coupling function parameters from section 5.3.1.

Filter applied to differentiator - Addition of a first order filter with time constant 5 seconds to the differentiator input results in a smaller initial reduction in rate of change of frequency, i.e gradient of the initial frequency in plot iii), compared to the base case. However at around time t = 3 sec the turbine power response, plot i), becomes similar from then on to the base case.

Inertia coupling gain doubled - This adjustment provides a doubling of torque magnitude per unit rate of change of frequency and doubling of rotor speed change compared to the base case. A further reduction in rate of change of frequency to

0.17Hz/sec occurs and a lengthening of the time to the minimum frequency to t = 10 sec. Since wind turbine 'responsive' capacity represents 2/3 of the system capacity the increased response in this case results in a reduction in rate of change of frequency and hence a less than doubling in the magnitude of the turbine response output.

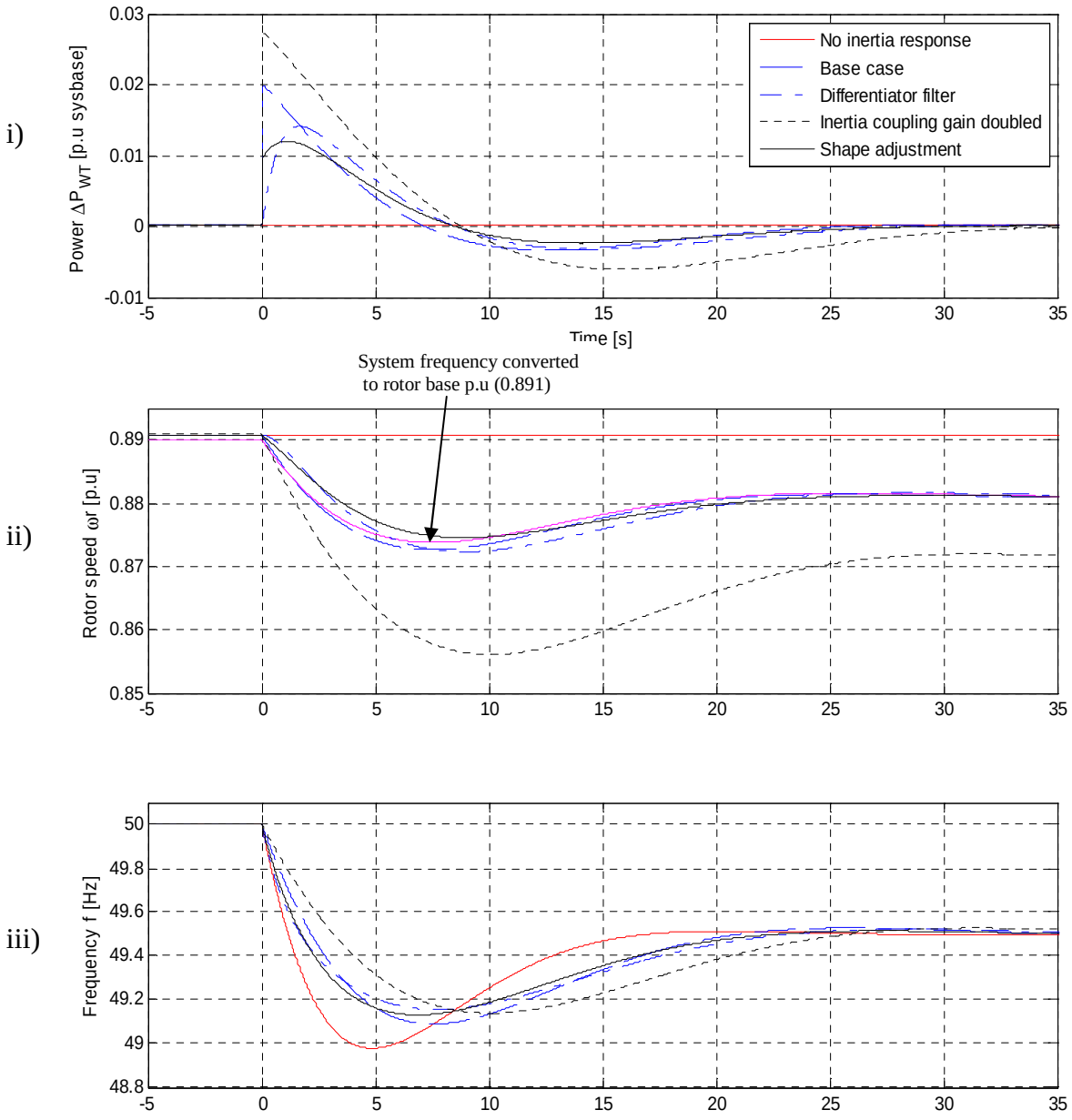

Figure 5.7 – Parameter adjustment of inertia coupling function. Wind turbine power response (i), rotor speed (ii) and system frequency (iii).

Shape adjustment - This is achieved by changing the relative contributions from the two parts of the inertia coupling function. The first part is derived from the rate of change of frequency and the value of H_{WT}, this essentially controlling the magnitude of the initial peak. The second part is the torque compensator component which determines the speed coupling. Trebling of K_T and division of K_c by three results in rotor speed change the same as the base case but with a reduction of the initial power peak by approximately half. The initial sharp increase in power at t = 0 sec similar to the base case is retained giving the response a 'knee' shape.

A characteristic of the inertia coupling function is that turbine rotor speed is made to closely follow system frequency (section 2.3.1). The solid magenta line of Figure 5.7 ii) is the accompanying system frequency from plot iii) converted to a base of 0.891p.u (the initial speed of the turbine for the base case, Table 5.1, medium wind speed). Turbine rotor speed is shown to follow system frequency, thus demonstrating the capability to replicate inertial response such as would occur if the turbine was coupled directly via a synchronous machine. The value for the torque compensator gain $K_{T,}$ 2.7, was obtained by trial and error and is a characteristic of the turbine power curve.

Support performance for the inertia coupling function after parameter adjustment is summarized in Table 5.6.

Table 5.6 – System frequency support performance for the inertia coupling function after parameter adjustments

Description	**Rate of change of frequency-initial 2 sec (Hz/sec)**	**Minimum frequency (Hz)**	**Overshoot (%)**	**Time to minimum (sec)**
No inertia response	0.37	48.98	104	5
Base case	0.22	49.09	82	7.5
Filter applied to differentiator	0.27	49.16	68	8
Inertia coupling gain doubled	0.17	49.13	74	10
Shape adjustment	0.27	49.13	74	6.5

Effect of wind speed and power extraction curve constant speed region

The inertia coupling function, using the 'base case' parameters from Table 5.5, is compared for operation at three different wind speeds (Table 5.1). To enable side by side comparison, for this section, system inertia H_{eq} is held constant at 2.17 sec which is the value of system inertia for the base case. Variation in wind speed in the model would normally affect system inertia according to Eq(5.6) and thus result in a different rate of change of frequency and thus a different quantity of response provided from the inertia function.

Lastly comparison is made at the medium wind speed using maximum power extraction curve Figure 5.4b) which includes a near constant speed region, instead of curve Figure 5.4a).

The resulting turbine power response is shown in Figure 5.8 with generation loss applied at t = 0 sec. For all the wind speeds, low, medium and high the power response profiles are nearly identical and will result in system frequency support similar to that of the base case shown Figure 5.7(b). This similarity in power response is due to the gradient of the maximum power extraction curve and gradients of the turbine torque curves being similar for the three wind speeds simulated.

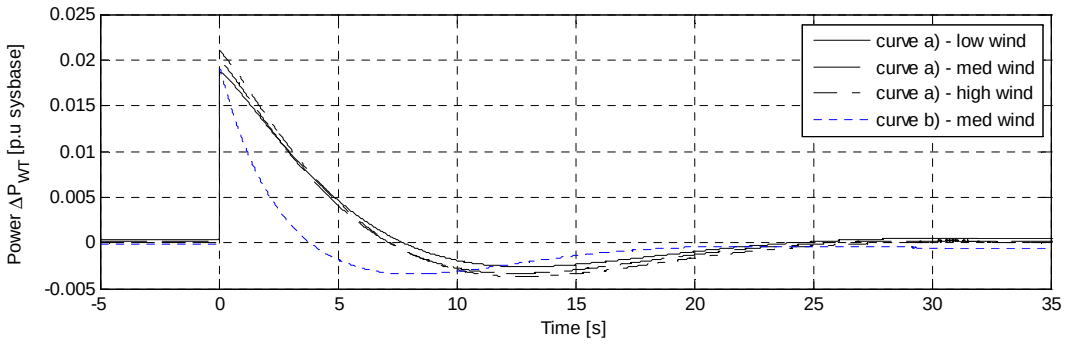

Figure 5.8 – Wind turbine power response ΔP_{WT} using maximum power extraction curve a) of Figure 5.4 for low , medium and high wind and curve b) with medium wind.

Power response using the near constant speed maximum power extraction curve b), shows a marked decline after the initial step increase compared to curve a). The response becomes negative at around t = 4 sec which is 1 second longer than the

response from the inertia coupling function without torque compensator shown in Figure 5.6i)(a-ii). This reduction in power response is due to the torque compensator (explained section 2.3.1) no longer being sufficient to make-up for the reducing value of T_{Pmax} as rotor speed reduces.

5.4 System performance with WT inertial response

Simulations are undertaken to illustrate the effect of demand size, generation loss size and speed of inertia response on the capacity of synchronous plant needed for primary response.

System sizing

The 2020 'Gone Green' scenario predicts peak and minimum demands of 57.5GW and 23GW respectively and a wind capacity of 26.8GW (National Grid 2011b). For the simulations, 60, 45 and 30 GW was chosen to represent peak, medium and minimum demand. Coincidence of the low demand (23GW) with wind output greater than 75% is estimated to be less than 3 times a year (National Grid 2011b) hence a larger (less extreme) minimum demand of 30GW is taken to be more representative for the purposes of this investigation (where wind output is high).

Wind capacity is set to 20GW, operating at an output of 14.2GW (medium wind speed, Table 5.1), this representing approximately 50% of the peak output from predicted 2020 installed wind capacity. With demand at 30GW this approximates to a '50% wind penetration' scenario.

Settings used for the simulations are summarized in Table 5.7

Table 5.7 – System, synchronous responsive plant and wind turbine setup

Item	Setting
System	Demand 60, 45 and 30GW, Wind capacity 20GW
Synchronous plant for primary response	Governor droop R = 10%, Plant capacity adjustable
Wind turbine	Wind output 14.2GW, Maximum power extraction curve Figure 5.4 a), Inertia Coupling function $K_T = 2.7$ $K_c = 1$

5.4.1 Variation of demand size and generator loss

For each demand size a generation loss is applied with the quantity of primary response synchronous plant adjusted[25] such that statutory frequency limits (Table 2.1) are met. The effect of wind capacity and inclusion of inertia response is shown for each case. Simulations are then repeated with a larger generation loss.

Results - 1320 MW loss

System frequency is shown in Figure 5.9 i) to iii) for a 1320MW generation loss at t = 0 sec. The respective rate of change of frequency, time to minimum frequency and synchronous plant capacities are shown in Table 5.8.

i)

ii)

iii)

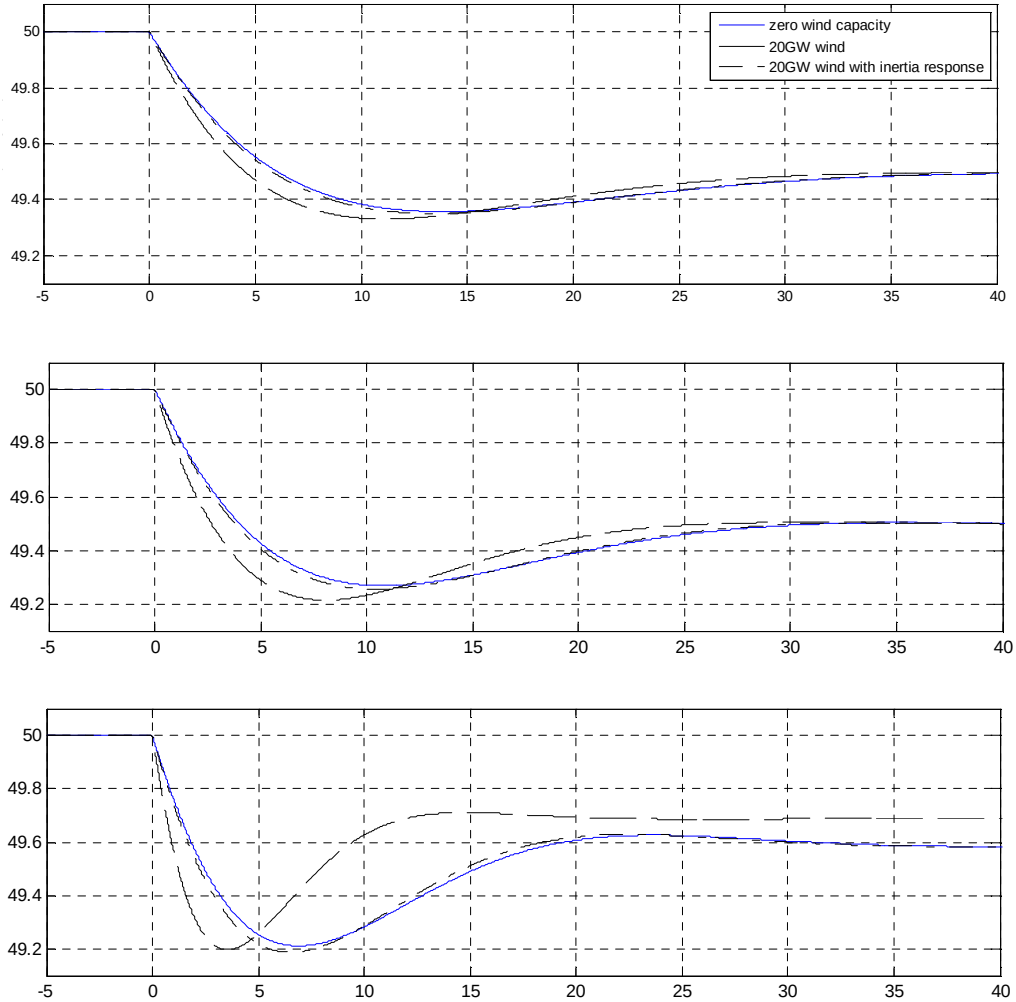

Figure 5.9 - System frequency for 1320MW generation loss with quantity of synchronous responsive plant adjusted to meet mandatory frequency limits.

[25] The quantity of synchronous plant providing governor response was found by trial and error. For a mathematical method of calculating the level of response needed see Kundur (1994).

i) Demand 60GW – Primary response synchronous plant capacity of 7GW is required for all cases to meet the steady state frequency limit of 49.5Hz. The 20GW wind case results in a lower frequency minimum and an earlier time to minimum but these are well within limits.

ii) Demand 45GW – Similar to i) frequency is controlled to within limits, in this case needing an increase in the primary responsive plant to 8.5GW for all three cases to meet the steady state limit. This increase is due to reduced contribution from load sensitivity to frequency. The minimum frequency without inertia response is approaching the 49.2 Hz limit.

iii) Demand 30GW – In all cases the steady state frequency is higher than required at 49.6 and 49.7Hz. An increase in the quantity of synchronous responsive plant is needed for all cases in order to prevent the minimum frequency limit being exceeded. For the zero wind capacity case 13GW of synchronous responsive plant is needed, for the 20GW wind case 18GW of synchronous responsive plant is needed and for the 20GW wind with inertia response case 13GW of synchronous responsive plant is needed. Note that for at 30GW demand, only 10GW of responsive synchronous plant was needed to meet the steady state limit (shown section 5.3).

The largest rate of change of frequency 0.35Hz/sec occurs at demand 30GW with 20GW wind and shows a substantial increase (66%) compared to the zero wind capacity case. Time to minimum frequency is below 10 seconds at demand 45GW with 20GW wind and all cases for demand 30GW where a value between 7 and 3.5 sec is obtained.

Results - 1800MW loss

The 1800MW generation loss gives similar characteristic system frequency profiles to Figure 5.9. The rate of change of frequency, time to minimum frequency and synchronous plant capacities are shown in Table 5.8.

The necessity to increase the primary response, to prevent the minimum frequency limit being exceeded, occurs at 45GW and below, rather than only at 30GW for the 1320GW loss. With 30GW demand the quantity of primary response synchronous plant needed (25 to 36 GW) exceeds the capacity of synchronous plant

on the system, 14GW, for all cases. (For the 1320MW loss this capacity shortfall only occurs for demand 30GW with 20GW wind).

Time to minimum frequency is below 10 seconds in all cases except demand 60GW with zero wind capacity and demand 60GW with 20GW wind with inertia response, the lowest value being 2.3 seconds for demand 30GW with 20GW wind without inertia response. Rate of change of frequency for this last case exceeds 0.5Hz/sec during the first second.

Table 5.8 – Synchronous plant sizes, rate of change of frequency and time to minimum frequency for three demand and two generation loss sizes where (u) corresponds to zero wind capacity, (v) to 20GW wind and (w) 20GW wind with inertia response.

Demand (GW)	**Total synchronous plant (GW), System H_{eq}(sec)**		**Primary response synchronous plant capacity (GW)**			**Rate of change of frequency initial 2 sec, 1 sec (Hz/sec)**			**Time to minimum frequency (sec)**		
	(u)	**(v&w)**	**(u)**	**(v)**	**(w)**	**(u)**	**(v)**	**(w)**	**(u)**	**(v)**	**(w)**
1320MW loss											
i) 60	58.7, 4.4	44.5, 3.3	7	7	7	0.12	0.14	0.12	14	11	14
ii) 45	43.7, 4.4	29.5, 3.0	8.5	8.5	8.5	0.15	0.20	0.15	11	8	11
iii) 30	28.7, 4.3	14.5, 2.2	13	18	13	0.21	0.35	0.23	7	3.5	6.5
1800MW loss											
i) 60	58.2, 4.4	44.0, 3.3	12	12	12	0.15	0.19	0.15	10.5	8.5	10.5
ii) 45	43.2, 4.3	29.2, 2.9	15	18.5	15	0.20	0.26	0.20	8.0	5.5	7.5
iii) 30	28.2, 4.2	14.0, 2.1	25	36	25	0.28	0.40, 0.57	0.30	4.7	2.3	4.5

5.4.2 Interaction with synchronous response

Wind turbine inertia response is constrained by use of the first order filter, time constant 5 seconds, applied to the inertia function differentiator input (case (r) section 0). Settings for the simulation are as shown in Table 5.7 with demand 30GW, this giving the approximate ‘50% wind penetration’ scenario. Synchronous plant capacity for primary response is set to 13GW.

Components of response

For a generation loss the 'net power disturbance' is equalled (see Figure 5.1) by the sum of the synchronous response P_{gov}, the wind turbine response ΔP_{WT} and the power associated with the change in speed of the rotating mass P_{acc} :

$$\Delta P_{load} \text{ - generator disturbance} = P_{gov} + \Delta P_{WT} - P_{acc} \qquad (5.7)$$

The magnitude of P_{acc} determines the rate of change of frequency (Eq(2.7)).

Results

Synchronous response P_{gov}, combined response P_{gov} + ΔP_{WT} and net power disturbance are shown Figure 5.10 i) to iii) for a generation loss of 1320MW at t = 0 sec.

i)

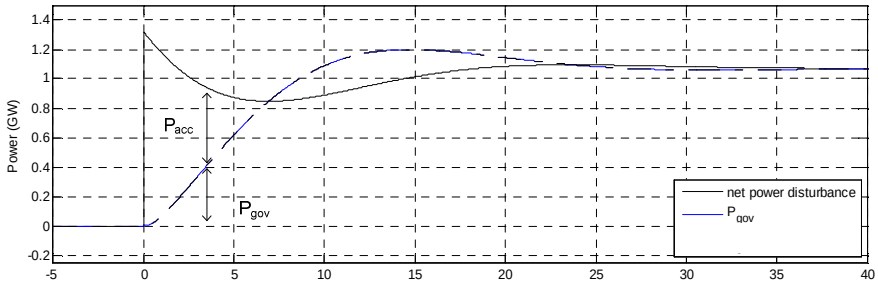

ii)

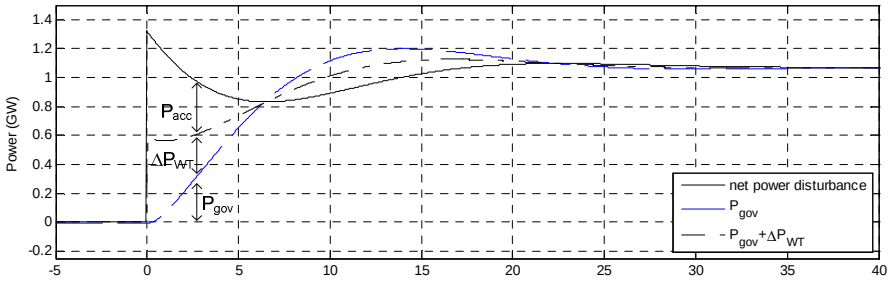

iii)

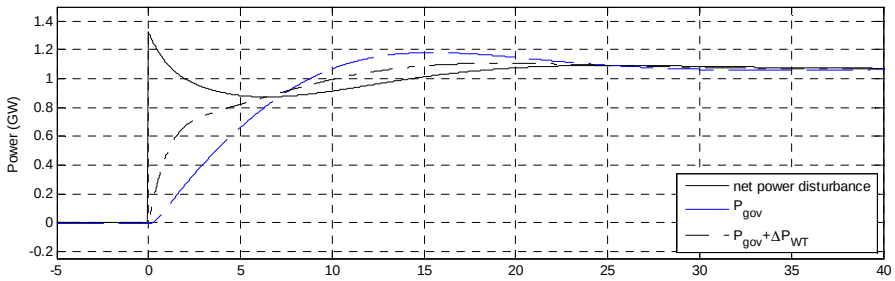

Figure 5.10 - Synchronous response P_{gov}, combined response (P_{gov} + wind turbine response ΔP_{WT}) and net power disturbance for i) wind capacity zero, ii) wind with inertia response and iii) inertia response with addition of the df/dt filter.

i) Wind capacity zero – Synchronous response P_{gov} is 1.09GW at t = 10 sec, peak response 1.20GW and the steady state response 1.07GW. The accelerating power P_{acc} magnitude is indicated which gradually reduces until the synchronous response equals the net power disturbance at t = 7 sec this also being the point at which the frequency minimum is reached. The net power disturbance at this point has reduced from an initial 1320MW to 850MW due to the effect of load frequency sensitivity.

ii) Wind with inertia response – Synchronous response is similar to i) with responses at t = 10 sec, peak and steady state of 1.11, 1.20 and 1.07GW respectively. Of the initial 1.32GW disturbance at t = 0, wind turbine inertia response provides just under half (0.59GW) of the power to meet the net disturbance with the remaining power shortfall being met by the release of rotational K.E of magnitude P_{acc}.

iii) Inertia response with addition of df/dt filter – Synchronous response is again similar to i) with 10 second and peak values of 1.07 and 1.18GW respectively. Initial rate of change of frequency is high due to the magnitude of P_{acc} being equal to the net disturbance. Wind turbine inertia response peaks at t = 2 sec at a value of 0.40GW (0.02 machine p.u).

The effect on frequency of application of the df/dt filter was shown in 0 (parameter adjustment) to be minimal, a slight improvement in the minimum frequency occurring.

Response levels and ramp rates are summarised in Table 5.9.

Table 5.9 – Levels of response with and without inertia response constrainment

	Equivalent to 5.4.1	**Synchronous response 10 sec, peak, steady state**		**Ramp Rate[26]**		**Wind Turbine response peak**		**Ramp Rate[27]**	
		GW	**On machine base p.u.**	**GW.sec^{-1}**	**On machine base p.u.sec^{-1}**	**GW**	**On machine base p.u.**	**GW.sec^{-1}**	**On machine base p.u.sec^{-1}**
i)	1320 iii)(u)	1.09, 1.20, 1.07	0.084, 0.092, 0.082	0.126	0.049	0	-	0	-
ii)	1320 iii)(w)	1.11, 1.2, 1.07	0.085, 0.092, 0.082	0.131	0.050	0.59	0.030	Step	-
iii)	1320 iii)(w) with df/dt filter	1.07, 1.18, 1.07	0.082, 0.091, 0.082	0.134	0.051	0.40	0.020	0.20	0.010

5.5 Discussion

Inertia response

The inertia coupling function, chosen for further evaluation, showed the following characteristics:

- Control of turbine rotor speed to mimic the change in rotor speed of synchronous plant during the load generation imbalance. This resulted in system frequency deviation similar to that which would occur with entirely synchronous generation.
- Change in turbine rotor speed small enough not to affect steady state power output of the turbine. A distinct re-acceleration function as applied to the step power function was therefore not needed.
- Capability to adjust power ramp rate via the df/dt filter and smoothing of the power output peak via parameter adjustment. Adjustability of these characteristics may be beneficial for reduction of wind turbine structure,

[26] Measured over first 5 seconds
[27] Measured over first 2 seconds

blade and drive-train loadings. Use of the filter may in fact be necessary to avoid amplification of noise.

Operation of the turbine in the constant speed region (see Figure 5.4b) of the maximum power extraction curve results in less than optimum power production. Further reduction in turbine speed for inertial response will result in a further decrease in power. Inertia response whilst operating in the constant speed region would require adjustment or modification of the inertia coupling function presented and closer assessment of the shape of the turbine power curve.

Provision of an increased inertial response by increasing of the coupling gain K_c was shown. The extent of this capability to 'artificially' increase the turbine inertia would similarly depend on the shape of the turbine power curve when operating away from the maximum power point such as occurring during operation in the constant speed region. For comparison a C_p curve for the GE 3.6MW DFIG turbine is shown in Appendix B2.

System performance with WT inertia response

The quantity of synchronous plant for provision of primary response was shown to increase as demand dropped and when generation loss was larger. At low demand and with the larger generation loss the 49.2Hz lower frequency limit became dominant with extra response needed to meet this limit, steady state frequency deviation being well above 49.5Hz. These results were in keeping with those shown in Pearmine, Song & Chebbo (2007b).

Adequate restoration of system performance (rate of change of frequency, time to minimum frequency and frequency minimum) with WT inertia response was shown in all cases. Constrainment of inertia response with the df/dt filter showed no significant interaction with the synchronous response. For the cases of wind operating without inertia response a substantial increase (approximately 40%) in the quantity of synchronous plant for primary response was needed at low demand.

For the 1800MW disturbance, time to minimum frequency was substantially less than 10 seconds. Existing grid connection codes specify synchronous response to be provided within 10 seconds (National Grid 2010b). Modelling of the synchronous response (5.2.2) may not be accurate for these rapid frequency deviations. Rate limited and peak limited synchronous response models which may represent

response more accurately for these cases are shown in Pearmine, Song & Chebbo (2007a).

5.6 Conclusion

The modelling studies undertaken showed that:

- Introduction of 'de-coupled' variable speed wind turbines necessitated an increase in the quantity of synchronous plant providing primary response. This became more pronounced as demand reduced and with the larger generation loss.
- Restoration of system performance was possible by inclusion of an inertia response from the wind turbines. This negated the need for an increase in the synchronous plant capacity providing primary response.
- 'Synthesis' or 'restoration' of turbine inertia was possible using the 'inertia coupling' function (Figure 5.5a-i), which forced turbine speed to closely track system frequency.
- Application of a filter to the inertia coupling differentiator, in order to reduce possible noise and reduce turbine loadings, did not adversely affect the inertia response provided or adversely interact with the response from synchronous plant.
- The inertia response was unaffected by a range of wind speeds tested. Some reduction of response output occurred when operating within the constant speed region of the maximum power extraction curve but this was considered to be rectifiable by suitable modification of the controller.

The step power function reviewed in chapter 2 showed capability to extract maximum K.E from the turbine for system support. The inertia coupling function is arguably simpler in that it does not need triggering or turbine re-acceleration after use. Capability to provide increased support, if desired, was shown possible by increasing the 'gain' of the inertia coupling. Further evaluation of the function in 0 and consideration of interaction with synchronous response 5.4.2 showed no major issues. Hence the inertia coupling function Figure 5.5 a-i) is selected for experimental testing in chapter 6.

6 Experimental testing of wind turbine inertia response

6.1 Introduction

Two areas of testing were undertaken using the test rig described in Chapter 4. The first was functional testing in order to confirm correct operation of the generator vector control (described 3.4.2) and correct operation of the turbine maximum power control (described 4.4.1 and 4.4.2). The second area of testing was implementation of the inertia coupling function (described section 2.3.1 and simulated in 5.3). The tests are described in the following sections.

Note that for both the functional tests and the inertia response test, the test rig was operated at a reduced output[28] in order to minimise electrical noise.

6.2 Functional tests

6.2.1 Generator torque control

This test examined the operation of the generator vector control which was implemented as shown Figure 4.12. The test rig was operated in manual speed control mode with the speed reference ω_{ref_man} set to 0.9p.u. The maximum power extraction control block (Figure 4.1), which normally supplies the generator torque reference, was bypassed and a step increase (doubling) in q-axis current reference, i_{q_ref}, directly applied to the q-axis current control loop.

Results

Figure 6.1(i) to (iii) shows the performance of the generator q-axis control loop and also the coupling effect on the d-axis control loop for a step increase in i_{q_ref}, from 0.2 to 0.4p.u, at approximately t = 0.4 sec. The d-axis current reference was set to 0.15p.u. The results are explained below:

(i) q-axis current, i_q, showed an immediate step change with the reference. Power output from the grid converter, P_{grid}, also immediately rose, but relatively slowly, and reached a steady state after 0.3 sec. Rotor speed, ω_r, was seen to dip momentarily as the speed control loop responded. The change in q-axis current was seen to cause an immediate disturbance in the d-axis current, i_d, of approximately 0.06p.u magnitude.

[28] Under normal operation a signal value of 1p.u corresponds to a power output of 800W from the test rig.

(ii) & (iii) These two plots show the terminal voltage setpoints, V_d and V_q, input to the PWM and applied at the generator terminals by the VSC. Also shown are the two components which make up the respective V_d and V_q setpoints which are $V_{d'}$, $V_{q'}$, the outputs from the PI control, and V_{d_spd} and V_{q_spd}, the (speed voltage) cross coupling terms[29].

At the start of the step increase in i_{q_ref}, the q-axis voltage V_q, plot (ii), showed a large drop in voltage from (approx) 0.5 to 0.35p.u and then returned to a steady state value, at t = 1.1 sec, slightly lower than before the step (indicated as ΔV_q).

The d-axis voltage V_d, plot (iii) showed a slow increase from 0.3 to 0.6 p.u beginning at t = 0.4 sec and settling by around t = 0.7 sec. This increase (indicated as ΔV_d) is due to the change in q-axis current. The change in the output from the d-axis control loop was composed principally of the cross decoupling term V_{d_speed}.

[29] Note that both of the cross coupling terms were passed through first order filters (time constant 0.03 sec) to prevent the introduction of noise from one axis to the other.

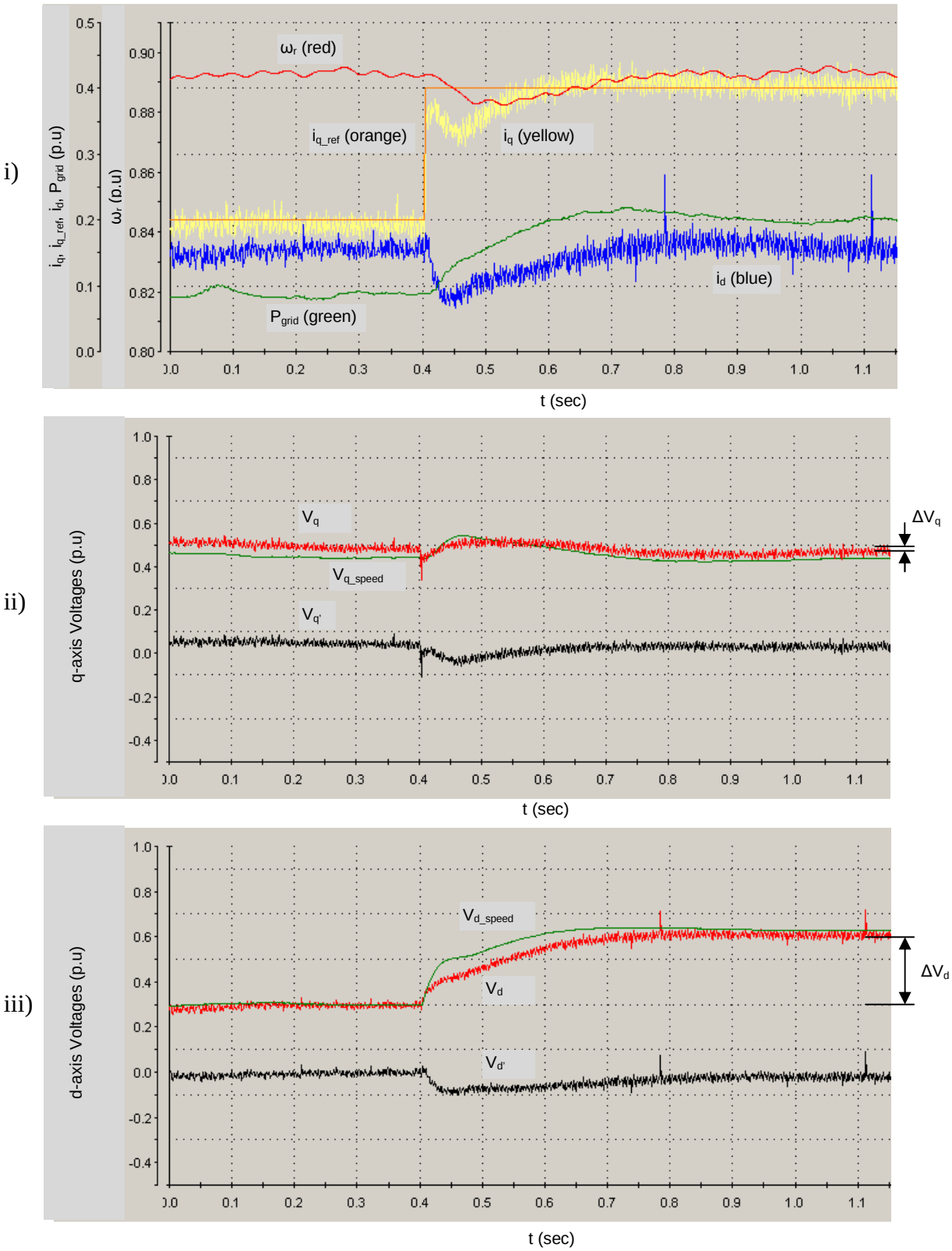

Figure 6.1 – Generator step torque test showing (i) q-axis and d-axis currents, (ii) control signal components for V_q and (iii) V_d.

The corresponding changes in generator phase currents during the test are shown in Figure 6.2(i) with a magnified view shown (ii). A step increase in the phase currents occurred at t = 0.41 sec. Concurrent with q-axis current and output power shown in Figure 6.2, the phase currents also exhibited a large settling time reaching their steady state value approximately 0.5 sec after the step.

i)

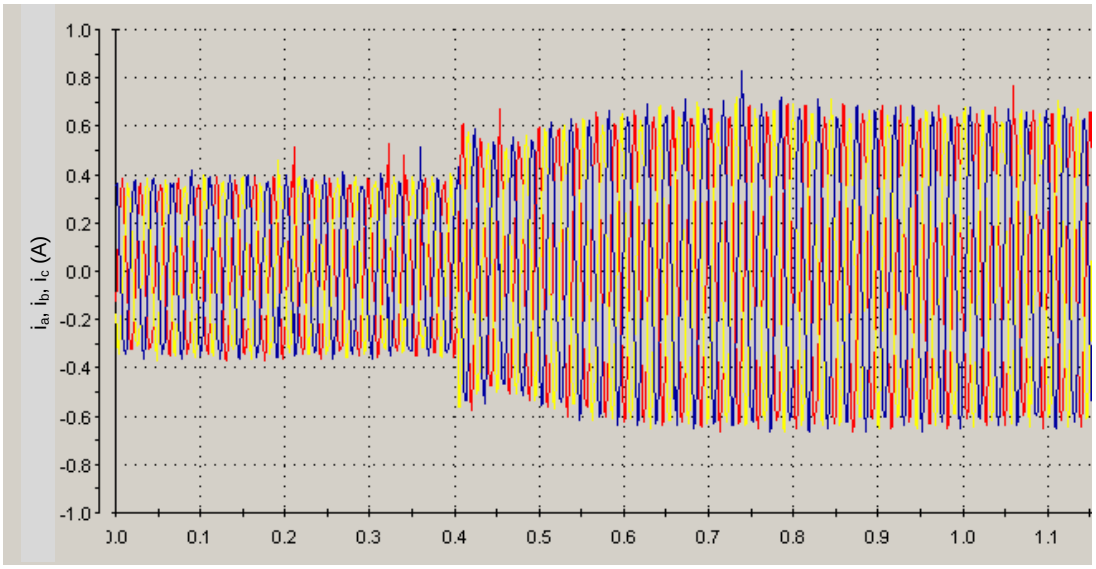

ii)

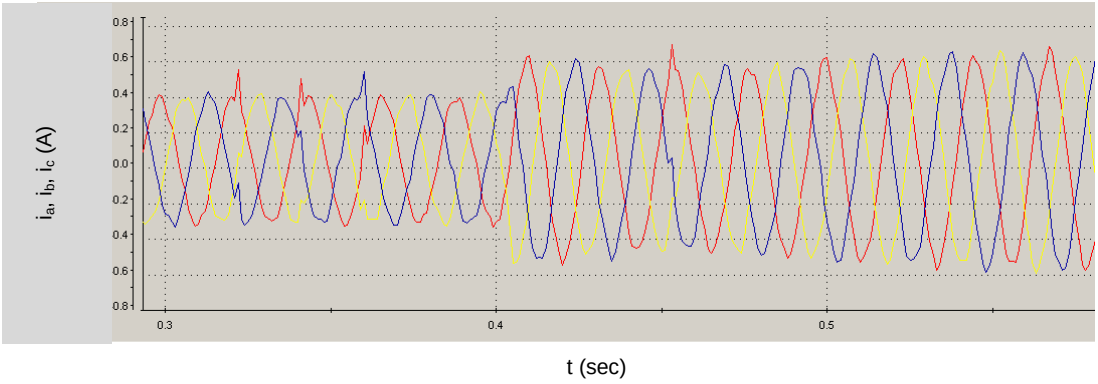

Figure 6.2 – Generator phase currents during the step torque test (i) and magnified view (ii).

6.2.2 Turbine maximum power control

This test examined the operation of the maximum power extraction control and the emulation of aerodynamic torque.

A step increase from 10.2m/s to 11.6m/s was applied to the wind speed input U_{wind} (shown Figure 4.11).

Results

Figure 6.3 shows the plot of wind speed input U_{wind}, rotor speed ω_r, aerodynamic torque T_{aero} and the generator's (maximum power) torque reference T_{Pmax} verses time. Point **a** corresponds to the steady state values of torque just before the step change in wind speed, when T_{aero} is equal to T_{Pmax}. Point **b** is the new aerodynamic torque after the step change at t = 1.5 sec. The turbine accelerated until the new equilibrium operating point was attained, point **c**, at approximately t = 12 sec.

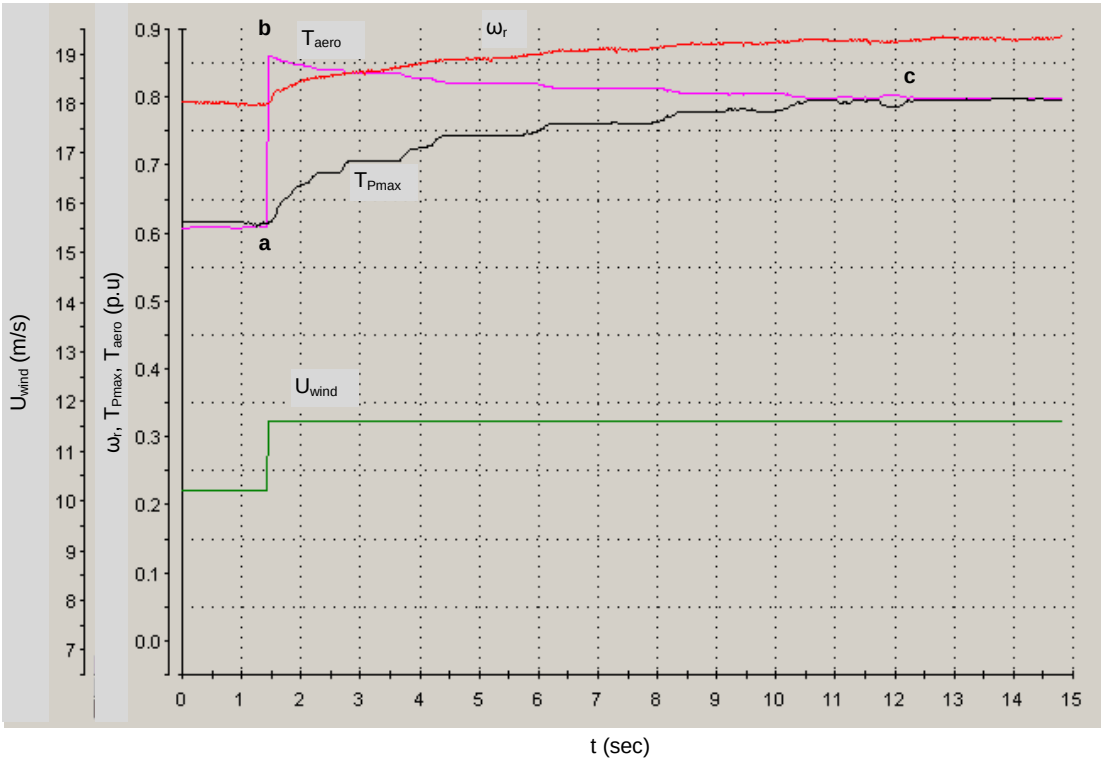

Figure 6.3 – Test rig response to step change in wind speed, 10.2 to 11.6 m/s, showing aerodynamic torque, generator reference torque and rotor speed.

The results for the test are also shown in an x-y plot format in Figure 6.4 with T_{aero} and T_{Pmax} on the y-axis and ω_r on the x-axis. Superimposed onto the plot is a graph

of the turbine's torque/power verses speed characteristics (Figure 5.4) and maximum power extraction curve (Figure 4.15). The track of operating points during the test is shown between points **bc** for the aerodynamic torque and between points **ac** for the maximum power torque reference.

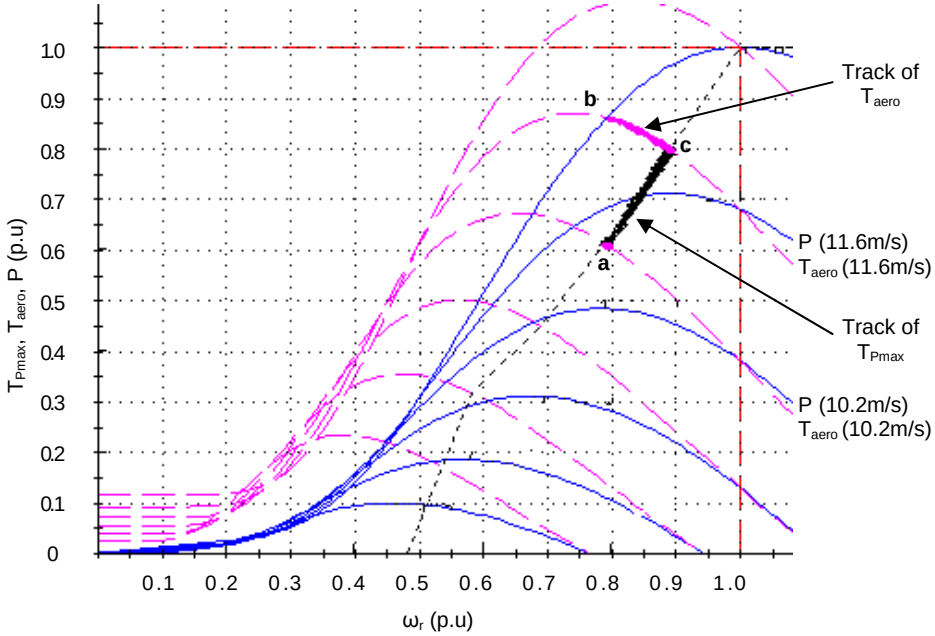

Figure 6.4 - Test rig response to step change in wind speed showing the track of generator torque and aerodynamic torque during the test.

The correct functioning of the test rig inertia scaling function (4.4.1) was confirmed by the results from this test (calculations shown in Appendix A5).

6.3 Wind turbine inertia response test

The inertia coupling function, Figure 5.5(a-i) was chosen for testing and was introduced into the generator torque speed control (as indicated in the Figure) by subtraction of the additional accelerating torque, $T_{SI,}$ from the generator maximum power setpoint T_{Pmax}. This test simulated the change in grid frequency by the injection of a frequency test signal into the wind turbine control system via the inertia function's frequency input. The profile of the test signal was based upon the frequency deviation shown in Figure 5.7(iii) for the case where the inertia coupling gain K_c is doubled.

The inertia coupling function was tested with parameter variations (i), (ii), and (iii), as listed in Table 6.1. The simulations performed in Chapter 5 which closely correspond to this experimental test are also listed. Note that to help reduce noise, for the first test, (i), the differentiator filter's time constant T_{dif} is set to 1 sec instead of the zero used in the simulation. Similarly for the last test, (iii), the filter time constant is left high at 5 sec. These differences are highlighted in bold.

Table 6.1 – Parameter settings for the experimental inertia response test and corresponding simulations and parameters from Chapter 5.

Experimental test (Figure 6.5)	**Corresponding simulation (Figure 5.7, Table 5.5)**
(i) Small time constant for the differentiator filter $K_c = 1$, $\mathbf{T_{dif} = 1}$, $K_T = 2.7$	(q) 'base case' $K_c = 1$, $T_{dif} = 0$, $K_T = 2.7$
(ii) Filter applied to differentiator $K_c = 1$, $T_{dif} = 5$, $K_T = 2.7$	(r) Filter applied to differentiator $K_c = 1$, $T_{dif} = 5$, $K_T = 2.7$
(iii) Inertia coupling gain doubled and differentiator filter time constant 5 sec $K_c = 2$, $\mathbf{T_{dif} = 5}$, $K_T = 2.7$	(s) Inertia coupling gain doubled $K_c = 2$, $T_{dif} = 0$, $K_T = 2.7$

6.3.1 Results

Results for the test are shown in Figure 6.5. Rotor speed, ω_r, and the frequency test signal, Δf, are both in p.u. Similar to Figure 5.7 in Chapter 5, the frequency signal is shown with its p.u base converted from 50 Hz to the base of the rotor speed before the disturbance (0.891p.u). The accelerating torque from the inertia coupling function, T_{SI}, and the change in power output to the grid, ΔP_{grid}, are both in p.u and shown multiplied by 10. This is necessary since a change in system frequency of approximately 1Hz (only 0.02p.u) results in a relatively small exchange of K.E for a synchronised rotating generator. The test results are explained below:

(i) Small time constant for the differentiator filter – This case demonstrated the inertia coupling function's ability to force rotor speed to closely follow system frequency. The additional torque demand, T_{SI}, added to the torque speed control, has a sharp rise and peaks 2.5 sec after the start of the frequency disturbance. The power output to the grid also changes with a similar profile to T_{SI}. At t = 30 sec the output T_{SI} remains slightly higher than its original value of zero. This steady state increase is from the torque compensator part of the inertia coupling function (explained

2.3.1) which acts to counteract the drop in the torque reference T_{Pmax}, from the maximum power extraction curve. The change in the generator q-axis current reference, i_{q_ref}, and the measured q-axis current, i_q, also show a similar change to T_{SI}, a step increase followed by a gradual decline.

(ii) Filter applied to differentiator - Rotor speed is again demonstrated to be coupled to system frequency. However due to the increased time constant of the filter, which reduces the rate of rise of T_{SI}, a slower change in rotor speed occurs and the rotor speed does not match system frequency until t = 20 sec. The peak value of the change in power output to the grid is 0.01p.u, this being lower compared to (i) which was 0.015p.u.

(iii) Inertia coupling gain doubled and differentiator filter time constant 5 sec - This case resulted in a quicker rise time for T_{SI} and doubled the change in rotor speed, hence doubling the quantity of K.E exported to the grid during the speed change (area under the plot of ΔP). The peak change in power was just over 0.015p.u. At the end of the disturbance, t = 27 sec, the rotor speed was still changing indicating a settling time much greater than in the case of (i) or (ii).

Note that the plots of P_{grid} and i_q are not smooth and appear to have a noise component of approximate period 2.5 sec. This was identified as problem with the controller PLLs and is not related to the torque control or synthetic inertia function.

i)

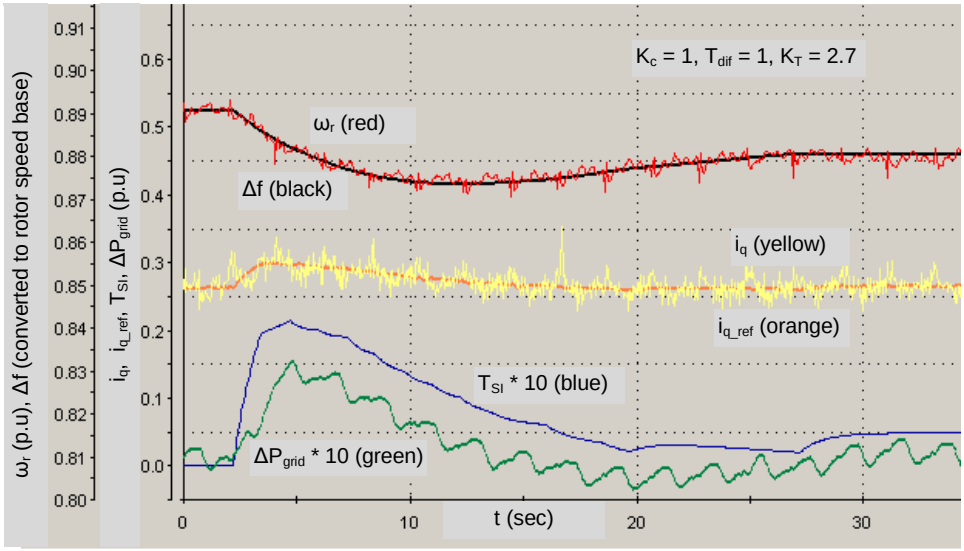

ii)

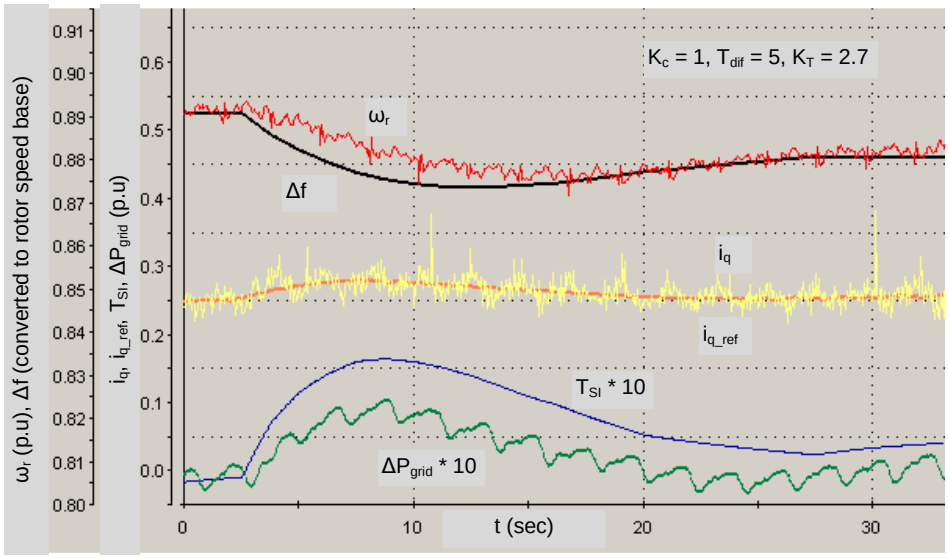

iii)

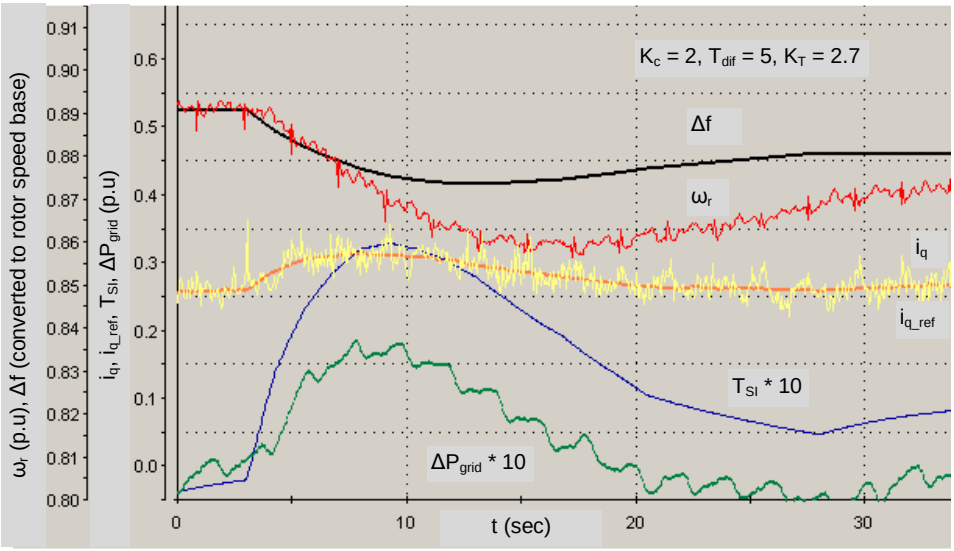

Figure 6.5 – Increase in power output and decrease in rotor speed with the inertia coupling function during application of the frequency test signal.

6.4 Discussion

6.4.1 Functional tests

Generator torque control

The q-axis current response of the generator vector control to a step change in i_{q_ref} was almost immediate and quicker than 50msec. This speed of response is in keeping with the expected response time, other similar sized test rigs (Chinchilla et al. 2006), (Pena et al. 1996), (Konghirun & Xu 2006) having response times between 5 and 10msec. The immediate change in rotor speed confirms that the torque response was rapid and the immediate jump in phase currents showed a balanced change. The relatively slow rise in the grid output power, seen in Figure 6.1, will be attributable to the speed of response of the grid active power control and the outer control loop for regulation of the dc link voltage.

The rapid change in q-axis current was seen to create a disturbance in the d-axis current. A large change in the required d-axis voltage, when i_q changed, due to the speed voltage (3.2.3) was also clearly evident. This change in steady state voltage which accompanies the change in torque matches the changes in steady state voltage shown in the phasor diagram of Figure 3.2. Since the X/R ratio of the machine is 19:1 the change in d-axis voltage ΔV_d is of a similar ratio greater than the change in q-axis voltage ΔV_q. Analysis of the disturbance effects when q-axis current changes and its effect on torque is discussed in Novotny & Lipo (1996).

Turbine maximum power control

The response from the maximum power extraction control and the function which emulates aerodynamic torque showed turbine acceleration as expected; a rapid initial acceleration which gradually diminished as the difference between the aerodynamic and generator torque reduced with the increase in speed. This behaviour was easily monitored in real time during the test using the x-y plot (Figure 6.4).

6.4.2 Inertia response test

Unlike the simulations undertaken in Chapter 5, for the experimental test a filter was applied to the inertia coupling function's differentiator input, for all cases. The sensitivity to noise due to the differentiator in the inertia coupling function was evident by the profile of T_{SI} for case (i) with a filter time constant of 1 sec. The test

frequency input Δf consists of discrete samples at 0.25 sec, so is not smooth and introduced an element of noise. However the addition of the filter, time constant 1 sec, for the first case, (i), produced identical results to that shown in the simulation in terms of the change in turbine power output and the capability to couple rotor speed to system frequency. The other cases (ii) and (iii) also correlated with the simulations of Chapter 5.

6.5 Conclusion

The following conclusions are made regarding the test rig and the demonstration of turbine inertia response:

- Vector control scheme derived in Chapter 3 and described in Chapter 4 was demonstrated to achieve fast control of torque via q-axis current.
- Performance of the q-axis current loop was demonstrated to be influenced by the regulation of the d-axis current.
- Turbine maximum power control and the emulation of aerodynamic torque for the test rig functioned correctly.
- 'Open loop' testing of an inertia response function demonstrated the capability to closely couple turbine rotor speed to system frequency.
- Change in power output of the turbine during the 'inertia response' was demonstrated to be adjustable by the selection of the filter time constant applied to the inertia coupling function's differentiator. Capability to double the effective inertia of the turbine was also demonstrated by adjustment of the inertia coupling function's overall gain.

7 Conclusion

This chapter gives an overview of the research undertaken, draws overall conclusions and makes recommendations for future research.

7.1 UK system modelling studies

A model was developed for the simulation of frequency on the mainland UK system. This work included derivation of a simplified model for the synchronous generator to represent the behaviour of Full Power Converter turbines equipped with such generators. The two distinct types of inertia response functions, the inertia coupling function and the step power/torque function were modelled by the introduction of a simple auxiliary torque signal into the existing turbine torque speed control loop.

Simulations using the model illustrated the likely positive and negative effects on primary frequency control for the UK when a high penetration of variable speed wind turbines with and without inertia response are introduced. Results were shown for a spread of demand levels and also two different sizes of generation loss, 1320GW and 1800GW. A basic comparison of the inertia functions was also included and consideration of the affect of steady state wind speed and the constant speed region of the maximum power extraction curve on the inertia response capability.

This work provides evidence which suggests:

- Impact on the wind turbine, in terms of performance requirements, for providing inertia response will likely be small, changes in torque/power output (and rotor speed) required during the frequency disturbances was relatively small (around 0.02pu for the frequency disturbances simulated). A quantitative comparison of the typical loadings experienced by a turbine during operation would be necessary to qualify this (see recommendations for future work 7.4).
- Commercial case for implementing inertia response may exist for the UK system; for the lower demand and larger loss scenarios an increase in synchronous plant response was needed (11GW in the most extreme case) to compensate for the reduction in system inertia due to a large quantity of wind turbines without inertia response. A reduction in the necessary quantity

of scheduled synchronous plant by the provision of wind turbine inertia response may be commercially attractive since the inertia response functions do not inherently reduce the energy production of the turbine. A more detailed consideration of the scheduling of conventional plant and reserve, across different operating scenarios, would be required to quantify the commercial benefit (see recommendations for future work 7.4).

- Use of the differentiator in the inertia response function is not necessarily prohibitive; when a first order filter was used on the function's differentiator input for noise reduction, the initial rate of change of system frequency increased by approximately 25% and the peak magnitude of the frequency deviation reduced by approximately 10%. In terms of the performance of system frequency regulation the first affect is considered detrimental and the second beneficial.

7.2 Experimental testing

A laboratory based test rig was constructed which consisted of a Full Power Converter bridge and a synchronous generator driven by a dc machine to represent aerodynamic torque input. Power converters, utilising discrete MOSFET devices, were designed and constructed by the candidate and gate drivers also constructed employing a single Integrated Circuit for the gate driver. Vector control of both the generator converter and grid converter was implemented on a dedicated hardware control platform using graphical based software for program description.

Tests confirmed correct operation of the generator vector control, turbine maximum power extraction control and emulation of aerodynamic torque by the dc machine.

The inertia coupling function was implemented and a test frequency deviation injected into the inertia function's input to represent a large load generation imbalance. The experimental results, Fig 6.5, were found to compare closely to those of the modelled turbine, Fig 5.7.

This work demonstrated that:

- The simplified model of synchronous generator as developed, was representative of the behaviour of the wind turbine test rig's electrical machine and power converters in terms of the speed of torque response; speed of response in the experimental test to a step change in torque was less than 50msec, the time constant used for the synchronous generator model was 20msec.
- Differentiator noise issues are not prohibitive in an experimental implementation.
- Vector control of the synchronous generator was sufficiently fast to implement the inertia response function; use of the filter on the input to the differentiator reduced the required rate of rise and magnitude of the additional torque response.

7.3 Overall Conclusions

The following overall conclusions are made:

- Simulations undertaken indicate that the inertia coupling function is arguably more applicable for use in the UK than the step type inertia response. Studies undertaken by another author show the step function to be applicable in particular to a hydro dominated system. This is further supported by a review of the grid codes; the only existing inertia response requirement is for the Canadian Hydro-Quebec (a hydro-electric dominated) system which specifies a step type inertia response. The draft grid code for the EU indicates an inertia coupling type response.
- The simplified model developed of the synchronous generator gave adequate representation for the system frequency modelling studies undertaken.
- Experimental testing further confirms the possibility of providing an inertial response from a variable speed wind turbine and the suitability of the inertia coupling function for this purpose.

7.4 Further work

Recommendations for further work are subdivided into the following areas:

- System modelling - The model developed for the frequency simulation studies was simplistic and did not take into account other types of generating plant or electrical aspects. Before use in further studies an evaluation of the suitability/accuracy of the model may be useful.
- System studies (a) - Stability analysis to investigate robustness of system frequency control and assess if introduction of inertial response from a large number of turbines using a heavily delayed response is problematic.
- System studies (b) - A more sophisticated consideration of the scheduling of generating plant and consideration of the inclusion of governor response from (new) conventional plant which may have enhanced frequency response capabilities.
- Turbine modelling (a) - Investigation of the sensitivity of a turbine to operating away from its maximum power point and hence further quantification of the capability to provide inertial response. This might involve representation of the torque speed control loop using a more realistic PI based speed control as shown in Bossanyi (2000) and representation of the dynamics of the rotor torque production.
- Turbine modelling (b) - Quantitative assessment of the loadings experienced by a turbine during operation. This might encompass drive-train, blade and tower loadings during variable wind conditions using a program such as Bladed®. As indicated in 7.1, this would enable the performance requirements for providing an inertia response to be assessed against existing turbine performance capabilities/constraints[30].
- Experimental work - Closed loop testing of the inertia response function on a small scale power system (i.e. 15kW). This will enable further assessment of the inertia coupling function and also the use of the filter on the differentiator's input for the reduction of noise. Use of commercially supplied power converters on the test rig would be recommended for the

[30] An example study looking at turbine loading issues and aspects of control implementation for the addition of turbine fault ride through capability is given in Bossanyi et al. (2009).

further experimental work since the test rig constructed for the research shown in this thesis was felt unrepresentatively noisy.

8 References

ANSI/IEEE, 1993. *C37.106-1987 Guide for Abnormal Frequency Protection for Power Generating Plants*,

Anaya-Lara, O. et al., 2009. *Wind Energy Generation: Modelling and Control*, Wiley.

Bolton, W., 1998. *Control Engineering*, Longman.

Bose, B., 2002. *Modern Power Electronics and AC Drives*, Pearson.

Bossanyi, E., 2000. The Design of closed loop controllers for wind turbines. *Wind Energy*, 3(3), pp.149–163. Available at: http://doi.wiley.com/10.1002/we.34 [Accessed August 2, 2011].

Bossanyi, E., Ramtharan, G. & Savini, B., 2009. The importance of control in wind turbine design and loading. In *2009 17th Mediterranean Conference on Control and Automation*. IEEE, pp. 1269–1274. Available at: http://ieeexplore.ieee.org/xpl/freeabs_all.jsp?arnumber=5164721 [Accessed November 4, 2011].

Bourlis, D., 2009. Gain Scheduled Controller with Wind Speed Estimation via Kalman Filtering for a Stall Regulated Variable Speed Wind Turbine. In *44th Universities Power Engineering Conference, 2009*. pp. 1–5.

Brisebois, J., Transénergie, H. & Aubut, N., 2011. Wind Farm Inertia Emulation to Fulfill Hydro-Québec's Specific Need. , 7, pp.1–7.

Burton, T. et al., 2001. *Wind Energy Handbook*, John Wiley & Sons Ltd.

Cedeno, W. & Laplante, P., 2007. An Overview of Real-time Operating Systems. *Journal of the Association for Laboratory Automation*, 12(1), pp.40–45.

Chapman, S., 2005. *Electric Machinery Fundamentals* 4th ed., McGraw-Hill.

Chinchilla, M., Amaltes, S. & Rodriguez-Amenedo, J.L., 2004. Laboratory set-up for wind turbine emulation. *2004 IEEE International Conference on Industrial Technology, 2004. IEEE ICIT '04.*, 1, pp.553–557. Available at: http://ieeexplore.ieee.org/lpdocs/epic03/wrapper.htm?arnumber=1490352.

Chinchilla, M., Arnalte, S. & Burgos, J C, 2005. Power limits of grid-connected modern wind energy systems. *Renewable Energy*, 31, pp.1455–1470.

Chinchilla, M., Arnaltes, S. & Burgos, J.C., 2006. Control of Permanent-Magnet Generators Applied to Variable-Speed Wind-Energy Systems Connected to the Grid. *IEEE Transactions on Energy Conversion*, 21(1), pp.130–135. Available at: http://ieeexplore.ieee.org/lpdocs/epic03/wrapper.htm?arnumber=1597329.

Committee on Climate Change, 2008. *Building a low-carbon economy - The UK's contribution to tackling climate change*, Available at: http://www.theccc.org.uk/.

Conroy, J.F. & Watson, R., 2008. Frequency Response Capability of Full Converter Wind Turbine Generators in Comparison to Conventional Generation. *IEEE Transactions on Power Systems*, 23(2), pp.649–656. Available at: http://ieeexplore.ieee.org/lpdocs/epic03/wrapper.htm?arnumber=4494589.

Courtecuisse, V. et al., 2008. Experiment of a wind generator participation to frequency control. In *2008 Wind Power to the Grid - EPE Wind Energy Chapter 1st Seminar*. IEEE, pp. 1–6.

Department of Energy and Climate Change, 2011a. *Planning our electric future: a White Paper for secure, affordable and low-carbon electricity*, Available at: http://www.decc.gov.uk/.

Department of Energy and Climate Change, 2011b. *UK Renewable Energy Roadmap*, Available at: http://www.decc.gov.uk/.

Department of Trade and Industry, 2007. *Meeting the Energy Challenge - A White Paper on Energy*, Available at: http://webarchive.nationalarchives.gov.uk/+/http://www.berr.gov.uk/energy/whitepaper/page39534.html.

EON-Netz, 2006. *Grid Code - High and extra high voltage - Status 1*, Available at: www.eon-netz.com.

EON-Netz, 2008. *Requirements for Offshore Grid Connections in the E.ON Netz Network*, Available at: www.eon-netz.com.

EirGrid, 2009. *EirGrid Code Ver 3.3 (Wind Grid Code Only)*, Available at: http://www.eirgrid.com/.

Ekanayake et al., 2008. Frequency Response From Wind Turbines. *Wind Engineering*, 32(6), pp.573–586.

Ellis, G., 2004. *Control system design guide* 3rd ed., Elsevier.

Entso-e, 2010. *Requirements for Grid Connection Applicable to all Generators - working draft*, Available at: https://www.entsoe.eu/.

Erinmez, I.A. et al., 1998. NGC Experience with frequency control in England and Wales - Provision of frequency response by generators. *Response*.

Fox, B., Flynn, D. & Bryans, L., 2007. *Wind Power Integration - Connection and system operational aspects*, IET.

Gallegos-Lopez, G., Gunawan, F.S. & Walters, J.E., 2005. Optimum Torque Control of Permanent-Magnet AC Machines in the Field-Weakened Region. *IEEE*

Transactions on Industry Applications, 41(4), pp.1020–1028. Available at: http://ieeexplore.ieee.org/lpdocs/epic03/wrapper.htm?arnumber=1468279.

Heier, S., 2006. *Grid Integration of Wind Energy Conversion Systems* 2nd ed., John Wiley & Sons Ltd.

Hydro - Quebec, 2009. *Transmission provider technical requirements for the connection of power plants to the hydro-quebec transmission system*, Available at: www.hydroquebec.com/.

International Rectifier, Six-Output 600VMGDs Simplify 3-Phase Motor Drives, Application Note AN-985. Available at: http://www.irf.com/technical-info/appnotes/an-985.pdf.

Jamieson, P., 2011. *Innovation in Wind Turbine Design*, John Wiley & Sons Ltd.

Johnson, K.E. et al., 2006. Control of variable-speed wind turbines: standard and adaptive techniques for maximizing energy capture. *IEEE Control Systems Magazine*, 26(3), pp.70–81. Available at: http://ieeexplore.ieee.org/lpdocs/epic03/wrapper.htm?arnumber=1636311 [Accessed December 20, 2011].

Kayikci, M. & Milanovic, J.V., 2009. Dynamic Contribution of DFIG-Based Wind Plants to System Frequency Disturbances. *IEEE Transactions on Power Systems*, 24(2), pp.859–867. Available at: http://ieeexplore.ieee.org/lpdocs/epic03/wrapper.htm?arnumber=4808229.

Konghirun, M. & Xu, L., 2006. A Fast Transient-Current Control Strategy in Sensorless Vector-Controlled Permanent Magnet Synchronous Motor. *IEEE Transactions on Power Electronics*, 21(5), pp.1508–1512.

Krause, P., Wasynczuk, O. & Sudhoff, S., 2002. *Analysis of Electric Machinery and Drive Systems*, IEEE.

Kundur, P., 1994. *Power System Stability and Control* N. J. Balu & M. G. Lauby, eds., McGraw-Hill.

LEM, Isolated voltage and current transducers - Characteristics - Applications - Calculations - 3rd edition. Available at: http://www.lem.com.

Lalor, G., Mullane, a. & O'Malley, M., 2005. Frequency Control and Wind Turbine Technologies. *IEEE Transactions on Power Systems*, 20(4), pp.1905–1913. Available at: http://ieeexplore.ieee.org/lpdocs/epic03/wrapper.htm?arnumber=1525120.

Littler, T., Fox, B. & Flynn, D., 2005. Measurement-based estimation of wind farm inertia. *2005 IEEE Russia Power Tech*, (1), pp.1–5. Available at: http://ieeexplore.ieee.org/lpdocs/epic03/wrapper.htm?arnumber=4524432.

Manwell, J., McGowan, J. & Rogers, A., 2002. *Wind Energy Explained - theory, design and application* 1st ed., John Wiley & Sons Ltd.

Miller, N.W. et al., 2003. Dynamic modeling of GE 1.5 and 3.6 MW wind turbine-generators for stability simulations. *2003 IEEE Power Engineering Society General Meeting (IEEE Cat. No.03CH37491)*, (July), pp.1977–1983. Available at: http://ieeexplore.ieee.org/lpdocs/epic03/wrapper.htm?arnumber=1267470.

Ming, Y. et al., 2004. Modeling of VSC-HVDC and Its Active Power Control Scheme. In *International Conference on Power System Technology*. pp. 21–24.

Mohan, N., Undeland, T & Robbins, W., 2003. *Power Electronics: Converters, applications and design* 3rd ed., John Wiley & Sons, Inc.

Molinas, M. et al., 2005. Control of Wind Turbines with Induction Generators Interfaced to the Grid with Power Electronics Converters. In *International Power Electronic Conference, IPEC, Japan 2005*.

Moore, I., 2011. *Review of Transmission System Connection Requirements*, Available at: MooreIF@Cardiff.ac.uk.

Morren, J., Pierik, J. & Dehaan, S., 2006. Inertial response of variable speed wind turbines. *Electric Power Systems Research*, 76(11), pp.980–987. Available at: http://linkinghub.elsevier.com/retrieve/pii/S0378779605002713 [Accessed July 24, 2011].

Mott MacDonald, 2010. *UK Electricity Generation Costs Update*, Available at: http://www.decc.gov.uk/assets/decc/statistics/projections/71-uk-electricity-generation-costs-update-.pdf.

Mullane, A. & O'Malley, M., 2005. The Inertial Response of Induction-Machine-Based Wind Turbines. *IEEE Transactions on Power Systems*, 20(3), pp.1496–1503. Available at: http://ieeexplore.ieee.org/lpdocs/epic03/wrapper.htm?arnumber=1490603 [Accessed November 25, 2011].

National Grid, 2008. *Balancing Principles Statement*, Available at: http://www.nationalgrid.com/.

National Grid, 2011a. *Gone Green 2011 - Key facts and figures*, Available at: http://www.nationalgrid.com.

National Grid, 2011b. *Operating the Electricity Transmission Networks in 2020 - June 2011 Update*, Available at: http://www.nationalgrid.com.

National Grid, 2010a. *Procurement Guidelines Report 1 April 2009 to 31 March 2010 Version 2*, Available at: http://www.nationalgrid.com/.

National Grid, 2010b. *The Grid Code - issue 4 rev 5*, Available at: http://www.nationalgrid.com/.

Novotny, D. & Lipo, T., 1996. *Vector Control and Dynamics of AC Drives*, Oxford University Press.

Pearmine, R. et al., 2006. Identification of a load–frequency characteristic for allocation of spinning reserves on the British electricity grid. *IEE Proceedings - Generation, Transmission and Distribution*, 153(6), p.633. Available at: http://ieeexplore.ieee.org/xpl/freeabs_all.jsp?arnumber=4015885 [Accessed December 21, 2011].

Pearmine, R., Song, Y. & Chebbo, A., 2007a. Experiences in modelling the performance of generating plant for frequency response studies on the British transmission grid. *Electric Power Systems Research*, 77(12), pp.1575–1584. Available at: http://linkinghub.elsevier.com/retrieve/pii/S037877960600277X [Accessed November 3, 2011].

Pearmine, R., Song, Y. & Chebbo, A., 2007b. Influence of wind turbine behaviour on the primary frequency control of the British transmission grid. *Power*, (2), pp.142 – 150.

Pena, R., Clare, J.C. & Asher, G.M., 1996. Doubly fed induction generator using back-to-back PWM converters and its application to variable-speed wind-energy generation. *IEE Proceedings - Electric Power Applications*, 143(3), p.231. Available at: http://link.aip.org/link/IEPAER/v143/i3/p231/s1&Agg=doi.

Rabelo, B. & Hofmann, W., 2002. DSP-based Experimental Rig with the Doubly-Fed Induction Generator for Keywords. In *Proceedings of PEMC'2002 Dubrovnik, Croatia*. pp. 1–12.

Rabelo, B., Hofmann, W. & Gliick, M., 2004. Emulation of the Static and Dynamic Behaviour of a Wind-Turbine with a DC-Machine Drive. In *35th Annaul IEEE Power Electronics Specialists Conference*. pp. 2107–2112.

Ramtharan, G., Ekanayake, J.B. & Jenkins, N., 2007. Frequency support from doubly fed induction generator wind turbines. *Engineering and Technology*, pp.3–9.

Rashid, M., 2001. *Power Electronics Handbook*, Academic Press.

Raychem, MOSFET Device Protection. , (V). Available at: www.pbi.co.kr/bbs/data/Raychem.../03.E10_mosfet_(164_168).pdf.

Rebours, Y.G. et al., 2007. A Survey of Frequency and Voltage Control Ancillary Services—Part I: Technical Features. *IEEE Transactions on Power Systems*, 22(1), pp.350–357. Available at: http://ieeexplore.ieee.org/lpdocs/epic03/wrapper.htm?arnumber=4077135.

Tarnowski, G.C. et al., 2009. Variable speed wind turbines capability for temporary over-production. In *Power & Energy Society General Meeting, 2009. PES '09. IEEE*. pp. 1–7.

The Parliamentary Office of Science and Technology, 2011. *Carbon Footprint of Electricity Generation - POSTnote Update*, Available at: http://www.parliament.uk/post.

Thiringer, T. & Luomi, J., 2001. Comparison of reduced-order dynamic models of induction machines. *IEEE Transactions on Power Systems*, 16(1), pp.119–126. Available at: http://ieeexplore.ieee.org/lpdocs/epic03/wrapper.htm?arnumber=910789 [Accessed January 5, 2012].

Ullah, N.R., Thiringer, T. & Karlsson, D., 2008. Temporary Primary Frequency Control Support by Variable Speed Wind Turbines— Potential and Applications. *IEEE Transactions on Power Systems*, 23(2), pp.601–612. Available at: http://ieeexplore.ieee.org/xpl/freeabs_all.jsp?arnumber=4480153 [Accessed August 10, 2011].

Williams, T., 1991. *The Circuit Designers's Companion* 1st ed., Newnes.

dSPACE, 2009. Manual for PPC1103.

Appendix A - Test rig implementation and commissioning

A1 – Inverse dq transformation

The inverse transforms of Eq(3.1, 3.2 and 3.3) implemented in the controller are as follows (Kundur 1994):

$$i_a = i_d\cos\theta - i_q\sin\theta + i_0$$

$$i_b = i_d\cos\left(\theta - \frac{2\pi}{3}\right) - i_q\sin\left(\theta - \frac{2\pi}{3}\right) + i_0$$

$$i_c = i_d\cos\left(\theta + \frac{2\pi}{3}\right) - i_q\sin\left(\theta + \frac{2\pi}{3}\right) + i_0$$

A2 – Converter bridge and gate driver schematics

The circuit schematic for a single phase of one of the converter bridges is shown in Figure A2.1. The MOSFET device package has gate, drain and source pins located on pins 1, 2, and 3 respectively with the metal package body being internally connected to the drain. This means the heat sinks are live. Note local decoupling caps across each bridge (V_{cc} to GND) are not shown and the snubber components (right-hand side of the schematic) were not populated. The gate driver circuit schematic is shown in Figure A2.2

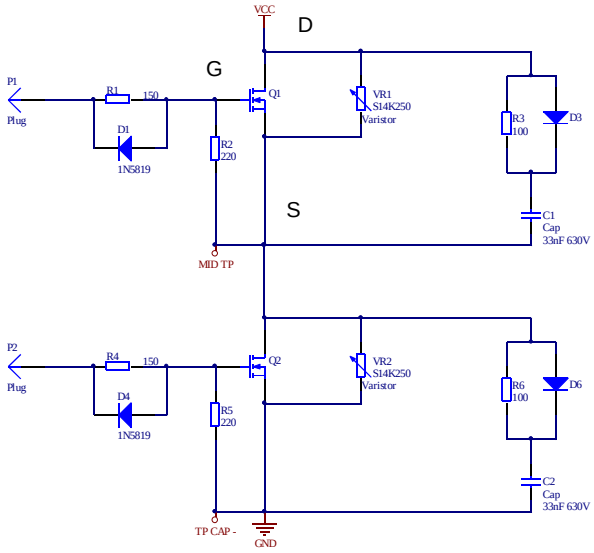

Figure A2.1 – Bridge converter circuit schematic (single phase shown)

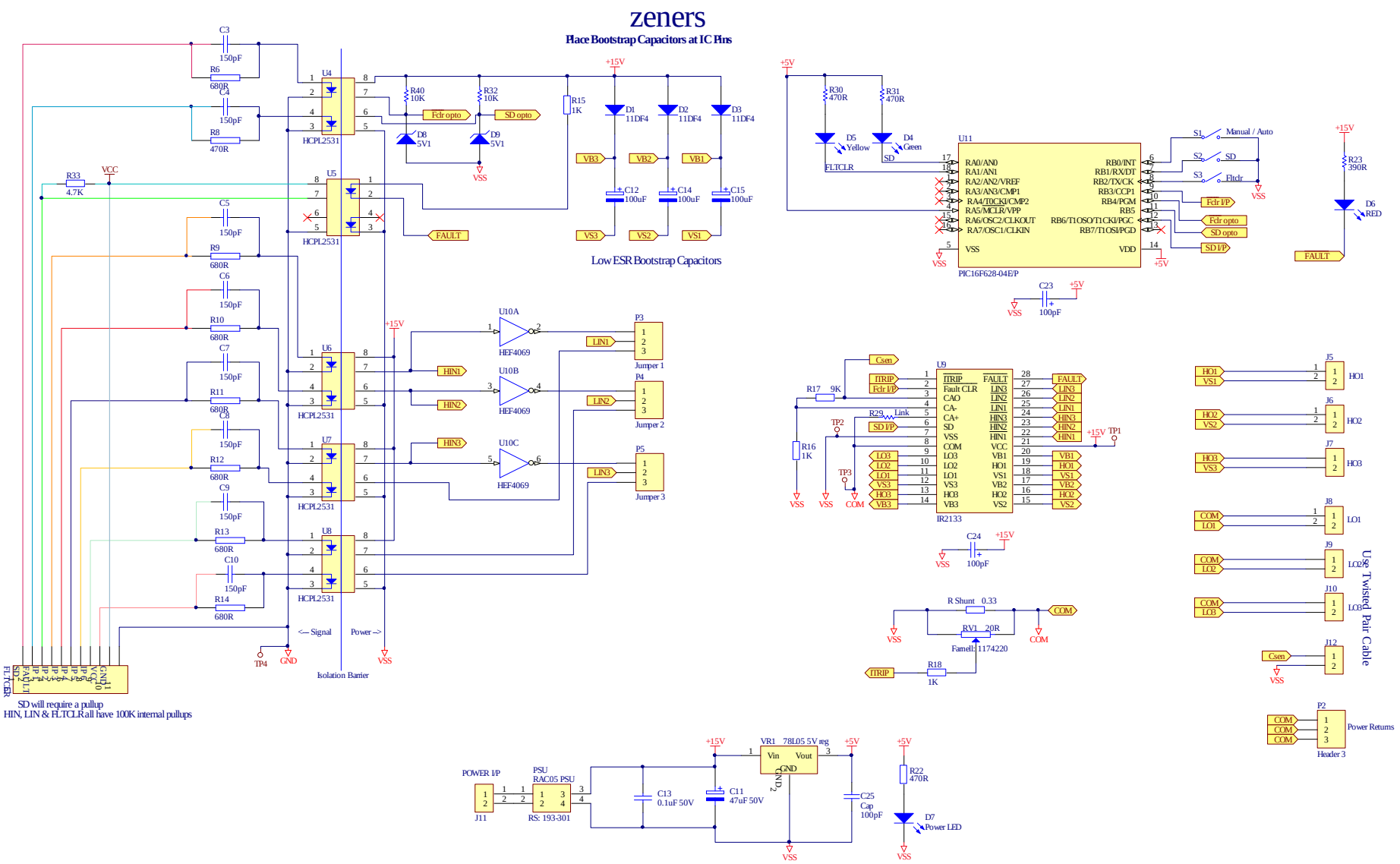

Figure A2.2 – Gate driver board circuit schematic

A3 – Parameter measurement

To provide values of inductance and resistance for use in the grid and converter control schemes of Figure 4.12 and Figure 4.13 the parameters for the synchronous machine and the transformer are experimentally measured using open circuit and short circuit tests (Chapman 2005).

Synchronous machine parameters

Firstly, voltage verses field current was measured with the machine open circuit, the open circuit characteristic for the machine is shown Figure A3.1 (left). Secondly, armature current verses field current was measured with the machine short circuited, the short circuit characteristic for the machine is shown Figure A3.1 (right). The synchronous machine was then directly connected to a resistive load bank where rated field current was found to be 1.18A for a terminal voltage of 230V at unity power factor, the corresponding per phase load was measured at 260W.

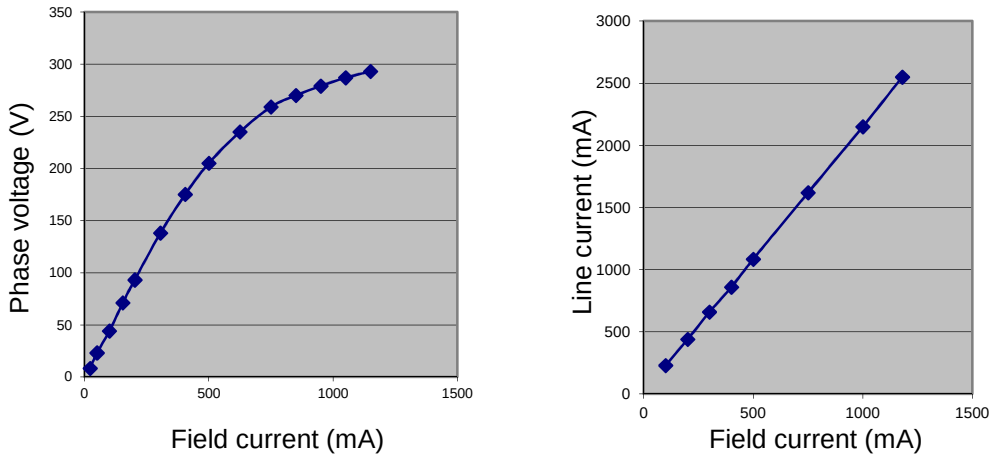

Figure A3.1 – Open circuit characteristics (left) and short circuit characteristics (right) for the synchronous machine.

The saturated reactance of the machine X_s is given by

$$X_s = \frac{E_{int}}{I_{arm}}$$

where E_{int} is the internal voltage of the machine obtained from the open circuit test and I_{arm} is the rated armature current obtained with the short circuit test, both at rated field current. Hence from the data in Figure A3.1

$$X_s = \frac{293}{2.55/\sqrt{3}} = 199\Omega$$

A third test determined the resistance of the machine by passing a dc short circuit current through a single phase winding which developed 5.34V across the phase at 0.497A. Thus

$$R_a = \frac{V}{I} = \frac{5.34}{0.497} = 10.75\Omega$$

Converting to p.u, with VA base S_b chosen as 800VA and the voltage base V_b chosen as 230V

$$Z_b = \frac{V_b}{S_b} = \frac{230^2}{800} = 66\,\Omega$$

hence

$$X_s = \frac{199}{66} = 3.0\text{p.u}, \quad R_a = \frac{10.75}{66} = 0.16\text{p.u}$$

Transformer parameters

The approximate equivalent circuit of a transformer is obtained by neglecting the excitation branch and adding the primary and secondary impedances giving an equivalent series impedance Z_{eq} composed of a resistance R_{eq} and reactance X_{eq} (Chapman 2005).

A short circuit test was performed by shorting the primary terminals of the transformer (the inverter side) and measuring the voltage, current and power on the secondary side with secondary current equal to rated. Rated current for the transformer is

$$i_{LL} = \frac{S_b}{V_{LL}} = \frac{800}{400\sqrt{3}} = 1.15\text{A}$$

The short circuit test using a primary phase current I_P of 1.21A (close to rated) gave a per phase primary voltage V_P = 50.0V, and a per phase primary power P_P of 31W (measured using a Wattmeter). The equivalent impedance, X_{eqP}, and resistance, R_{eqP}, referred to the primary side are calculated, using the following procedure:

The impedance referred to the primary side is

$$\left|Z_{eqP}\right| = \frac{V_P}{i_P} = \frac{50.0}{1.21} = 41.3\Omega$$

and the power factor (PF) is given by

$$PF = \frac{P_P}{V_P I_P} = \frac{31}{50.0 \text{ X } 1.21} = 0.51 \text{ lagging}$$

Hence

$$R_{eqP} = 0.51 \text{ X } 41.3 = 21.1\Omega$$

and $$X_{eqP} = \sqrt{\left(Z_{eqP}{}^2 - R_{eqP}{}^2\right)} = 35.5\Omega$$

Converting to p.u using the system base and impedance base used for the synchronous generator

$$R_{eq} = \frac{21.1}{66} = 0.32\text{p.u}, \quad X_{eq} = \frac{35.5}{66} = 0.54\text{p.u}$$

A4 - Measurement of generator L_{dq}

The d and q-axis inductance was experimentally measured using the control screen shown in Figure A4.1 using the following procedure:

a) Set i_d and i_q both equal to zero (via i_{dq_ref}). Adjust L_{ad} so that V_q consists of only V_{q_speed}, the q-axis speed voltage. (i.e. the output from the PI compensator, $_{Vq'} = 0$).
b) Set $i_d = 0$ and set i_q non-zero (via the i_{dq_ref}). Now adjust L_q until $V_{d'}$ from the d-axis PI compensator is zero.
c) Repeat procedure b) but for other axis. i.e Set $i_q = 0$ and set i_d non-zero (via the i_{dq_ref}). Now adjust L_d until $V_{q'}$ from the q-axis PI compensator is zero.

Note in Figure A4.1 the superscript '*' means 'ref'.

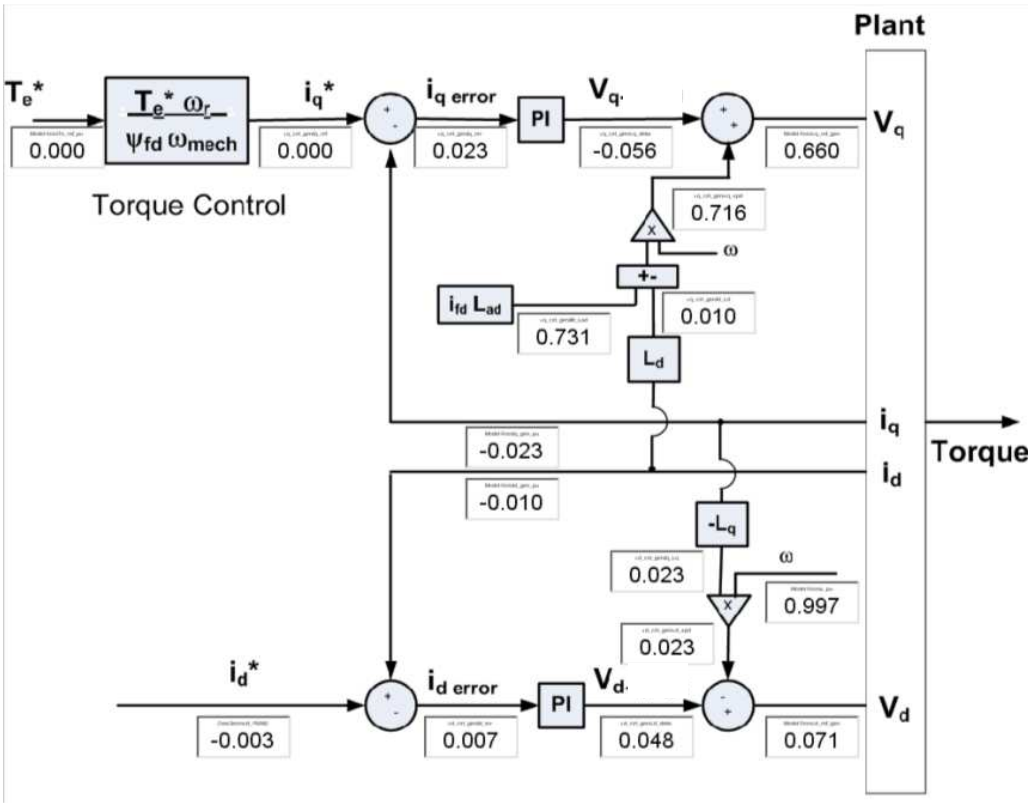

Figure A4.1 – Control 'mimic' from the test rig user interface showing values of i_{dq}, V_{dq} and the PI control values in real-time.

A5 - Test rig inertia scaling function check

Correct functioning of the test rig inertia scaling function (4.4.1) is confirmed using the results from Section 6.2.2. Considering the acceleration over the first half second between t = 1.5 and 2.0 sec in Figure 6.3:

The average value of the accelerating torque T_{acc} is approximately 0.2p.u and the rate of change of speed

$$\frac{d\omega_r}{dt} = \frac{0.1}{2.75} = 0.036 \text{ p.u sec}^{-1}$$

Rearranging Eq(2.4)

$$H = \frac{T_{acc}}{2\frac{d\omega_r}{dt}}$$

and using the experimentally measured values the inertia constant is

$$H = \frac{0.2}{2 * 0.036} = 2.78 \text{ sec}$$

This compares well with the intended 'scaled' test rig inertia of 2.97 sec as calculated in section 4.6.1.

Appendix B - Generator and turbine modelling

B1 - Electrical machine properties and electrical machine control

Inertia for a range of rotating machine sizes

The inertia constant calculated for a range of electrical machine sizes is shown in Table B1.1. Electrical power verses the per unit inertia constant H is plotted in Figure B1.1. Note that the vertical axis is logarithmic.

Table B1.1 – Inertia constants for a range of electrical machines

Machine	Mech. Power (kW)	Current (I_L)	P.F	Electrical Power (kW)	Inertia J (kgm^2)	Speed ($rads^{-1}$)	Machine K.E (kW.s)	H (sec)
WP[31]-DF90LRX	1.1	2.43	0.78	1.3	0.0034	157.1	0.04	0.03
Test Rig	-	-	-	0.8	0.022	157.1	0.17	0.22
WP-DF132-STX	5.5	10.6	0.84	6.2	0.03	157.1	0.37	0.06
PMGO-10K-200[32]	-	-	-	10.0	6.61	20.94395	1.45	0.14
WP-UDF200LNX	30	54	0.86	32.2	0.31	157.1	3.83	0.12
WP-UDF315SNE	110	191	0.87	115.3	3.2	157.1	39.49	0.34
BU[33]-DF450LA	710	1164	0.91	734.7	41	157.1	505.95	0.69
GE 1.5MW DFIG[34]	-	-	-	1545.0	75	150.7964	852.73	0.55
Jones . (2005)[35]	-	-	-	1650.0	75	157.1	925.52	0.56
2MW DFIG[36]	-	-	-	2000.0	130	157.1	1604.23	0.80

[31] WP – Range of induction motors by Brook Crompton www.brookcrompton.com
[32] Outer rotor design Permanent Magnet motor of type used by Ben.Whitby@Cardiff.ac.uk
[33] Larger size range of induction motors by Brook Crompton www.brookcrompton.com
[34] *GE 1.5 MW General Data* available http://www.pes-psrc.org/c/C17/GE%20Data%20Sheets.pdf
[35] From '*Estimating Wind Turbines Mechanical Constants*' A.G. González Rodríguez et al. available http://www.icrepq.com/icrepq07/361-gonzalez.pdf
[36] From Anaya-Lara (2009)

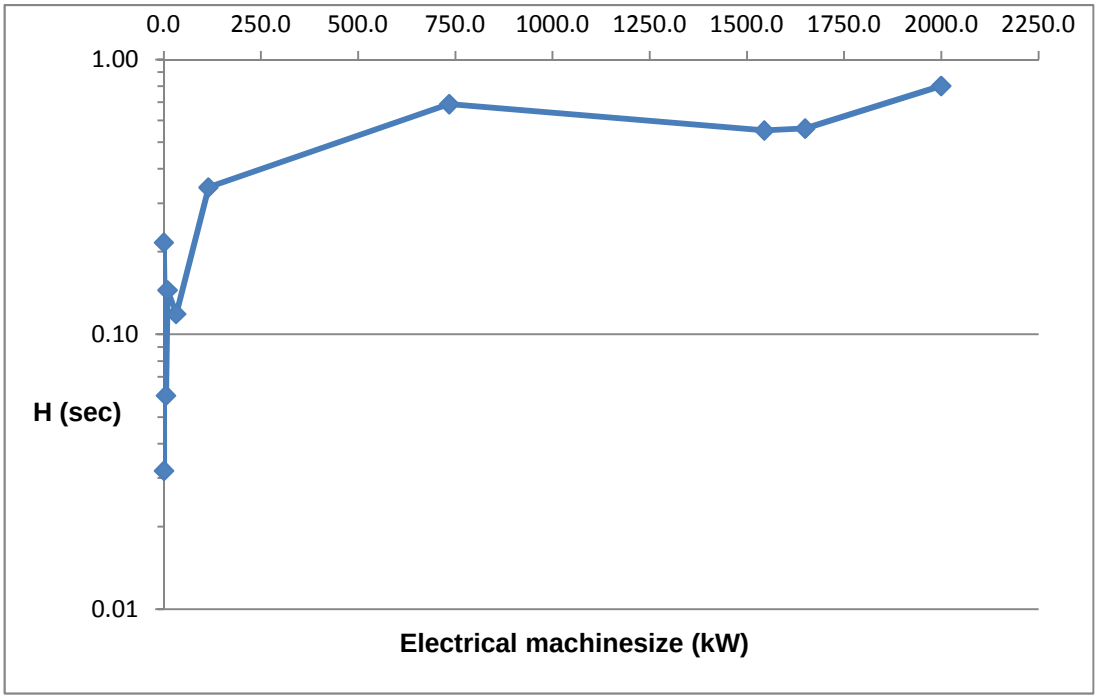

Figure B1.1 – Per unit inertia constant for a range of electrical machine sizes (vertical axis logarithmic)

Induction generator proportionality of torque to slip

As stated in section 2.2.1, a simplified induction generator circuit model (Kundur 1994) yields the following relationship between slip and electromagnetic torque T_e

$$T_e = 3\frac{p_f}{2}\left(\frac{R_r}{s\omega_s}\right)\frac{V_e^2}{(R_e + R_r/s)^2 + (X_e + X_r)^2} \qquad (2.10)$$

where p_f is the number of poles, V_e, X_e , R_e are the equivalent stator voltage, reactance and resistance respectively and R_r and X_r are the rotor resistance and reactance referred to the stator side.

Removing the constants p_f, ω_s, and V_e equation 2.10 shows a relationship between torque and slip as below:

$$T_e \propto \left(\frac{1}{s}\right)\frac{1}{(R_e + R_r/s)^2 + (X_e + X_r)^2}$$

Expanding the left hand side of the denominator

$$T_e \propto \frac{1}{s\left({R_e}^2 + \frac{2R_eR_r}{s} + \frac{{R_r}^2}{s^2}\right) + s(X_e + X_r)^2}$$

$$T_e \propto \frac{1}{s{R_e}^2 + 2R_eR_r + \frac{{R_r}^2}{s} + s(X_e + X_r)^2}$$

As s approaches zero it can be seen that $1/(R_r^2/s)$ will become the dominant term and hence for small values of slip torque is proportional to slip as below

$$T_e \propto \frac{s}{{R_r}^2}$$

Phasor representation of dq quantities

Components of flux linkage, voltage and current in the dq reference frame can be represented as phasors similar to as is conventionally done for current and voltage in the stationary reference frame (Kundur 1994). These dq quantities and their orientation are illustrated in Figure B1.2 where E_{int} is the internal voltage of the machine, E_T the terminal voltage, I_T current and X_s the impedance. Flux linkages are located 90 degrees behind their corresponding voltages and out of phase with their respective currents; field flux linkage λ_{fd}, stator flux linkage $\lambda_s = \lambda_{dq}$, and armature reaction flux linkage λ_a. The component of armature reaction flux linkage due to current in the d-axis is indicated as λ_{id}. Note as speed ω_r increases the magnitudes of E_{fd} and E_T will increase proportionally according to Eq(3.1), (3.2) & (3.4).

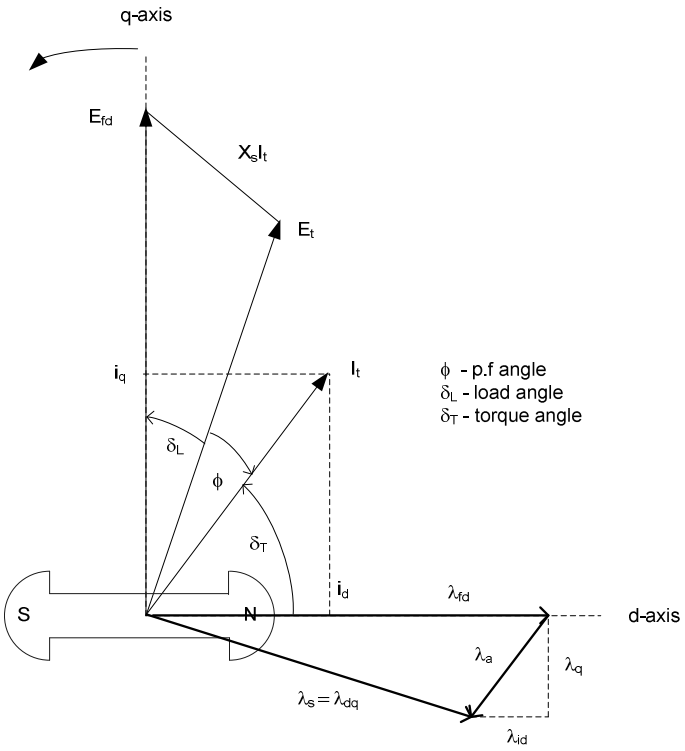

Figure B1.2 – Phasor representation of voltages, currents and flux linkages for the synchronous machine (winding resistances ignored and dq-axis inductances L_d, L_q assumed equal).

Load angle δ_L is the angle by which internal voltage leads terminal voltage, power factor angle φ is the angle by which current lags terminal voltage and torque angle δ_T is the angle by which terminal current leads the d-axis (or the angle of the armature reaction field to the rotor field). Figure B1.2 shows operation of the synchronous machine as a generator (E_{fd} leads E_T) and supplying reactive power (E_{fd} cos $\delta_L > E_T$)

B2 - Wind turbine

Model equation and C_p curve

The 'wind turbine' block supplied in MATLAB Simulink® is utilised for both the modelling and experimental work in the thesis. It is uses the function below:

$$C_p = c_1\left(\frac{c_2}{\lambda_i} - c_3\beta - c_4\right)e^{\frac{-c_5}{\lambda_i}} + c_6\lambda \quad \text{(B2.1)}$$

where C_p is the coefficient of performance, λ is the tip-speed ratio, β is the blade pitch angle and λ_i is calculated from tip speed ratio and pitch angle as below

$$\frac{1}{\lambda_i} = \frac{1}{\lambda + 0.08\beta} - \frac{0.035}{\beta^3 + 1}$$

The coefficients used, c_1 to c_6, were 0.5176, 116, 0.4, 5, 21 and 0.0068 respectively. Further information about this function is given in Heier (2006) and also the MATLAB® on-line help (http://www.mathworks.co.uk/). The resulting plot of C_p verses tip speed ratio is shown in Figure B2.1.

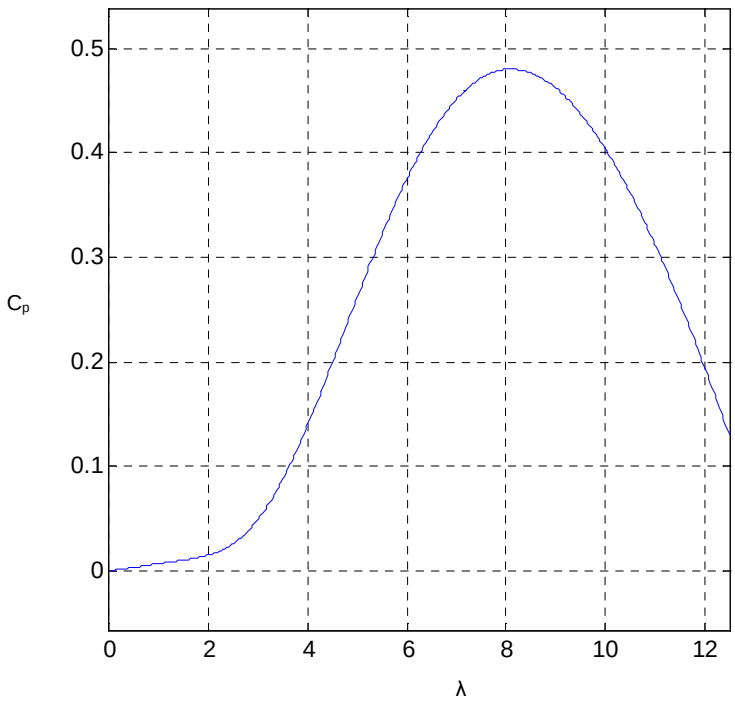

Figure B2.1 – Coefficient of performance verses tip speed ratio for the turbine used in the thesis (pitch angle $\beta = 0$)

C_p curve for GE 3.6MW DFIG turbine

The coefficient of performance verses tip speed ratio for the GE3.6MW turbine is shown in Figure B2.2 (right) for comparison with that of the turbine used in the thesis (left). The GE turbine is seen to be less sensitive to the tip speed and hence will be expected to have greater extractable reserves of K.E.

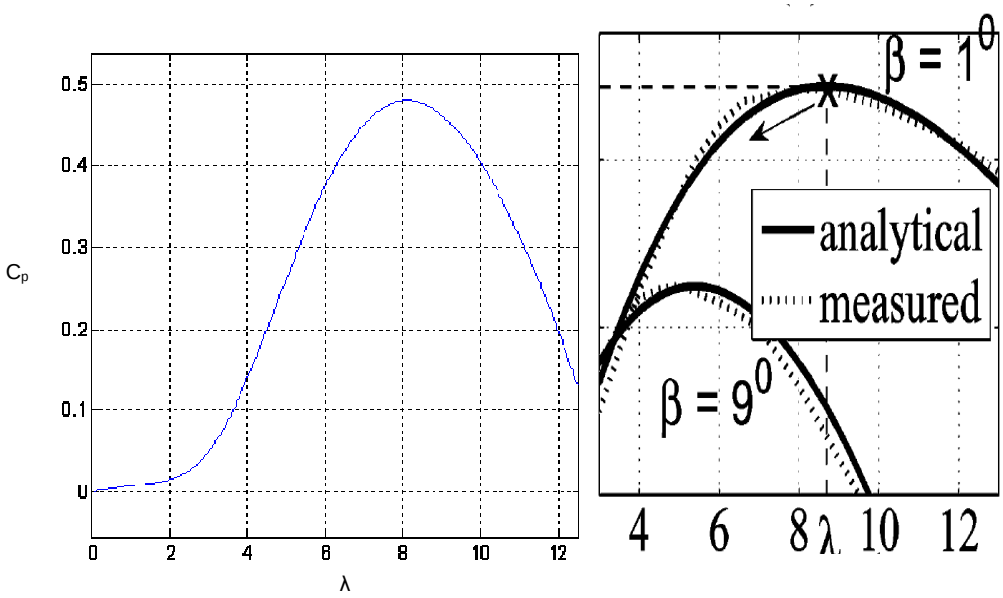

Figure B2.2 – Coefficient of performance curve from previous Figure (left) compared with that of the GE 3.6MW DFIG (right) (Ullah 2008).

B3 - Steam turbine schematic

Schematic for the simplified steam turbine as modelled in 5.2.2 is shown in Figure B3.1.

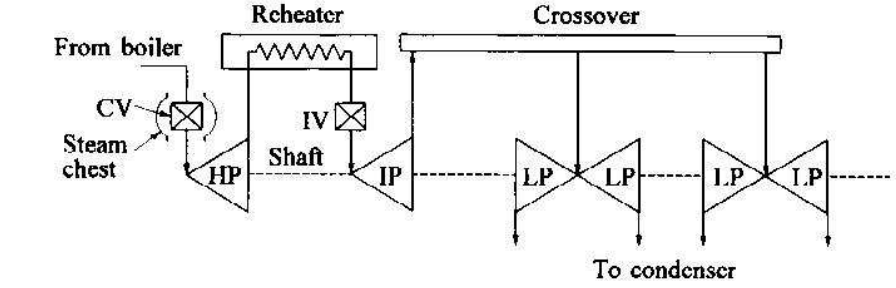

(a) Turbine configuration

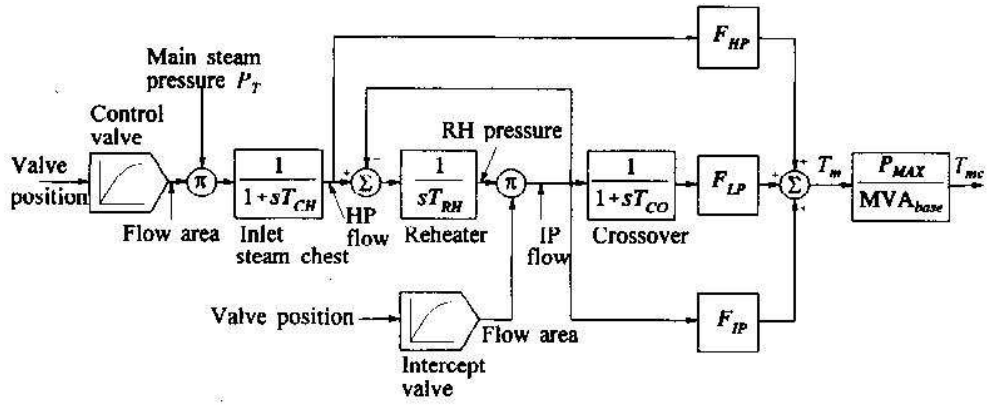

(b) Block diagram representation

Parameters

T_{CH} = time constant of main inlet volumes and steam chest
T_{RH} = time constant of reheater
T_{CO} = time constant of crossover piping and LP inlet volumes
T_m = total turbine torque in per unit of maximum turbine power
T_{mc} = total turbine mechanical torque in per unit of common MVA base
P_{MAX} = maximum turbine power in MW
F_{HP}, F_{IP}, F_{LP} = fraction of total turbine power generated by HP, IP, LP sections, respectively
MVA_{base} = common MVA base

Figure B3.1 – Single reheat tandem-compound steam turbine (Kundur 1994).